

Physical alterations to erythrocytes following sublethal mechanical stresses

Author

McNamee, Antony

Published

2020

Thesis Type

Thesis (PhD Doctorate)

School

School Allied Health Sciences

DOI

[10.25904/1912/1044](https://doi.org/10.25904/1912/1044)

Rights statement

The author owns the copyright in this thesis, unless stated otherwise.

Downloaded from

<http://hdl.handle.net/10072/394320>

Griffith Research Online

<https://research-repository.griffith.edu.au>

Physical alterations to erythrocytes following sublethal mechanical stresses

Antony P. McNamee
BExSc (Hons)

Biorheology Research Laboratory
Griffith University Mechanobiology Laboratory (GUMBL)
Menzies Health Institute Queensland
Griffith University
Australia

Submitted in fulfilment of the requirements of the degree of Doctor of Philosophy
February 2020



Correspondence

Antony P. McNamee

Biorheology Research Laboratory

Griffith University Mechanobiology Laboratory (GUMBL)

Menzies Health Institute Queensland

Griffith University

Australia

Telephone: +61 7 5552 7540

Email: mcnamee.ap@gmail.com

Declaration and copyright statement

This work has not previously been submitted for a degree or diploma in any university. To the best of my knowledge and belief, the thesis contains no material previously published or written by another person except where due reference is made in the thesis itself.

.....

Antony P. McNamee

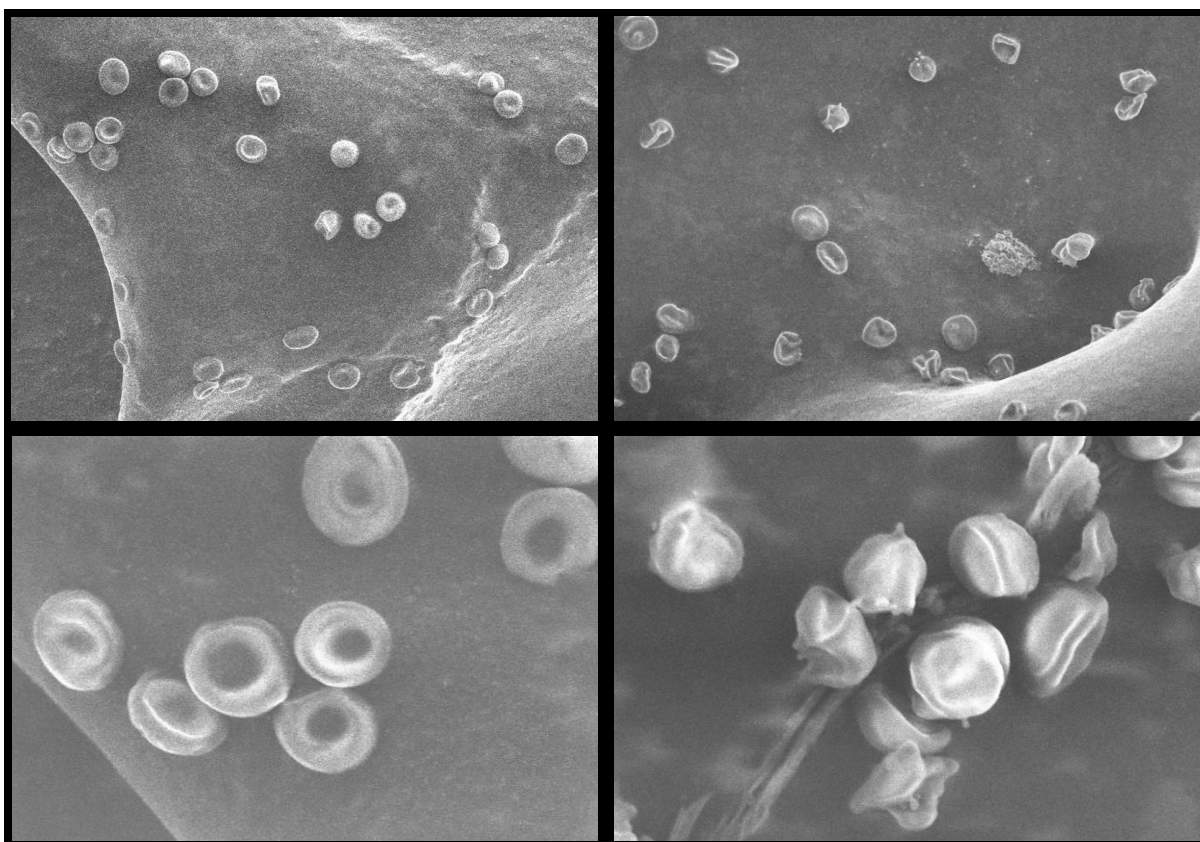


Fig. 1. Scanning electron micrograph of blood cells before (left) and after (right) exposure to sublethal mechanical shear stress.

Acknowledgements

As this dissertation draws to a close, I find myself contemplating on my fortunate journey, overwhelmed with gratitude for all the individuals that helped me to reach this momentous achievement.

Firstly, Dr Michael Simmonds, it is almost unbelievable that our paths first crossed more than seven years ago! I am truly indebted to you for tapping into my love of science and making me realise my 'itchy mind' and thirst for knowledge. Our many stimulating discussions and debates on scientific and other worldly issues regularly sparked motivation and compulsion to learn more. Your support, guidance, and mentorship facilitated my professional and personal growth by leaps and bounds. From undergraduate, postgraduate, to doctoral supervision, thank you for continually believing in me and allowing me to pave my own path. I look forward to our continued discoveries together and seeing just how far this rabbit warren goes.

Secondly, Prof Geoff Tansley, thank you for all your guidance, encouragement, and support. Your approachable nature and strive for excellence makes you a superb role model to the international artificial organs field, and a high-calibre Prof! Undeniably, you taught me on numerous occasions the true power of the whiteboard. I look forward to our continued work together into the future.

To my father, Peter McNamee, you would have made a fine academic. Your diverse expertise excels in many fields. I am not sure whether to thank you or apologise for the countless hours I stole you away to have scientific discussions, math and physics debates, learn your worldly wisdoms, or just consume an inordinate amount of coffee. Indeed, when times were at their toughest, your insights were ever inspiring. You are an exceptional role model and mentor, and

your vast knowledge of theoretical and applied science forever motivates me to continue onwards and upwards.

I sincerely wish to thank my many colleagues, at my home institution and elsewhere (especially my fellow labmates), for their continued interest, consistent engagement, intellectual discussion, and ongoing collaboration.

To my friends and family, you have always provided endless support, encouragement, and love. You were always there for a brew when I needed it most, and you never shied away when I would 'nerd out' about my science of blood 'homogoblins'.

Finally, to the love of my life, Caity, if I had not been waiting for you outside your lecture theatre all those years ago, I never would have had the fortuitous encounter with Dr Simmonds that started this wonderful endeavour. Unquestionably, you are my grounding force and soulmate. We have discussed on numerous occasions about your award of a 'PhT' ('Put hubby Through'), and honestly, without you I would not have survived this doctorate (nutritionally or otherwise). Thank you for coming along this journey with me. You were always there for me when I needed an arm for support, ear to listen, or a shoulder to lean on. I look forward to our continued adventures together, and exciting future to come.

Preface

I wish to open this thesis with an empirical truth that should not be misconstrued:

Artificial organs are medical miracles that do save human lives ...

...however, they still need improvement.

Cardiovascular disease remains the leading cause of death globally, with the prevalence continuing to rise in the developed world. As heart disease progresses into its end-stages, individuals urgently require transplantation of a new heart. Unfortunately, due to the scarcity of healthy donor organs, individuals can be bound to prolonged waitlists that extend beyond their foreseeable prognosis.

If only we could keep patients alive a little longer...

... If only we could create new organs that would heal this individual.

Since the development of the first artificial kidney (1943) and total artificial heart (1952), rapid advancements in technology have improved the viability of artificial organs, such that rather than solely being a transitional 'bridge to transplant', artificial organs are becoming a feasible therapeutic end-point. Home dialysers are now a reality, and implanted devices for cardiac support can extend survival beyond ten years of extra life.

Artificial organs make life saving medical procedures a possibility...

... In fact, artificial organs make life saving procedures routine practice!

Due to improved technology and medical therapies, the paradigms of artificial organ development have transitioned. Rather than device success being measured by the ability to mechanically mimic specific organ function, patient centred outcomes and quality of life are now of immense importance.

Undeniably, the future will contain individualised medicine that will rapidly return patients back to an active and healthy life.

The works contained within this dissertation will identify that the interface of artificial organs propagates the pathogenesis of blood dysfunction, partly explaining the aetiology of currently unresolved clinical complications. The intention of these works is not to ignite fear that artificial organs should not be used; but rather, these works should provide hope, knowing that by uncovering current tribulations of artificial organs, we will be able to strive for novel solutions for the betterment of humanity.

I hope that during my career in science, medicine, and engineering, the current problems will be of the past, and we will instead be striving to resolve the next great paradigm. Likely, biological substitutes will replace our current mechanical solutions, allowing self-regeneration and repair of damaged tissues. Perhaps humanity's role model will be realised in the Mexican axolotl salamander, who is able to regenerate missing limbs, as well as parts of their brain, heart, and spinal cord!

While the future of science and medicine remains exciting and unknown, one aspect remains certain, collaborative efforts at the interface of clinical practice, science, and engineering are the key to unlocking the complex truths. Science in isolation is antiquated. As such, I sincerely wish to thank my many colleagues, at my home institution and elsewhere, for their collaboration, intellectual discussion, and ongoing support.

I appreciate the universality of the concepts theorised, and desire to help those in need.

A.P. McNamee

Abstract

Mechanical circulatory support (MCS) devices, extracorporeal membrane oxygenators, and dialysis machines are mechanical systems designed to replace and/or support the functionality of specific biological organs. These devices have been extensively developed over recent decades and are increasingly utilised in acute and chronic care, greatly improving patient outcomes and extending survival. Given these devices integrate into the human vasculature, the efficacy of mechanical circulation depends on: successful surgical implantation and infection prevention, long-term functional performance without mechanical failure, and biological compatibility minimising damaging interactions with blood (i.e., haemocompatibility).

With improved device design, many current generation MCS devices have the capacity to adequately meet the required functional demands of associated biological organs, operating within parameters that avoid overt haemolysis and other extremes of inadequate haemocompatibility. Nevertheless, unfortunately the use of MCS remains plagued with severe secondary systemic complications which implicate impaired blood health and a functional decline of blood flow. While many precipitating determinants of these secondary complications remain unresolved, the accumulating clinical evidence indicates that the current haemocompatibility criteria is insufficient in predicting declines in blood function without the development of haemolysis (i.e., sublethal damage).

Blood trauma may be induced by non-physiological flow environments, largely due to elevated shear forces, turbulence, and collision with other cellular and artificial surfaces within MCS. Consequently, fragmentation of red blood cells (RBCs), shortened cell life-spans, and decreased cell function may be observed at microvascular levels, leading to the development of acute tissue ischaemia, propagating chronic systemic complications (e.g., multi-system organ failure –

where mortality is unavoidable). While there is need for improved, more sensitive, markers of haemocompatibility that can detect declining RBC function in non-haemolysed blood, only limited studies have investigated this sublethal trauma.

The aim of the present dissertation was to mechanistically elucidate how non-physiological shear environments, typical of MCS, can adversely affect blood function and flow independent of haemolysis, leading to the development of multi-system organ failure and death. The dissertation provides a comprehensive discussion into the haemorheological alterations that occur following exposure of blood to shear stresses that are suprphysiological (i.e., >10 Pa) and subhaemolytic (i.e., less than that required to induce haemolysis), providing novel characterisation and avenues for future inspection.

The findings of the current dissertation greatly enhance the understanding of the processes involved in the accumulation of functional blood damage observed in MCS, while progressing current understanding of red cell physiology. Further, the collective findings may in part explain current clinical complications associated with the use of MCS, possibly identifying rheological aetiologies for ischaemic complications, angiodysplasia, and the vascular related incidence of neurological complications.

The collective studies conceivably provide the basis for the development of a more sensitive and holistic indicator of haemocompatibility, while facilitating the development of numerical models that will allow *in silico* optimisation that will rapidly accelerate the advancement of future MCS devices. Understanding the haemorheological interactions associated with blood trauma will also assist the clinical management of current patients exposed to various forms of mechanical circulation, providing potential avenues for targeted rheological pharmacotherapy and improved patient care.

Publications arising from this dissertation

Published Chapters:

Chapter III:

McNamee AP, Tansley GD, Simmonds MJ. *Sublethal mechanical trauma alters the electrochemical properties and increases aggregation of erythrocytes*. *Microvascular Research*. 2018;120:1-7. doi: 10.1016/j.mvr.2018.05.008. PubMed PMID: 29803580.

Chapter VI:

McNamee AP, Horobin JT, Tansley GD, Simmonds MJ. *Oxidative stress increases erythrocyte sensitivity to shear-mediated damage*. *Artificial Organs*. 2018. **42**(2): p. 184-192.

Publications under review:

Chapter IV:

McNamee AP, Fitzpatrick T, Tansley GD, Simmonds MJ. *Exposure to sublethal and supraphysiological shear stress alters erythrocyte dynamics in subsequent low-shear flows*. Under review.

Chapter V:

McNamee AP, Tansley GD, Simmonds MJ. *Sublethal mechanical shear stress increases the elastic shear modulus of red blood cells but does not change capillary transit velocity*. Under review.

Publications contributing to this dissertation:

McNamee AP, Richardson K, Horobin JT, Kuck L, Simmonds MJ. *Susceptibility of density-fractionated erythrocytes to subhaemolytic mechanical shear stress*. *The International Journal of Artificial Organs*. 2019 Mar. **42**(3):151-7.

McNamee AP, Tansley GD, Sabapathy S, Simmonds MJ. *Biphasic impairment of erythrocyte deformability in response to repeated, short duration exposures of supraphysiological, subhaemolytic shear stress*. *Biorheology*. 2016. **53**(3-4): pp. 137-49.

Relevant abstracts presented to scientific conferences

McNamee AP., Tansley GD., Simmonds MJ., “Biophysical alterations to erythrocytes exposed to sublethal shear stresses”, 8th Meeting of the International Federation for Artificial Organs, PE12-5, Osaka, Japan (November 2019).

McNamee AP., Tansley GD., Simmonds MJ., “Sublethal damage to erythrocytes alters low-shear blood flow”, XLV European Society for Artificial Organs Congress, P34, Madrid, Spain (September 2018).

McNamee AP., Tansley G., Simmonds MJ., “Subhaemolytic mechanical trauma increases RBC aggregation by altering cell electrochemistry”, Joint meeting of: The European Society for Clinical Hemorheology and Microcirculation, The International Society for Clinical Hemorheology, and, The International Society of Biorheology, O1-3, Krakow, Poland (July 2018).

McNamee AP., Tansley G., Simmonds MJ., “Subhaemolytic mechanical damage alters erythrocyte behaviour in subsequent low-shear flows”, Joint meeting of: The European Society for Clinical Hemorheology and Microcirculation, The International Society for Clinical Hemorheology, and, The International Society of Biorheology, O1-4, Krakow, Poland (July 2018).

McNamee AP., Richardson K., Kuck L., Robertson K., Simmonds MJ., “Susceptibility to mechanical damage of density-fractionated red blood cells”, Joint meeting of: The European Society for Clinical Hemorheology and Microcirculation, The International Society for Clinical Hemorheology, and, The International Society of Biorheology, P24, Krakow, Poland (July 2018).

McNamee AP., Tansley G., Simmonds MJ., “Shear stress exposure alters the electrochemical and physical properties of erythrocytes”, Conference of the 44th European Society for Artificial Organs and 7th International Federation for Artificial Organs, O80, Vienna, Austria (September 2017).

McNamee AP., Horobin J., Tansley G., Simmonds MJ., “Oxidative stress increases susceptibility of red blood cells to shear-mediated damage”, Conference of the 44th European Society for Artificial Organs and 7th International Federation for Artificial Organs, P21, Vienna, Austria (September 2017).

McNamee AP., Horobin J., Tansley G., Sabapathy S., Simmonds MJ., “Biphasic responses of RBC function following repeat exposures to short duration, supraphysiological, subhaemolytic shear stress”, 18th Conference of the European Society for Clinical Hemorheology and Microcirculation, OC32, Lisbon, Portugal (June 2016).

McNamee AP., Horobin J., Tansley G., Simmonds MJ., “Oxidative stress increases erythrocyte susceptibility to mechanical damage”, 24th Annual Conference of the Society for Free Radical Research (Australasia), P17, Gold Coast, Australia (December 2016).

McNamee AP., Tansley G., Horobin J., Sabapathy S., Simmonds MJ., “The effects of supraphysiological shear stress on erythrocyte function”, Gold Coast Health and Medical Research Conference, Australia (December 2015).

Contents

CORRESPONDENCE.....	I
DECLARATION AND COPYRIGHT STATEMENT	III
ACKNOWLEDGEMENTS	V
PREFACE	VII
ABSTRACT	IX
PUBLICATIONS ARISING FROM THIS DISSERTATION	XI
RELEVANT ABSTRACTS PRESENTED TO SCIENTIFIC CONFERENCES.....	XII
CONTENTS.....	XV
LIST OF FIGURES	XXI
CHAPTER I.	
INTRODUCTION.....	1
<i>Blood fluidity and organ perfusion</i>	<i>1</i>
<i>Blood fluidity, chronic disease, and the clinical paradox</i>	<i>3</i>
<i>Biomedical devices and haemocompatibility</i>	<i>4</i>
REVIEW OF THE LITERATURE	5
<i>Haemorheology and the red blood cell.....</i>	<i>5</i>
<i>RBC aggregation.....</i>	<i>7</i>
<i>RBC deformability.....</i>	<i>10</i>
<i>RBCs in shear flow.....</i>	<i>10</i>
<i>Haemorheology in circulation.....</i>	<i>11</i>
<i>Haemodynamics</i>	<i>13</i>
<i>Mechanical circulatory support and blood compatibility: the clinical problem</i>	<i>15</i>
<i>Blood damage and the haemolytic threshold</i>	<i>17</i>
<i>Sublethal mechanical blood trauma</i>	<i>18</i>

<i>Changes in the RBC membrane and microvesicle release</i>	20
<i>Accelerated ageing and eryptosis</i>	21
OVERARCHING OBJECTIVES AND EXPERIMENTAL AIMS	23
CHAPTER II.	
SYSTEMS DESIGN AND CONTROL	25
SHEARING SYSTEMS	26
<i>Axisymmetric parabolic Poiseuille shearing system</i>	27
<i>Planar parabolic ‘slit flow’ shearing system</i>	31
<i>Annular Couette flow shearing system</i>	32
ELECTROPHORETIC MOBILITY CHAMBER.....	34
<i>Design specifications</i>	34
<i>Optimisation</i>	35
<i>Final design and deployment</i>	36
EKTACYTOSCOPE (COMBINED RHEOMETER-EKTACYTOMETER).....	38
<i>Design specifications</i>	39
<i>Optimisation</i>	40
<i>Final design and deployment</i>	42
<i>Analysis software</i>	44
MICROPIPETTE ASPIRATION SYSTEM.....	45
<i>Design specifications</i>	45
<i>Micropipette fabrication and forging</i>	45
<i>Micropipette control system</i>	48
<i>Pressure regulation</i>	49
<i>Final design and deployment</i>	49
<i>Analysis software</i>	51

CHAPTER III.

SUBLETHAL MECHANICAL TRAUMA ALTERS THE ELECTROCHEMICAL PROPERTIES AND INCREASES AGGREGATION OF ERYTHROCYTES 53

ABSTRACT.....	54
INTRODUCTION.....	55
MATERIALS AND METHODS.....	57
<i>Experimental overview.....</i>	<i>57</i>
<i>Subjects and sampling</i>	<i>58</i>
<i>Cell preparation.....</i>	<i>58</i>
<i>Application of shear stress</i>	<i>59</i>
<i>Isolation after shear stress.....</i>	<i>59</i>
<i>RBC aggregation and disaggregation shear rate threshold.....</i>	<i>59</i>
<i>RBC aggregability.....</i>	<i>60</i>
<i>RBC electrophoretic mobility</i>	<i>61</i>
<i>Preparation of RBC ghosts.....</i>	<i>62</i>
<i>Determination of sialic acid content</i>	<i>62</i>
<i>Statistical analyses.....</i>	<i>63</i>
RESULTS.....	63
<i>RBC aggregation and RBC aggregability</i>	<i>63</i>
<i>RBC disaggregation shear rate threshold.....</i>	<i>64</i>
<i>Bound and unbound sialic acid.....</i>	<i>65</i>
<i>Electrophoretic mobility and zeta potential.....</i>	<i>67</i>
DISCUSSION.....	68

CHAPTER IV.

EXPOSURE TO SUBLETHAL AND SUPRAPHYSIOLOGICAL SHEAR STRESS

ALTERS ERYTHROCYTE DYNAMICS IN SUBSEQUENT LOW-SHEAR FLOWS. 75

ABSTRACT..... 76

INTRODUCTION..... 78

MATERIALS AND METHODS..... 81

Blood sampling and preparation 81

Experimental design..... 81

Experiments One & Two: shear magnitudes that rigidify RBCs 82

Development of the ektacytoscope 83

Experiment Three: RBC treatment phase and ektacytoscope assessment 84

Data analysis..... 85

RESULTS..... 86

Experiment One: confirmation of shear magnitudes that rigidify RBCs..... 86

Experiment Two: RBC rigidity and low-shear EI..... 87

Experiment Three: coaxial ektacytometry and rheometry of RBC deformability..... 88

Experiment Three: histograms of RBC deformation 89

Experiment Three: RBC orientation at 0.3 and 5 Pa 91

DISCUSSION..... 92

CONCLUSIONS..... 96

CHAPTER V.

SUBLETHAL MECHANICAL SHEAR STRESS INCREASES THE ELASTIC SHEAR

MODULUS OF RED BLOOD CELLS BUT DOES NOT CHANGE CAPILLARY

TRANSIT VELOCITY 97

ABSTRACT..... 98

INTRODUCTION..... 99

MATERIALS AND METHODS.....	101
<i>Blood sampling and preparation</i>	101
<i>Experimental design</i>	101
<i>RBC preparation and treatment phase</i>	102
<i>Micropipette aspiration: rig design</i>	102
<i>Micropipette aspiration: shear elastic modulus</i>	104
<i>Micropipette aspiration: volume and capillary transit velocity</i>	106
<i>Statistical analysis</i>	107
RESULTS.....	108
<i>Haematology</i>	108
<i>Cell volume</i>	108
<i>Shear elastic modulus (pN·μm^{-1})</i>	110
<i>Normalised capillary transit velocity</i>	110
DISCUSSION.....	111
CHAPTER VI.	
OXIDATIVE STRESS INCREASES ERYTHROCYTE SENSITIVITY TO SHEAR-MEDIATED DAMAGE.....	117
ABSTRACT.....	118
INTRODUCTION.....	119
MATERIALS AND METHODS.....	121
<i>Subjects and sampling</i>	121
<i>Experimental design</i>	122
<i>Sample preparation – oxidative stress</i>	122
<i>Application of conditioning shear stress</i>	123
<i>RBC deformability measures</i>	124

<i>Data analysis</i>	124
<i>Statistical analysis</i>	126
RESULTS.....	127
<i>RBC deformability prior to conditioning shear stress</i>	127
<i>Effects of prior conditioning shear stress exposure on RBC deformability</i>	128
DISCUSSION	132
CHAPTER VII.	
CONCLUSION	137
SUMMARY OF FINDINGS	138
GENERAL DISCUSSION	140
<i>Sublethal damage and plastic deformation</i>	140
<i>Potential rheological and clinical implications</i>	141
<i>Thresholds of sublethal damage</i>	143
<i>Future Directions</i>	144
CONCLUSION	146
REFERENCES	149
APPENDIX: AUTOMATED MICROPIPETTE IMAGE ANALYSIS SOFTWARE ..	167
LIST OF ABBREVIATIONS AND SYMBOLS	173
SYMBOLS.....	173
UNITS OF MEASUREMENT	175
VARIABLES AND ABBREVIATED TERMS	178

List of figures

Fig. 1. SEM of blood cells before and after sublethal shear stress	III
Fig. 2. Implications of altered blood fluidity: The vicious cycle	3
Fig. 3. The non-Newtonian viscosity of blood	6
Fig. 4. Micrograph of RBC aggregates (rouleaux)	8
Fig. 5. RBC electrochemistry	9
Fig. 6. RBC tank treading (tracking a membrane 'bleb')	11
Fig. 7. Infographic of the physical properties of blood circulation	11
Fig. 8. Fluid streamlines with various Reynolds flows	13
Fig. 9. Velocity flow profile development in a cylindrical pipe	14
Fig. 10. Mortality and complications for patients receiving VAD support	16
Fig. 11. Characterisation of flow induced haemolysis	18
Fig. 12. RBC micrograph before and after sublethal shear stresses	19
Fig. 13. Identification of RBC sublethal mechanical damage point	20
Fig. 14. 'Leaky' cells with developed micropores following damage	21
Fig. 15. Step-down connection for the microtube shearing system	28
Fig. 16. Free body planar parabolic shear diagram	32
Fig. 17. Schematic of an annular 'bob' and 'cup' shearing system	33
Fig. 18. Initial design of the electrophoretic mobility chamber	35
Fig. 19. Schematic of the redesigned electrophoretic mobility chamber	37
Fig. 20. A single micrograph video frame of tracked RBCs over time	38
Fig. 21. CAD of a microscope stage for addition of laser diffractometry	40
Fig. 22. Initial (non-axial) system for combined rheometry-ektacytometry	41
Fig. 23. Combined slit-flow rheometer ektacytometer (i.e., the 'ektacytoscope')	43
Fig. 24. Final optimisation of ektacytoscope construction	44
Fig. 25. Schematic of constructed microforge for micropipette fabrication	47

Fig. 26. Schematic of single micropipette aspiration rig.....	50
Fig. 27. Micropipette system performing RBC aspiration.....	51
Fig. 28. Aggregation of RBCs following exposure to shear.....	64
Fig. 29. Disaggregation shear rate threshold (γ_{thr}) of RBCs following shear	65
Fig. 30. Sialic acid concentration of RBC ghosts and supernatant after shear.....	66
Fig. 31. Electrophoretic mobility of RBCs following exposure to shear.....	67
Fig. 32. Design schematic for the 'the ektacytroscope'.....	84
Fig. 33. RBC mechanical sensitivity following varied magnitude/duration of shear.....	86
Fig. 34. (A) Ektacytometry for Con and RBCs exposed to increasing duration of 100 Pa (B) Relationship of mechanical sensitivity index and EI at 0.3 Pa.....	88
Fig. 35. Coaxial ektacytometry-rheometry for RBCs previously exposed to 100 Pa	89
Fig. 36. EI frequency histograms for Con and PSE RBCs at various shear	90
Fig. 37. RBC orientation for Con and PSE in 0.3 and 5 Pa shear flows.....	91
Fig. 38. Schematic of RBC dynamics in 5 Pa shear flow for Con and PSE	93
Fig. 39. Schematic of a dual micropipette aspiration rig	104
Fig. 40. Micropipette aspiration principle for determining the shear modulus (μ).....	105
Fig. 41. Micropipette aspiration measurement of a single RBC	106
Fig. 42. Identification of RBC $d(x)/d(t)$ for capillary transit velocity (v)	107
Fig. 43. Cell volume of RBCs following shear and heat treatment.....	109
Fig. 44. Micropipette aspiration micrograph for Con (A) and 100 Pa (B) RBCs.....	109
Fig. 45. Shear modulus (μ) of RBCs following shear and heat treatment.....	110
Fig. 46. Normalised capillary transit velocity and correlation with shear modulus	111
Fig. 47. RBC deformability for cells previously incubated with/without PMS	127
Fig. 48. $SS_{1/2}:EI_{max}$ for Con and PMS RBC	128
Fig. 49. $SS_{1/2}:EI_{max}$ for Con and PMS RBC following exposure to shears	129
Fig. 50. Surface mesh of Mechanical Sensitivity (%) for Con and PMS RBCs	130
Fig. 51. Δ Mechanical Sensitivity between Con and PMS samples.....	131

Chapter I.

Introduction

Blood fluidity and organ perfusion

Blood is an essential biological tissue that facilitates transport of oxygen and nutrients to metabolically-active tissues while enabling the elimination of waste products of cellular metabolism¹. Distribution of blood throughout the body relies upon a convective transport system, which requires a propulsive organ (i.e., the heart) for generating a pressure head, as well as conduits (i.e., the vascular system) that facilitate delivery of blood to distal tissues¹. The transport of oxygen and nutrients within the fluid media, and concurrent elimination of metabolic waste products, is the primary purpose of the circulatory system and is essential for mammalian life. Blood flow, and the consequential tissue oxygenation, is intrinsically-linked to the physical properties of the system, and is a highly sensitive homeostatic process². With any disturbances to the vascular network, propulsive organ, or cellular components of blood, the apparent viscosity of blood in a defined shear flow may become altered, changing blood fluidity (i.e., the reciprocal of viscosity) and heterogeneity of cell distribution across capillary beds, causing circulatory insufficiencies that propagate the development of disease.

The internal environment of the body is a carefully regulated closed system, where small alterations in the maintenance of normal blood fluidity can proliferate a 'vicious cycle' of deterioration, leading to systemic complications and chronic disease. Given the circulatory system networks all parts of the body, if small locations are influenced by insufficient circulatory distribution, systemic consequences may be observed, and a vicious cycle of self-propagating altered blood fluidity can be initiated (summarised in Fig. 2). The implications of hindered blood fluidity causing insufficient circulation may initially cause local hypoxia, acidosis, and accumulation of metabolic waste. These factors, if prolonged, can lead to tissue necrosis, changes to vascular reactivity, and alterations to the cellular and extracellular components of blood, thereby increasing blood viscosity. Blood viscosity is an important determinant of flow resistance, that if increased may worsen the initial circulatory insufficiency. It should be noted that in healthy individuals, vasomotor control compensates for minor alterations in blood fluidity; however, when vasculature autoregulation is compromised, as observed in some chronic disease states (e.g., cardiovascular and metabolic diseases), haemorheological abnormalities that could easily be compensated for in healthy individuals may have severe consequences.

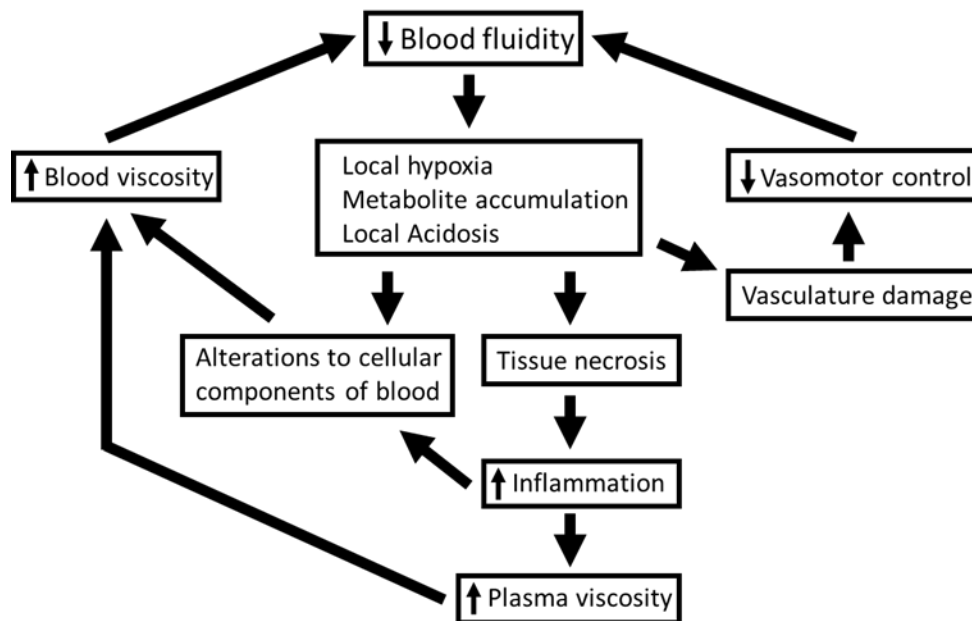


Fig. 2. Implications of altered blood fluidity: The vicious cycle. Adaption of Baskurt³.

Blood fluidity, chronic disease, and the clinical paradox

Cardiovascular diseases remain the leading cause of death worldwide (contributing to 27% of all deaths in Australia in 2017), and are the most expensive cluster of diseases to treat in Australia⁴. Therapeutic interventions for individuals with progressive cardiovascular disease requires combination pharmacotherapy, and commonly necessitates the use of extracorporeal life support and mechanical circulatory support devices to overcome failing organs. Given the integration of these devices with the human circulatory system, their efficacy is highly dependent on the static and dynamic interactions with blood (i.e., haemocompatibility). Although biomedical devices indicated for life support *are* medical marvels that *do* extend patient lives^{5,6}, unfortunately due to the non-physiological environment within these devices through which blood flows, all current mechanical circulatory support devices for haemodynamic support are plagued with dangerous, life-threatening complications. As patients indicated for life support are typically already at elevated risk of altered blood fluidity due to pre-existing chronic disease, concomitant exposure to the non-

physiological environments within life-support systems likely compounds the deleterious effects of pre-existing microcirculatory impairments and has a critical role in the accumulation of systemic complications attributed to blood trauma.

Biomedical devices and haemocompatibility

Biomedical devices for mechanical circulatory support have been in development for over seven decades and are widely used to replace various human organs in acute surgery, or in patients with chronic disease awaiting donor organs. While the design and manufacturing of devices for extracorporeal circulation has been greatly enhanced, blood damage has been an inevitable complication in the development process. Previously, the implantation of an artificial organ increased incidence of infection, had a high chance of mechanical failure, and caused complications of biological compatibility (including risk of foreign-body rejection syndromes). Unfortunately, the precise mechanisms of blood damage induced by these devices is still not well understood; however, with improved technology, manufacturing capabilities, and continual refinement of a haemocompatibility criteria over recent decades, device efficacy has substantially improved and patient survival has greatly increased^{5,6}.

While artificial organs increase the lifespan of patients with end stage chronic disease, many severe complications of microcirculatory dysfunction and ischaemic disease are still associated with their use. Current haemocompatibility criteria assesses thrombosis, coagulation, platelet count and activation, immune response, and haematology (RBC counts and haemolysis). Mechanical circulatory support systems have evolved such that they adequately meet the functional demands of replaced organs, and achieve current haemocompatibility criteria⁷⁻⁹, yet several significant complications have still been reported with long-term device use that are suggestive of blood damage and malfunction, without remarkable haemolysis. This damage, which is due to blood-interaction with non-physiological environments (i.e., contact

with foreign surfaces, elevated shear forces, turbulence, and cavitation), has the capacity to alter the rheological properties of blood, causing functional blood damage, rather than an absolute haemolytic damage¹⁰. The need to further refine the current haemocompatibility criteria to include cellular function and rheological properties of blood is required.

Review of the literature

Haemorheology and the red blood cell

The function of blood in mammalian circulation is to traverse the vascular network to facilitate: gas and heat exchange, delivery of nutrients and hormones, and the removal of metabolic waste from all tissues of the body. Blood is propelled throughout the vascular network by cardiac contraction from asystole and systole, generating a pressure head. When analysing the flow of blood in the body (i.e., haemorheology), blood is examined for how it responds to various pressures, force gradients, and shear stresses, against flow resistances created by the geometry of the vasculature and the flow properties of blood. For blood flow to be compatible with life, circulation must remain fast enough to support tissue perfusion, otherwise ischaemia and necrosis will occur.

Blood is a colloid emulsion (i.e., a two-phase suspension) consisting of red blood cells (RBCs), white blood cells, and platelets, suspended in a fluid phase (i.e., plasma)¹¹. Plasma is an aqueous solution of organic molecules, proteins and salts, which is a Newtonian fluid across the physiological range of shear rates when maintained at human body temperature (37°C)¹². Whole blood, however, is a non-Newtonian fluid, whereby its 'apparent viscosity' is dependent upon the magnitude of applied instantaneous shear rates: i.e., blood exposed to low-shear rates is more viscous than when exposed to high-shear rates. This characterises the 'shear thinning' property of blood (Fig. 3), and is vital for successful blood fluidity and circulation¹². The viscosity-

shear relationship is sensitive to haematocrit (i.e., percentage RBCs by volume of blood), plasma viscosity, the aggregation of RBCs, and the ability of RBCs to elongate, orientate, and deform¹³.

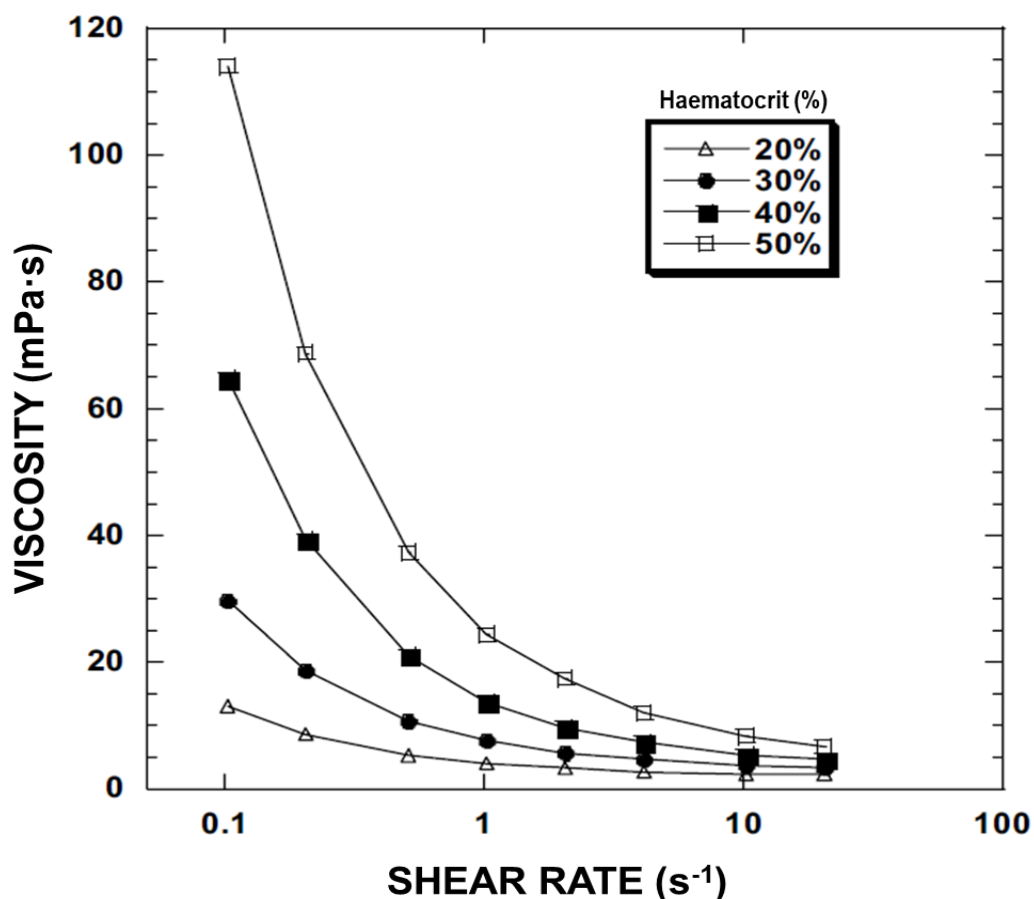


Fig. 3. The non-Newtonian ‘shear-thinning’ property of healthy whole blood samples is sensitive to haematocrit¹⁴.

RBCs are the most prominent haematological factor influencing haemorheology, constituting 36–50% of blood, with approximately 5 million cells in every microlitre. The cell itself is a viscous container of Newtonian fluid consisting of haemoglobin which binds and exchanges oxygen and carbon dioxide with tissues it perfuses. The average cytosolic volume is ~90 femtolitres, and is surrounded by a membrane comprised of a cytoskeletal protein network and lipid bilayer. Relative to its volume,

due to the unique biconcave morphology of the RBC (Fig. 5, Fig. 12), the surface area of the cell membrane is ~40% larger than that of a sphere with same volume. For an RBC to survive the tortuous vessels of circulation, the cell must leverage its increased surface area to bend, fold, and deform through the various geometries of the vasculature. A single RBC circulates the body approximately every 60 seconds for a lifespan of ~120 days before the cell is sequestered from circulation by the spleen or immune system. With alterations to the mechanical properties of blood cells, survival in circulation will likely be shortened.

RBC aggregation

RBC aggregation is a major determinant of *in vivo* blood fluid dynamics/resistance and *in vitro* rheological properties¹⁵. RBC aggregation is the reversible process where RBCs form stacks of branched aggregates (i.e., rouleaux; Fig. 4) at stasis or low shear rates, and is the major determinant of low-shear blood viscosity¹³. The reversible nature of RBC aggregation differentiates this process from RBC coagulation and agglutination, which are irreversible due to protein polymerisation or strong antigen-antibody attractive forces¹¹. RBC aggregation reflects a balance between pro-aggregating factors (e.g., plasma fibrinogen concentration) and disaggregating factors (e.g., mechanical shear and cell electronegative repulsive forces)¹⁶. Disease processes associated with increased RBC aggregation mainly act to decrease the overall electronegative (i.e., disaggregating) forces of RBCs, due to altered membrane lipid composition and/or modified membrane sialic acid content¹¹.

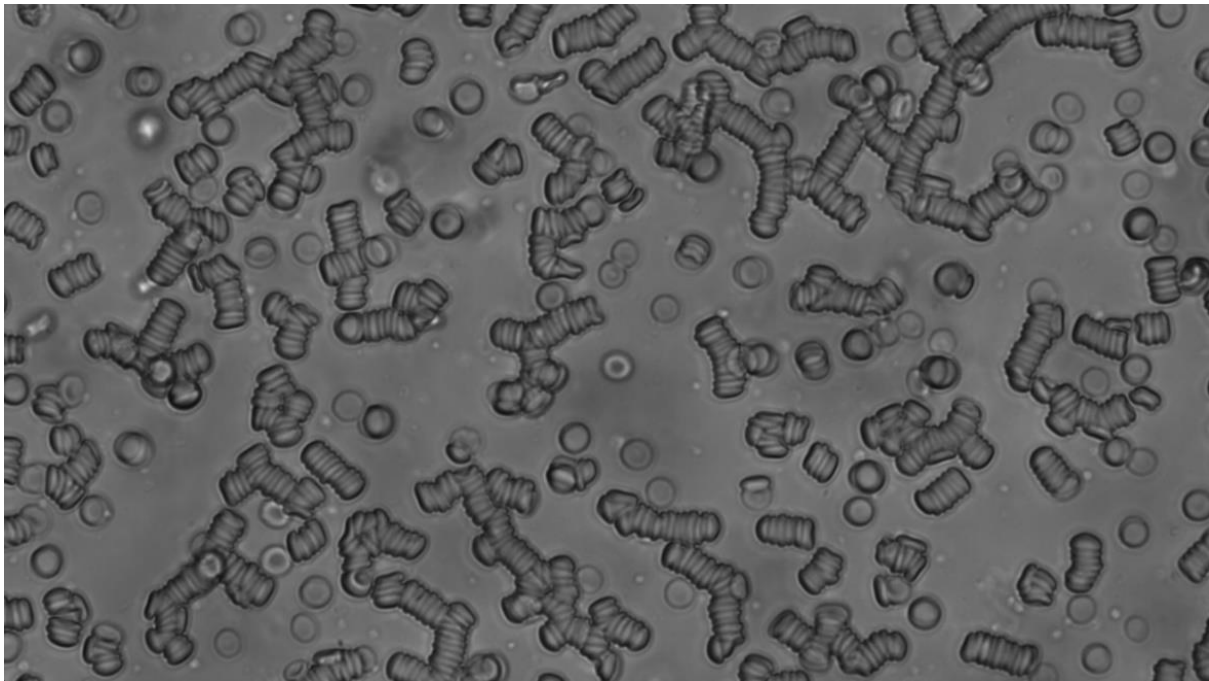


Fig. 4. Micrograph of red blood cell aggregates (rouleaux).

RBC sialic acids (primarily N-acetylneuraminic acids) are a family of nine carbon acidic monosaccharides located on the cell membrane within the glycocalyx (i.e., a permeable layer of glycoprotein-polysaccharides attached to the cell membrane). Sialic acids are distributed across the cell membrane and are reported to be involved in influencing morphology, membrane deformability, oxygen carrying capacity, and distribution of intracellular haemoglobin¹⁷. The distribution of sialic acids across the outer monolayer of the RBC membrane accounts for ~90% of the cell's net negative charge. RBCs in suspension have two ionic layers (Fig. 5): the negative net at the membrane's surface, and the electrostatically attracted compact layer of oppositely charged ions¹⁸. These two ionic layers are immobile, and the electrical potential difference between each layer defines a cell's zeta potential (ζ) and external repulsion force. Outside the immobile charge layer, ions in the diffuse layer are mobile and will interact with an RBC according to its zeta potential. With the normal ageing and senescence process of RBCs, sialic acid content is lost, resulting in decreased negative surface charge and thus zeta potential of the cell¹⁹. Jan and Chien²⁰ reported that the removal of sialic acid from RBC membranes with the incubation of the enzyme

neuraminidase was indicated to display significantly stronger aggregation compared to non-treated cells. Given the involvement of sialic acids in RBC electrochemistry, processes that remove sialic acid from the cell membrane are highly likely to induce altered blood rheology via promotion of RBC aggregability and interaction with other charged particles¹⁸.

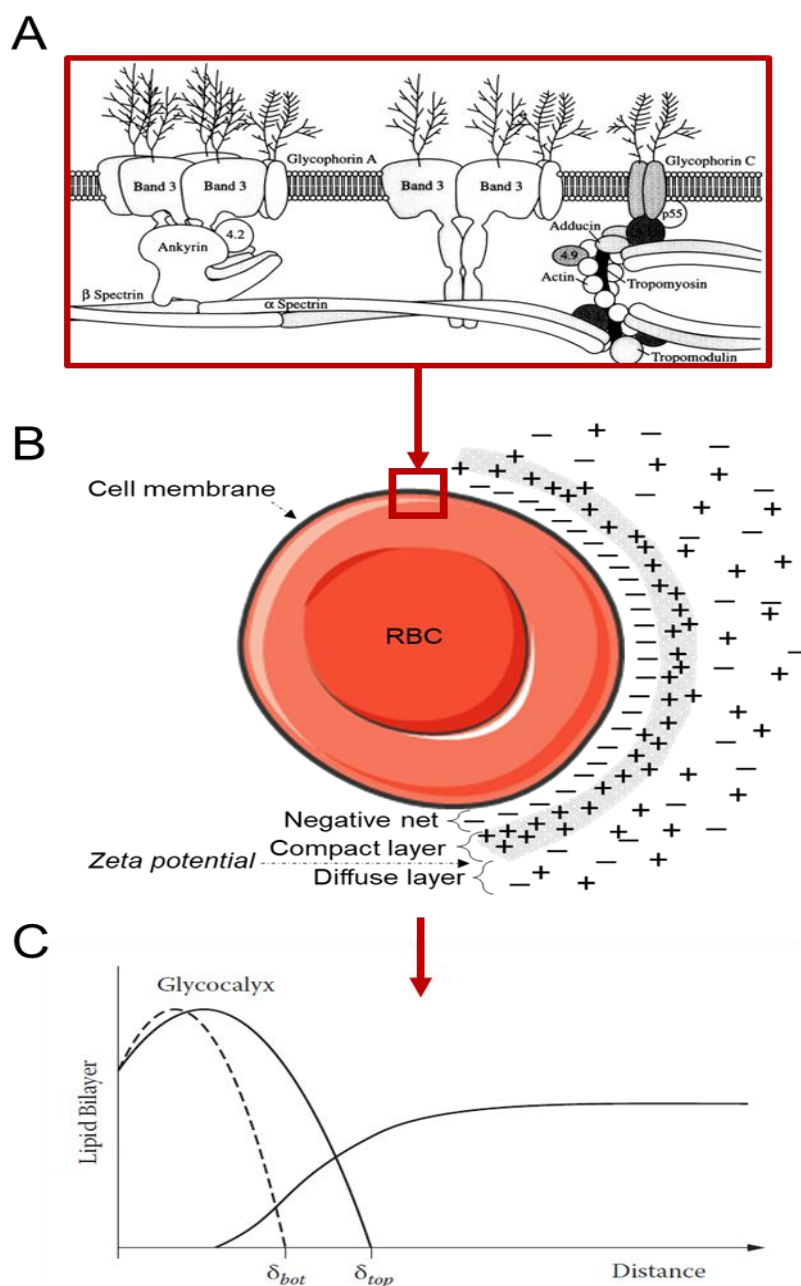


Fig. 5. RBC electrochemistry. (A) The composition of the RBC outer monolayer of the membrane and glycocalyx²¹ (especially sialic acids) influence (B) the cell's negative charge and zeta potential. (C) The theoretical changes in thickness of the glycocalyx between young (δ_{top}) and old (δ_{bot}) blood cells changes the zeta potential and interaction distance with other particles²².

RBC deformability

The deformability of RBCs is an essential attribute that defines the high-shear viscoelastic properties of blood and facilitates circulation through the microvasculature. The elasticity of RBCs allow for passage of the 8 μm cells through vessels as small as 2–3 μm in diameter²³. The RBC is well equipped to store the potential energy of the high-shear environments, and recover shape when the applied shear is removed¹. The primary determinants of RBC deformability include: the geometry of the cell, particularly the cell surface area-to-volume ratio; the cytosolic (i.e., intracellular) viscosity relative to that of plasma; and, the cell membrane's elastic properties²³. Potential secondary determinants of RBC deformability may be derived from intracellular biochemical processes that actively regulate RBC morphology in response to mechanical stimulation^{24,25}. Such biochemical stimulators that have been identified to influence RBC deformability are RBC-derived nitric oxide, intracellular calcium (Ca^{2+}) concentration, and adenosine triphosphate (ATP) concentration^{26,27}. The elastic nature of RBC, which also facilitates cell orientation in flow, is perhaps the most important cellular characteristic that facilitates blood flow through the various geometries of the vasculature.

RBCs in shear flow

The physical properties of RBCs have the ability to alter the local viscosity of blood, where distortions in fluid stability may occur due to poor deformability, lack of orientation, RBC rouleaux formation, and RBC tumbling instead of the typical 'tank-treading' movement^{11,28}. The typical movement of blood cells in flow involves tumbling at low shear rates and 'tank-treading' movements at high shear rates, where the membrane skeleton is able to freely rotate around the cytoplasm (illustrated in Fig. 6)²³. For RBCs to transition from tumbling to tank-treading, it has recently been reported that strong membrane deformations are required²⁹. As RBC function may become altered with the accumulation of varied levels of stress-strain history, the

viscoelastic properties of blood and the Fåhræus-Lindqvist effect may change when more rigid RBCs with hindered ability to deform become trapped in tumbling motions or lose orientation ability. These cells may cause greater local disturbances, extracting energy from the flow, generating localised low-pressure regions, thus increasing apparent viscosity.

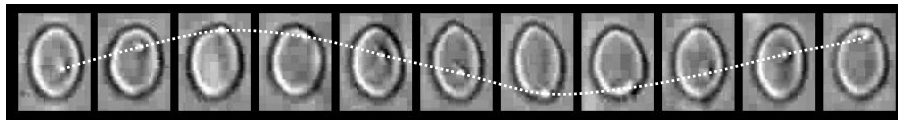


Fig. 6. Single red blood cell in a tank treading motion after exposure to mechanical damage (obtained through the course of this dissertation). A morphological alteration (i.e., a membrane ‘bleb’) induced by exposure to shear was tracked in shear flow.

Haemorheology in circulation

While the physical properties of blood are often investigated *in vitro* (due to feasibility), the understanding of *in vivo* application is vital for applied physiology.

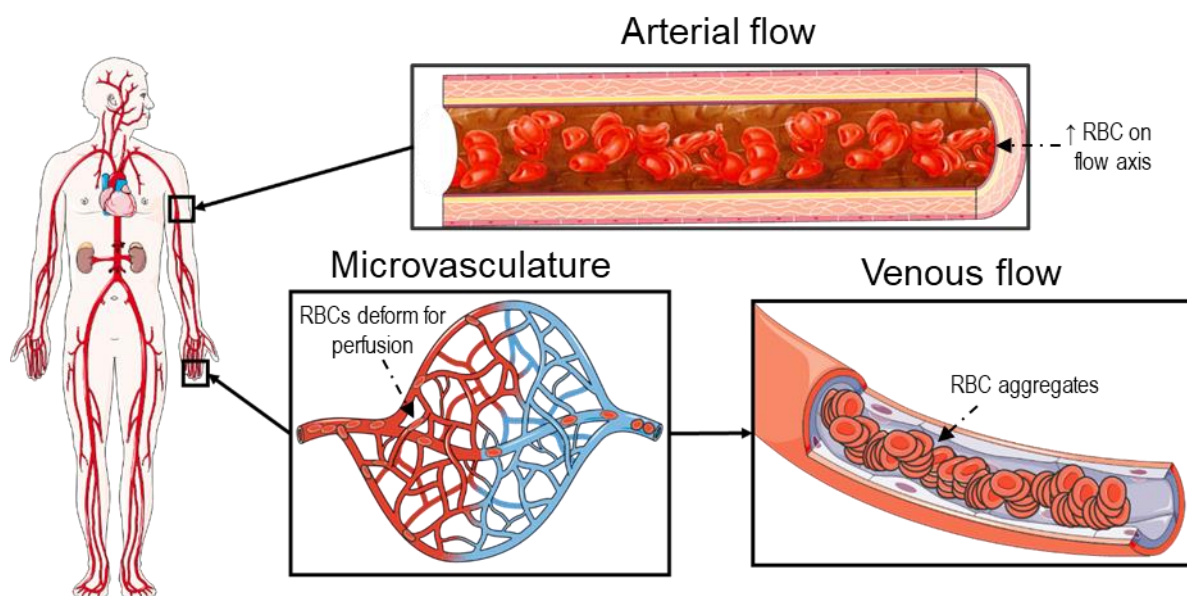


Fig. 7. The physical properties of blood are important for circulation through the body's arteries, capillaries, and veins.

- 1. Arterial circulation:** When blood is ejected from the left ventricle of the heart into the arterial circulation, the physical properties of RBCs immediately begin to define blood rheology in these high-velocity flows. Due to the governing Fåhræus-Lindqvist and Magnus effects, blood cells align with the axial column of highest velocity flows and marginate away from the higher-friction slower-flowing vessel wall region. RBC deformability facilitates cells to be able to 'slide' past one another in the axial column, while orientating and aligning with flow. Despite wall shear flows being too high in arterial circulation for aggregates to form, the shear profile varies radially across the vessel, decreasing to a minimum in the central region of flow (the axis), where aggregation may occur²⁸. The presence of RBC aggregation facilitates the attraction of more cells towards the central low-shear column further aiding the propagation of a lubricating cell-poor layer (predominantly comprised of plasma) in marginal flow.
- 2. Microvasculature:** As blood approaches the smaller vessels in the body, the cell-poor layer also facilitates conduit vessels to 'skim plasma', contributing to lower haemodynamic resistance by significantly decreasing haematocrit to ~10% in some capillary networks³⁰. This decrease in haematocrit must continue with RBC disaggregation until single blood cells are able to meet the entry conditions of the microvasculature. If RBCs do not disaggregate sufficiently, or are too rigid to meet the entry conditions of the microvasculature, sluggish flow or even complete flow-stasis may occur – this has negative implications for microvascular perfusion and tissue oxygenation.
- 3. Venous circulation:** Following microcirculatory flow, blood returns to the heart under the lower shear of the venous circulation. Given the low-shear environment, RBC aggregates form readily, until being disaggregated by the higher shears within the vena cava, heart, and arterial circulation.

Haemodynamics

Commonly, blood flow is described using Poiseuille's law: $Q = \frac{\pi \Delta p D^4}{128 L \eta}$; where p is pressure, D is the diameter of the vessel, L is the length of the vessel and η is the viscosity of the fluid. Although it is now recognised that the viscosity of blood is non-Newtonian in nature, the works of Hagen and Poiseuille are still often employed for their simplicity²⁸. As a result, when examining the *in vivo* movement of 'homogenous' blood through the large arteries of the body, and external to the body in *ex vivo* situations, theoretical and experimental environments are manipulated to meet the associated Hagen-Poiseuille assumptions. This means that the flow of blood is considered incompressible, Newtonian, and laminar, while flowing through a pipe of constant circular cross section, with a tube length markedly longer than its diameter, where the fluid does not accelerate while in the pipe. With these assumptions, the development of flow, the flow profile, and the movement of cells within streamlines of flow can be subsequently investigated.

For blood flow through cylindrical pipes, the Reynolds number reflects the balance between inertial and viscous forces acting within a fluid: lower values reflect predominantly viscous forces that maintain laminar (i.e., "smooth") flow, whereas higher values reflect predominantly inertial forces that induce turbulent flow. Within pipe flow (e.g., blood in a vessel), a Reynolds number under 2000 is indicative of laminar flow, values over 4000 reflect turbulent flow, and values between 2000 and 4000 represent transitional flow (Fig. 8)²⁸.

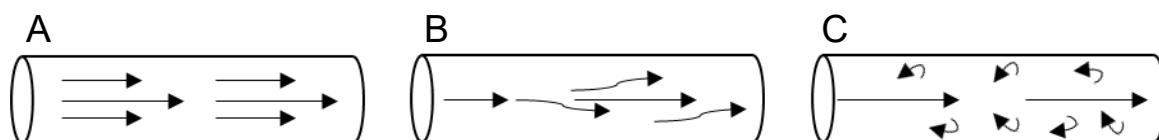


Fig. 8. Fluid streamlines with various categories of Reynolds numbers. (A) Laminar flow with a Reynolds number less than 2000. (B) Transitional flow with a Reynolds number between 2000 – 4000. (C) Turbulent flow with a Reynolds number greater than 4000.

Provided the Reynolds number indicates laminar flow and the moving fluid is given the required length of tubing for flow to develop, a characteristic (non-blunted) velocity flow profile is formed (illustrated in Fig. 9A). The velocity flow profile of blood is different to that of Newtonian fluids, due to the axial migration of RBCs (observed with the Fåhræus-Lindqvist effect³¹) and the formation of a lubricating cell-poor layer (predominantly plasma) in marginal flow, causing the apparent viscosity to differ radially across the vessel.

The length to development of the curvilinear flow profile (L_e), and the propagation of axial migration of RBCs, can only be assumed to occur after adequate development length of laminar flow entering a new tube. This is defined by the Reynolds number (Re) of the fluid and the diameter (D) of the vessel, which may be described by the equation: $L_e = 0.06ReD$ (Fig. 9B²⁸). It should be noted that the velocity flow profile can be predicted by the Navier-Stokes model; $v_r = v_{max} \left[1 - \left(\frac{r}{R} \right)^2 \right]$, where the fastest velocity occurs in the centre of developed flow, and can be determined by $v_{max} = \frac{\Delta p \cdot a^2}{4L\eta}$.

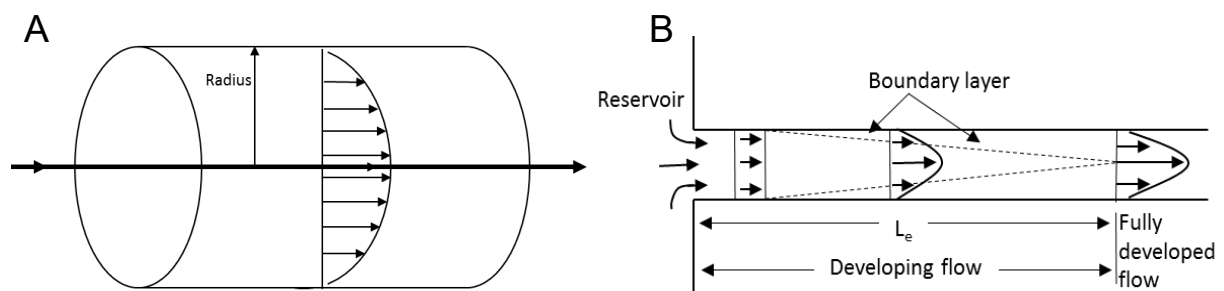


Fig. 9. (A) A typical velocity flow profile in a cylindrical pipe exhibiting laminar flow. (B) The progression of a fluid to fully developed flow within the entrance length of a pipe.

Mechanical circulatory support and blood compatibility: the clinical problem

Mechanical circulatory support (MCS) may acutely facilitate the function of important biological organs (e.g., heart, kidneys, lungs) and maintain circulation, filter toxins, or facilitate gas-exchange. In recent years, advances in MCS has enabled complete replacement of native organ function for periods extending beyond a decade³². These devices are thus essential in facilitating medical interventions or therapies in dire situations, and positively impact some of the largest clinical populations, including individuals suffering: end-stage renal failure, cardiac disease, and respiratory failure; as well as transfusion recipients following acute trauma, burns, and various cancers.

Primary limitations inherent to earlier generation designs of MCS typically involved infection, mechanical failure, and biological (in)compatibility. Improved design and manufacturing, however, with a focus on improved biological compatibility has resulted in reduced acute complications and improved patient survival^{33,34}. Prolonged reliance on MCS, however, such as in the case of ventricular assist devices (VADs) has resulted in the emergence of seemingly diverse secondary complications, including stroke, infection, and multi-organ failure that occur independent of the initial pathology (Fig. 10)³⁴. The precise mechanisms and processes that govern these secondary complications are poorly understood; however, blood trauma related to blood-device interactions has been implicated, where artificial conditions (e.g., foreign materials, surfaces) and non-physiological fluid properties (e.g., excessive shears, turbulence, cavitation) are dominant.

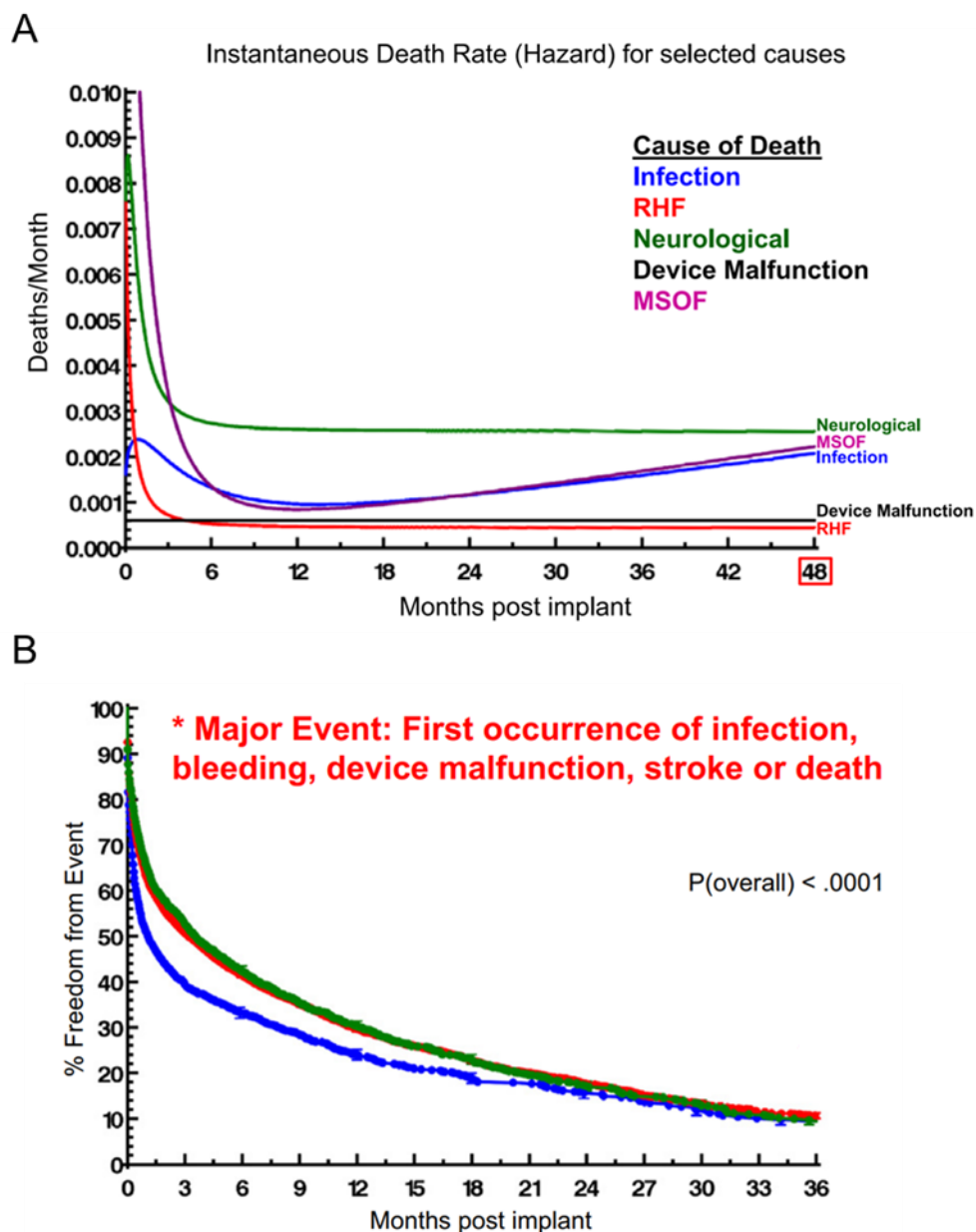


Fig. 10. Mortality rate (A) and prevalence of complications (B) post implantation for patients receiving VAD support³⁴.

The cell dysfunction associated with prolonged implantation of mechanical assist devices manifests in altered blood flow patterns, which may be quantified by excessive magnitudes of shear stress. Given that mechanical assist device recipients commonly have comorbidities associated with impaired organ perfusion and function (e.g., type 2 diabetes), the rheological responses to shear stress in artificial devices must be carefully quantified and minimised.

Blood damage and the haemolytic threshold

The complete destruction of red blood cells (RBCs) – i.e. haemolysis – is an important indicator of blood damage, and remains a prominent focus of haemocompatibility assessments. When RBCs are destroyed, their cytosolic contents (including haemoglobin) are released into the surrounding media (i.e., plasma) causing toxic effects by increasing free radical production and thrombus formation, while decreasing nitric oxide bioactivity and thus also vascular function³⁵. Due to the importance of avoiding overt haemolysis, current generation MCS devices have been developed to an extent that haemolysis occurs at almost negligible levels³⁴. The absolute tolerance of RBCs to shear stress was characterised by Paul et al.³⁶, who reported the haemolytic threshold as a dynamic function of magnitude and duration shear exposure (Fig. 11). Importantly, it must be noted that haemolysis is an endpoint absolute damage. Baskurt and Meiselman³⁷ found that RBCs repeatedly exposed to prolonged subhaemolytic shear stress acquired decreases in cell deformability, increasing subsequent membrane fragility, and decreased cell tolerance to further shear stress exposure³⁷.

Clinical data indicate that individuals exposed to MCS experience other delayed complications such as stroke, haemorrhagic events, neurological dysfunction, and multi-system organ failure^{34,38}. While the cause of these complications cannot currently be explained, it is likely that mechanical stresses in combination with other factors within MCS cause damage to blood that is sublethal (i.e., a functional damage occurring prior to haemolysis). Given that white blood cells and platelets account for only ~1 per 1,000 cells¹¹, we hypothesise that the dysfunction of RBCs is primal in the aetiology of microvascular complications leading to multi-system organ failure³⁷. While there is a need for identifying new markers which may detect RBC dysfunction in non-haemolysed blood previously exposed to supraphysiological shear stress, limited studies have investigated this sublethal blood trauma.

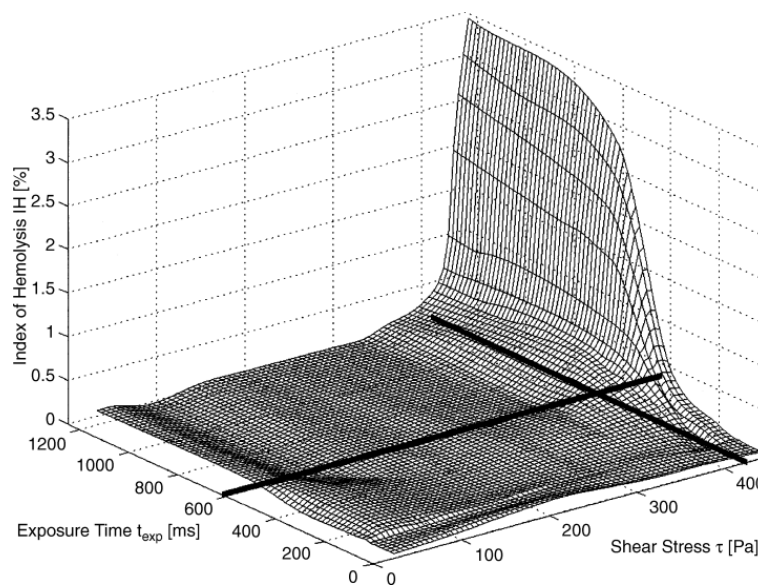


Fig. 11. Flow induced haemolysis by shear stress magnitude-duration combinations. The intersection of the black line (425 Pa, 620 ms) represents Paul et al.'s³⁶ haemolytic threshold.

Sublethal mechanical blood trauma

Under normal physiological conditions, RBCs are exposed to an array of magnitudes of shear stress throughout their traverse of the circulatory system. Physiological shear stresses range from 0–10 pascals (Pa) without inducing long-term damage to blood constituents³⁷. While physiological shear stress induces RBC deformation, activation of biochemical pathways, and the disaggregation of cell-cell aggregates, supraphysiological shear stress may impair RBC function even if haemolytic thresholds have not been reached. Prior investigations of this subhaemolytic damage have reported altered cellular metabolism, membrane function, and RBC deformability^{36,39-41}, resulting in immediate cell changes, causing functional alterations in blood fluidity, increased mechanical fragility^{42,43}, and early removal and sequestration from circulation⁴⁴. This sublethal damage has been observed in clinical devices, being reported in current MCS systems (e.g., haemodialysis, cardiopulmonary bypass, ventricular assist devices), resulting in altered blood cell

morphology^{45,46}, changed blood viscosity^{47,48}, and delayed anaemia⁴⁹. Given the severity of the associated complications occurring from sublethal blood damage, there is a necessity to extensively characterise and elucidate the mechanisms of functional blood cell deterioration that occur prior to complete cell destruction. It is thus also important to identify the boundaries of shear that delineate magnitudes that are tolerable, and thresholds that induce sublethal damage.

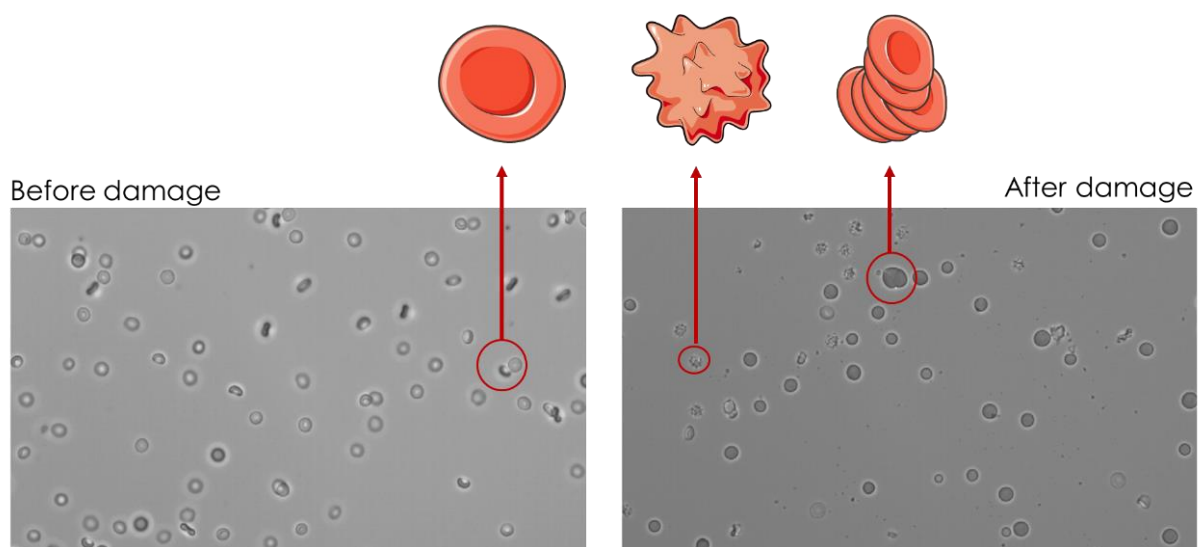


Fig. 12. Micrograph of RBCs before (left) and after (right) exposure to sublethal shear stresses. Note the dramatic alterations in morphology, aggregate formation, and cell fragmentation. Adaptation of McNamee et al.⁵⁰.

Understanding the rheological functioning of blood and its response to shear stresses within, and superseding, the physiological range is of scientific and clinical interest for predicting an individual's response/success to the use of MCS. To investigate and describe the changes in RBC populations following exposure to subhaemolytic shear stress, Simmonds and Meiselman⁵¹ employed a standardised method of assessing magnitude-duration effects of a conditioning shear stress on subsequent RBC deformability and mechanical sensitivity. The standardised method allowed for:

- i. characterisation of shear-mediated changes in RBC sensitivity to mechanical stress

(Fig. 13A); and, ii. identification of a “subhaemolytic damage point” – i.e. the critical point at which conditioning shear stresses induced mechanical damage to RBCs, significantly decreasing RBC deformability under subsequent shear exposure (Fig. 13B).

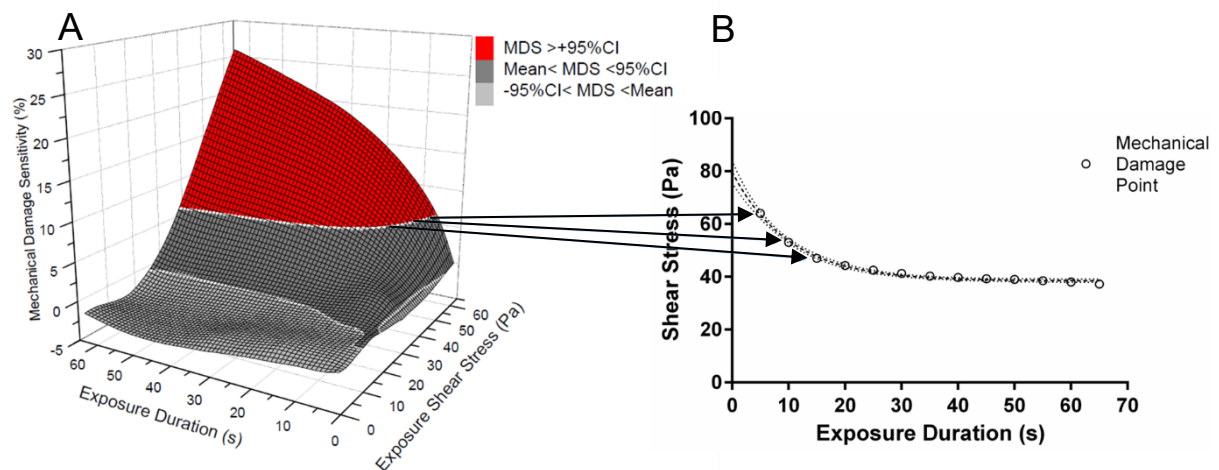


Fig. 13. (A) Shear mediated changes in RBC deformability following various combinations of shear stress conditioning. The red region indicates RBC populations above the mechanical damage point that have become significantly impaired in their ability to deform. (B) Illustrates the mechanical damage point as a function of magnitude and duration of shear exposure. Samples exposed to shear combinations above the mechanical damage threshold will observe subhaemolytic damage. Adaptation of Simmonds and Meiselman⁵¹.

Changes in the RBC membrane and microvesicle release

Supraphysiological shear stress and trauma associated with mechanical assist devices has been identified to induce conformational changes in the cytoskeleton of RBCs that leads to cell fragmentation, protein denaturation, and glycoprotein cleavage⁵²⁻⁵⁴. It has been hypothesised by Watanabe et al.⁵² that with exposure to supraphysiological subhaemolytic shear stresses, the lipid bilayer of the RBC may be progressively thinned, leading to the development of micro-pores and the leakage of microparticles. Microparticles and microvesicles are small phospholipid vesicles less than one

micrometre in diameter that are released from cells for intercellular communication and initiation of inflammation and coagulation. Prolonged storage of blood and damage from rotary blood pumps has been reported to increase RBC microparticle production^{55,56}. Sakota et al.⁵⁷ correlated blood damage from rotary blood pump MCS systems with increased RBC volume and decreased cell haemoglobin concentration, supporting the hypothesis that RBC sublethal trauma may induce the development of membrane micropores sizable enough to enable leakage of cytosolic haemoglobin (Fig. 14).

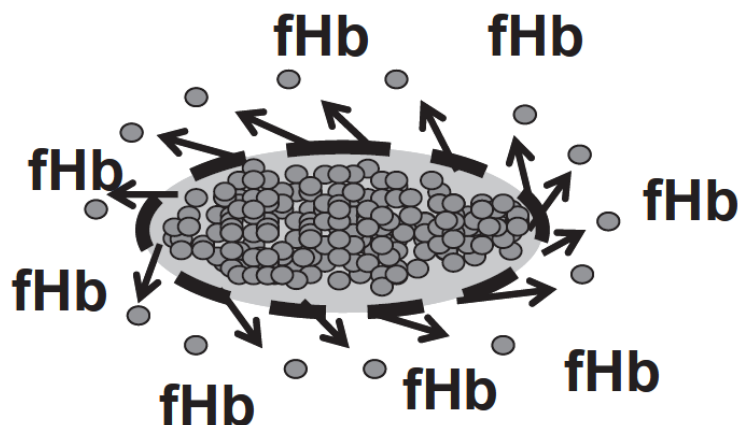


Fig. 14. Illustration of a RBC following damaging shear stress causing thinned portions of the cell membrane and the development of micropores from which cytosolic haemoglobin microparticles (Hb) will leak prior to complete destruction of the cell (i.e., haemolysis)⁵².

Accelerated ageing and eryptosis

The normal ageing of RBCs is a complex process which results in changes to cell morphology (i.e., size and volume) and to the lipid bilayer (i.e., altered roughness, charge, and glycoprotein expression). One glycoprotein that is highly important in the cell senescence process, is phosphatidylserine. Phosphatidylserine is a glycoprotein that is quantitatively a minor component of the lipid bilayer (~2-10%) and is normally restricted to the inner monolayer; however, during the early stages of apoptosis

(i.e., programmed cell death) phosphatidylserine becomes a cell marker as it is translocated to the external side of the lipid bilayer. This translocation marks the initiation of many biological processes that are important for physiological functioning for healthy cell regulation (e.g., apoptosis by signalling for removal by phagocytes, blood coagulation cascade in platelets, changes in the membrane structural support within the spectrin network interface)⁵⁸. Individuals exposed to MCS devices have displayed significantly decreased *ex vivo* RBC lifespan due to increases in RBC mechanical fragility⁴⁰. If erythropoiesis rates are not matched with rates of cell sequestration, a 'delayed anaemia' has been reported to occur⁴⁹. However, given the complications associated with the circulation of sublethally damaged RBCs are likely to persist until the cell lifecycle is complete, if erythropoiesis rates *are* matched with cell removal, accelerated cell turnover may assist in normalising abnormal haemorheology.

Overarching objectives and experimental aims

The primary objective of the current doctorate was to conduct works that contribute to gaining a more thorough understanding of the biophysical and functional changes that occur to RBCs following exposure to discrete shear stresses that are supraphysiological (and non-lethal), congruent with the shear environment that exists within current mechanical circulatory support systems.

The current doctoral thesis has four primary aims:

- A1.** Develop low-cost infrastructure that facilitates high quality inspection of the macro/micro mechanobiological properties of RBCs.
- A2.** Inspect how mechanical shear stresses interact with RBC membrane mechanics, electrochemistry, and deformability.
- A3.** Interrogate the effect of sublethal shear damage on subsequent haemodynamics in low-shear and capillary flows.
- A4.** Assess the potential compounding influence of damaging oxygen free radical species (often imparted by inline membrane oxygenators and some chronic disease) on the susceptibility of RBCs to shear damage.

Chapter II.

Systems design and control

To investigate the effects of sublethal shear stress on RBC structure and function, a suite of specific infrastructure was deemed necessary to be acquired and/or constructed. Aim 1 of the current thesis was to construct these systems for low-cost, without sacrificing the quality of the generated data. The following Chapter briefly describes the construction and implementation of the systems required for the experimentation included in the current doctoral program.

The different systems created in the current doctoral program are as follows:

- Shearing systems*
- Electrophoretic mobility chamber*
- Combined rheometer-ektacytometer: the 'Ektacytoscope'*
- Micropipette aspiration system*

Shearing systems

To effectively investigate the effects of shear stress on the physical properties of RBCs, the present thesis required a variety of specific shearing systems to be constructed. These systems needed to accurately and precisely control discrete levels of both magnitude and durations of shear stresses that were to be applied to RBCs. An important pre-experimental consideration, however, is that blood is non-Newtonian, thus its viscosity-shear relationship is difficult to manipulate and control. For the current doctoral program, some ecological validity was sacrificed to overcome the non-Newtonian properties of whole blood to enable more accurate shear control. To control the viscosity responses of blood, RBCs were isolated and resuspended in various concentrations of polyvinylpyrrolidone (PVP-PBS) solutions at a decreased haematocrit. Using a Brookfield cone-plate DV2+ viscometer (Middleboro, USA) with a CPE40 spindle, the viscosity of the solutions could be determined, manipulated, and adjusted.

Beyond controlling the suspension viscosity, to apply shear to blood cells, a simplified model of shear damage without the complexities of the flow environments within MCS devices (e.g., turbulence, recirculation, etc.) was required to be constructed. Adopting this reductionist approach allowed for shear specific effects to be studied, although would require future scaling to fully represent MCS systems. Given the complex flow environments within MCS have previously been reported to impart greater blood damage^{9,59} (likely due to extreme shears, combined with turbulent flows, variable flow profiles, and contact with non-physiological materials), any blood trauma observed in the current thesis is hypothesised to be further exacerbated when scaled to current generation MCS devices.

Three different types of shearing systems were used in the present thesis: i. a microtube (axisymmetric parabolic) Poiseuille shearing system, ii. a parallel plate 'slit

flow' (planar parabolic) Poiseuille shearing system, and iii. an annular Couette flow shearing system.

The following section describes characteristics of these systems, highlighting important design considerations that facilitated experimental deployment.

Axisymmetric parabolic Poiseuille shearing system

Part of the experimentation conducted for the present thesis sought to investigate the effect of shear stress on RBC aggregation with a model that partially represented *in vivo* circulatory flow. To construct a simplified model representative of the vessels in the body, a shearing system that also adopted Poiseuille tube flow was deemed necessary. Given that the microcirculation includes blood vessels smaller than 300 μm , the Poiseuille shearing system was constructed using linear segments of extruded polyethylene tubing with an inner diameter of 200 μm (Microtube Extrusions Pty Ltd, North Rocks, Australia). A Poiseuille tube flow shearing system would allow for the discrete manipulation of amplitude and duration of supraphysiological shear stress exposure to blood (and RBC suspensions) through manipulation of viscosity, flow velocity, tube inner diameter and length.

To attach the polyethylene tubing to a pressure head, the ends of the microtubing were sleeved with a 10 μL plastic pipette tip. Each plastic tip was adhered to a luer lock connector and adapted to a syringe at both the inlet and outlet (Fig. 15). The pressure head and flow velocity of the system were provided by two syringe pumps (8000Xs, New era Pump Systems Inc., Farmingdale, USA). The dual syringe pumps were utilised in a reciprocating protocol, i.e., with one pump infusing and the other withdrawing at a matched rate.

Once the viscosity of the RBC suspension was known and controlled, using the constructed shearing system, the flow rate and length of tubing was manipulated to control the magnitude and duration of shear stress exposure.

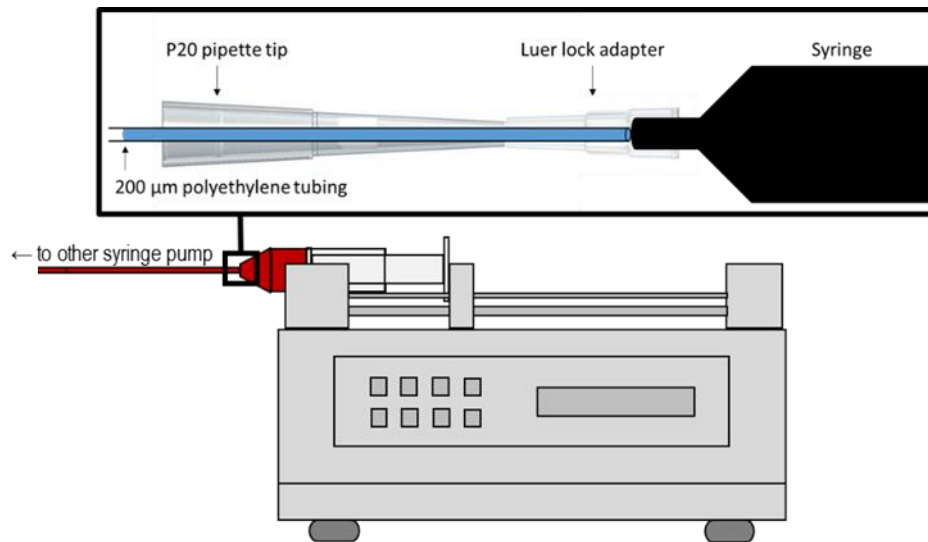


Fig. 15. Step-down created to facilitate the connection of a polyethylene tubing (I.D. 200 µm) to the pressure head generated by a syringe pump. The step-down connection required polyethylene tubing to be sleeved with a 10 µL plastic pipette tip, which was sealed to a luer lock adapter and connected to a syringe.

To determine the wall shear stress (τ_0) imposed by the cylindrical tubing, the Darcy-Weisbach equation was considered:

$$h_f = f \frac{Lv^2}{D2g} \quad (1.0)$$

Where h_f = friction head loss

f = the Darcy-Weisbach friction factor

L = length of the microtubing

v = velocity of the fluid

D = inner diameter of the microtubing

g = acceleration due to gravity.

When examining friction head loss, the Hagen-Poiseuille law for laminar flow can also be considered:

$$h_f = \frac{32vL\eta}{g\rho D^2} \quad (1.1)$$

Where momentum diffusivity is represented by the dynamic viscosity (η) per unit of density (ρ).

Using these variables, provided that fluid streamlines are laminar, the Reynolds number (Re) can be calculated with the following formula:

$$Re = \frac{\rho v D}{\eta} \quad (1.2)$$

Given the interrelationships of the Reynolds number (Eq. 1.2), the Darcy-Weisbach equation (Eq. 1.0), and Hagen-Poiseuille equation (Eq. 1.1), combination and simplification yields the friction coefficient:

$$f = \frac{64}{Re} \quad (1.3)$$

Provided the flow within the system is laminar and the shear stress distribution is linear across the length of the vessel (i.e., steady flow), wall shear stress is given by:

$$\tau_0 = \frac{f\rho v^2}{8} \quad (1.4)$$

As fluid velocity (v) is a function of both the flow rate (Q) and the vessel cross-sectional area, velocity can be given by:

$$v = \frac{4Q}{\pi D^2} \quad (1.5)$$

With the combination of the wall shear stress equation (Eq. 1.4), the calculation of the friction coefficient (Eq. 1.3), and the Re formula (Eq. 1.2), the equation can be simplified as follows:

$$\tau_0 = \frac{f\rho v^2}{8} = \frac{64\rho v^2}{8Re} = \frac{8\rho v\eta}{D\rho} = \frac{8v\eta}{D} \quad (1.6)$$

By substituting the function of fluid velocity (Eq. 1.5) into Eq. 1.6 the calculation of shear stress can be simplified to the form that is used throughout the present study.

$$\tau_0 = \frac{8(4Q)\eta}{(\pi D^2)D} = \frac{32\eta Q}{\pi D^3} \quad (1.7)$$

Once the flow rate for a given shear stress magnitude was determined, the duration of shear exposure was controlled by manipulating the segmental length of the polyethylene tubing.

Given the relationship between flow rate (Q), volume (V) and time (t):

$$Q = \frac{V}{t} \quad (1.8)$$

The volume of the cylindrical tubing is determined by the radius and segmental length:

$$V = \pi r^2 L \quad (1.9)$$

Provided a predetermined flow rate is known for a specific shear stress condition, when Eq. 1.8 and 1.9 are combined, the segmental length for a desired duration of shear exposure can be calculated:

$$L = \frac{Qt}{\pi r^2} \quad (2.0)$$

The length to full development of curvilinear flow profile (Le), and the propagation of axial migration of RBCs, can only be assumed to occur after adequate development length of laminar flow entering a new tube. The Le will thus be the region within the

microtubing where the fluid will be accelerating to the experimental shear stress, representing a region of systematic error; and, therefore it is important to characterise and minimise this variable. Le is defined by the Reynolds number (Re) of the fluid and the diameter (D) of the vessel, which may be described by the equation²⁸:

$$Le = 0.06ReD \quad (2.1)$$

Planar parabolic 'slit flow' shearing system

Following construction and implementation of the Poiseuille flow microtube shearing system, the design considerations for subsequent studies required a shearing system that also facilitated direct optical observation. The original polyethylene tubing was deemed inadequate for visualisation due to low optical clarity. While glass capillary tubes were originally considered, to accurately visualise blood cells through a glass cylinder, various oils of matched refractive index were required. Instead, a simpler parallel plate slit-flow microfluidic chamber was constructed. This chamber, which was fabricated of clear acrylic, sufficiently achieved the design specifications while being cost-effective to construct and implement. Provided laminar flow conditions were maintained, the shear profile was planar parabolic within the shear chamber; and, side wall shear effects were able to be neglected since the width (w) of the chamber was 20 times larger than its height (h). The chamber was sealed and connected to a pressure-head provided by dual reciprocating syringe pumps via clamped double O-rings.

The wall shear stresses in this system could be manipulated through the following relationship⁶⁰:

$$\tau = \frac{6\eta Q}{wh^2} \quad (2.2)$$

Importantly, in Poiseuille flow shearing systems, the shear profile across the axial region of the chamber is not constant, i.e., at different focal depths of visualisation, blood cells will be exposed to different levels of shear. Thus, when constructing the visualisation rig with the slit-flow system, it was important to maintain an accurate height of visualisation for comparative and precise data collection.

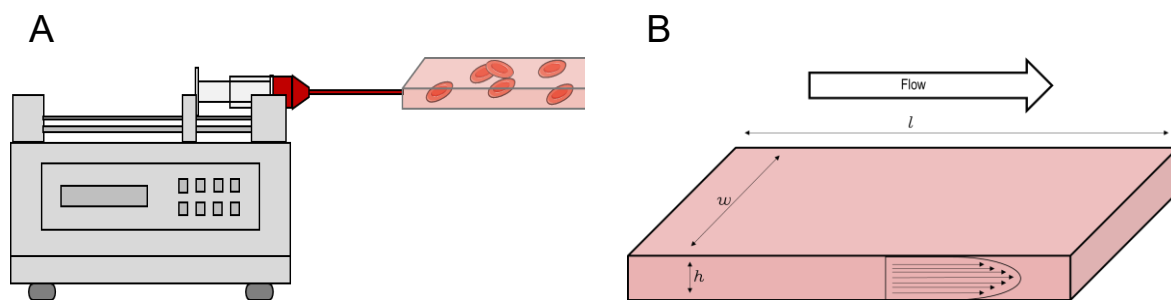


Fig. 16. (A) Schematic of simplified slit flow shearing system and (B) free body planar parabolic shear diagram.

Annular Couette flow shearing system

The final shearing system deployed for the current thesis required a uniform exposure of shear to all blood cells in flow irrespective of cell location (i.e., axial or marginated). For this design requirement, a commercial annular Couette flow shearing system and ektacytometer (Laser-assisted Optical Rotational Red Cell Analyser, Mechatronics, Hoorn, The Netherlands) was deployed for several thesis studies. Unlike Poiseuille flow, Couette flow induces shear stress between two parallel surfaces, between which the shear profile is constant across all locations in flow (provided the ΔP of the system is neutral). The Couette flow shearing system used in the current thesis was of a ‘bob’ and ‘cup’ design (Fig. 17), where the angular velocity (ω) of the outer cup could be manipulated to control the applied shear rate ($\dot{\gamma}$) of the system (Eq. 2.3⁶¹).

$$\dot{\gamma} = \frac{4\pi r_b r_c}{60(r_c^2 - r_b^2)} N \quad (2.3)$$

Where: r_b = radius of the bob

r_c = radius of the cup

N = number of revolutions per minute

Provided the viscosity (η) of the solution was known, the shear stress magnitude (τ) could be calculated:

$$\tau = \eta \dot{\gamma} \quad (2.4)$$

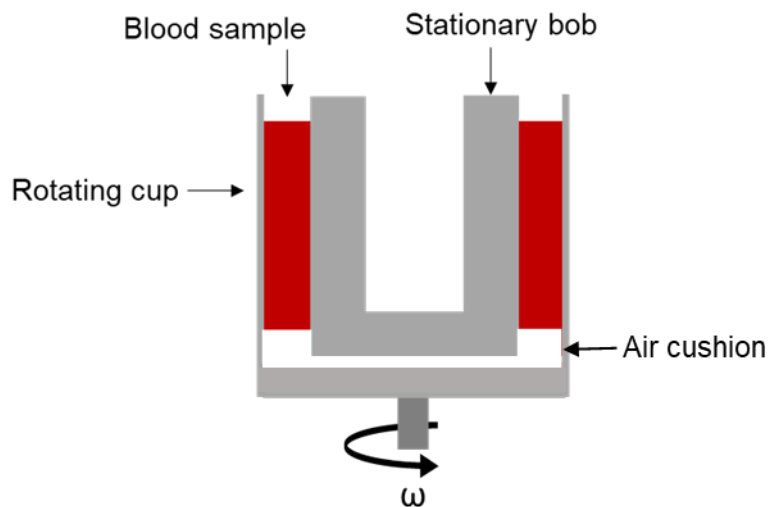


Fig. 17. Schematic of an annular 'bob' and 'cup' shearing system.

When deployed experimentally, to ensure all suspended RBCs were exposed to the same levels of shear, the outlet port of the annular couette shearing system was clamped to create an air cushion that prevented cell suspensions from collecting underneath the bob where shear stresses alter radially.

Electrophoretic mobility chamber

Part of the present thesis aimed to investigate the electrophysical properties of the RBC glycocalyx following exposure to sublethal shear. To determine the zeta potential of a particle, its electrophoretic mobility must first be determined. The electrophoretic mobility can be determined by measuring the velocity of particle movement towards a cathode or anode in the presence of an electric field. Thus, for the current thesis, to determine the zeta potential of blood cells, an electrophoretic mobility chamber (that concurrently facilitated RBC visualisation) was required.

Design specifications

The design specifications identified that the following characteristics were required:

1. The chamber must be electrically isolated and able to hold dilute RBC-PBS suspensions.
2. The chamber must have an optically clear bottom that would facilitate microscopy for RBC visualisation.
3. The chamber will be small, such that it could be a modular system able to be retrofitted to a microscope.
4. The microscope used must have a suitable camera able to image RBC movement in the electric field.
5. A power supply able to provide a sufficient electric field.
6. The electrodes and chamber materials must be compatible with short-term biological material interaction.

Optimisation

The initial designs of the electrophoretic mobility chamber leveraged a RheoMeditech chamber (Seoul, Korea) that was modified to have imbedded platinum electrodes and brass connectors (Fig. 18). The small acrylic chamber facilitated easy visualisation and good portability to fit into a microscope stage.

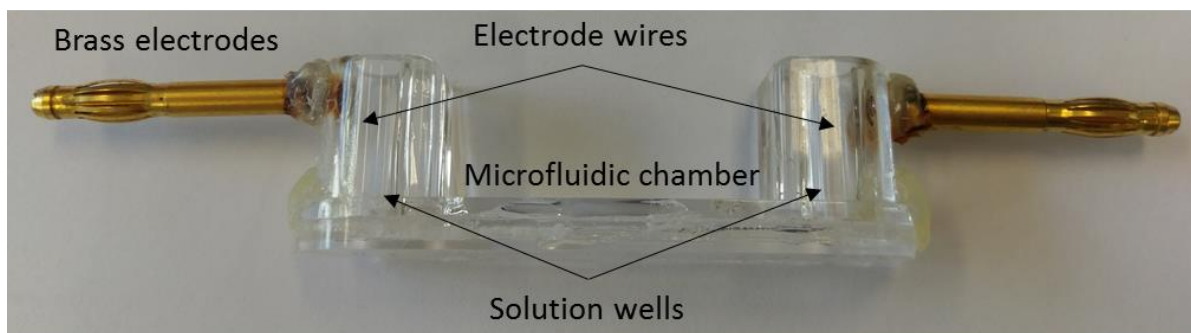


Fig. 18. Initial design of the electrophoretic mobility chamber for investigating RBC electrochemistry.

While this chamber was suitable for data collection, a considerable limitation was identified with its initial use: the substantial electric field generated by the apparatus resulted in an electrical potential and heat at the electrodes sufficient to cause electrolysis of the water solvent and dissociation into its component elemental gases. As the solution dissipated at the anode, a hydrodynamic water column pressure was generated in the opposite direction to the electrophoretic mobility movement, generating erroneous results. The design of this chamber was thus deemed inadequate, and the electrophoretic mobility chamber was redesigned to be an open system. An open 'bath-like' design without any separate chambers allowed dissociation of elemental gases, and thus solution dissipation, without generating differential water column pressure between either end of the device.

The initial optimisation processes identified that:

1. Clear acrylic was a suitable material for visualisation with brightfield and fluorescent microscopy.
2. Copper (Cu^{2+}) electrodes were insufficient for interaction with the phosphate buffered solution, deteriorating too rapidly due to electrochemical reduction-oxidation (redox) reactions. To stop electrode participation, inert Platinum (Pt) electrodes were instead implemented. Pt electrodes were far superior to Cu^{2+} and able to be reused for numerous measurements.
3. The elevated wells at the inlet and outlet of the Rheomeditech chamber was an inadequate structure as an electrophoretic mobility chamber, due to redox reactions generating uneven water columns and hence unwanted pressure gradients and subsequent fluid shifts.
4. The regulated DC power supply (MP3087, Powertech Systems Equipment Corp., Hacienda Heights, USA) set to 30 V and 80 mA could provide a sufficient electric field to rapidly induce RBC movement without temperature change.

Final design and deployment

The electrophoretic mobility chamber was redesigned and constructed with glass microscope slides in an open top, bath-like system (Fig. 19). The glass slides were fixed together with food-grade silicon sealant from the outer edge of the chamber. All optimisation processes identified from the initial tests were implemented into the redesigned chamber.

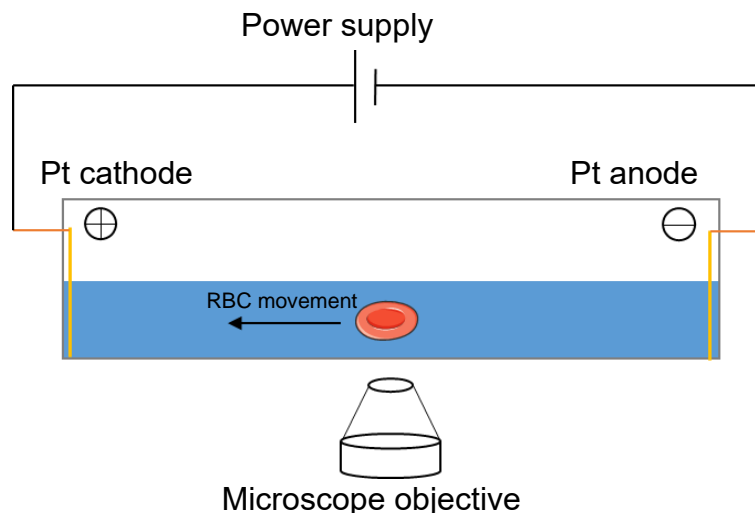


Fig. 19. Schematic of the redesigned electrophoretic mobility chamber used to measure RBC charge and zeta potential.

For experimentation, 5 μL of RBCs were suspended in 30 mL of PBS, and measurements were performed at a field strength of $203 \text{ V}\cdot\text{m}^{-1}$. The speed at which the RBCs travelled towards the cathode (positive electrode) was visualised using an Olympus IX70 inverted microscope (Olympus, Melville, USA) with an optiMOS high-speed camera (QImaging Corporation, Surrey, Canada) recording at 1 frame per second. Using the $40\times$ objective, images captured had a resolution of $162.5 \text{ nm}/\text{pixel}$, and the velocity of each cell tracked could be calculated by measuring displacement between each frame (Fig. 19). Data could then be exported for calculation of electrophoretic mobility and statistical analysis. Electrophoretic mobility (u) was determined by the quotient of the measured velocity of a tracked cell (v ; $\mu\text{m}\cdot\text{s}^{-1}$) for a given field strength (E ; $\text{V}\cdot\text{cm}^{-1}$):

$$u = \frac{v}{E} \quad (2.5)$$

Provided the dielectric constant of the buffer (ϵ) was known, the zeta potential (ζ) of each cell was able to be calculated using the Henry equation with the Smoluchowski approximation:

$$\zeta = \frac{\eta \times u}{\epsilon} \quad (2.6)$$

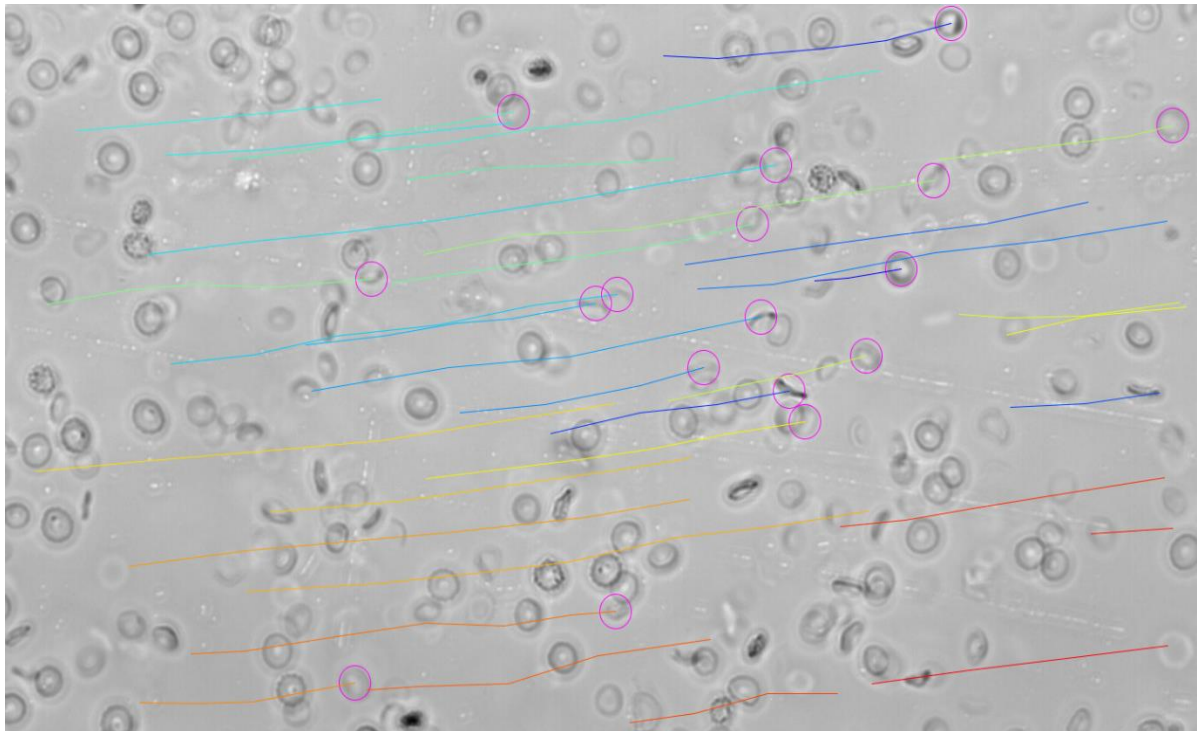


Fig. 20. A single micrograph video frame of tracked RBCs (circles) over time (coloured lines) in the applied electric field of the electrophoretic mobility chamber.

Ektacytoscope (combined rheometer-ektacytometer)

Current assessments of blood damage predominantly use indirect measurements, with quantification of changes in plasma haemoglobin concentration (representing haemolysis) being the international benchmark standard. More recent investigations of sublethal functional blood damage have deployed laser diffractometry techniques with an ektacytometer to assess intact blood cell deformability. Notably, blood cells with abnormal mechanical properties (e.g., shear rigidified^{50,62-64}, sickled blood cells⁶⁵, elliptocytes⁶⁶) have been reported to produce aberrant signals in small-scatter diffraction patterns generated by ektacytometry in low-shear flows. Numerous authors have proposed that this phenomenon is an erroneous measurement resultant of cell tumbling and non-alignment with flow (*see Chapter 4 for further details*).

Development of a system that could directly inspect blood cell movement and elongation while recording small-scatter diffraction patterns was identified necessary to elucidate this phenomenon. Further, such a system would constitute required infrastructure for future inspection of Fraunhofer diffraction patterns for RBC subpopulation isolation, and provide the foundations of a system that could be scaled into a device that could non-invasively yield real-time measures of accumulated blood damage.

Given Aim 3 of the present thesis required the construction of a new experimental rig that could investigate blood cell haemodynamics (especially cell orientation) using combined visualisation and ektacytometry techniques, the following section describes the construction and implementation of the 'Ektacytoscope'.

Design specifications

To assess ektacytometry and blood cell dynamics in low-shear flows, a new system with combined laser diffractometry and cell visualisation was needed to be created. The design specifications of the system were identified as follows:

1. The system must have a shearing chamber that can be discretely controlled, while also being suitable for optical inspection of blood cells.
2. The shear chamber must be able to support laser diffractometry and bright-field visualisation concurrently.
3. The visualisation component of the system must have appropriate magnification and resolution for the inspection of single blood cells.
4. The laser light must be able to yield small-scatter diffraction patterns without negatively impacting the sample (i.e., inducing unwanted sample heating).

Optimisation

Based on the desired specifications, the initial design was created by retrofitting a custom stage as a modular insert for an Olympus IX73 inverted microscope, leveraging the existing visualisation system. A laser was mounted on an external surface, and beam splitters controlled the laser light path. For the shearing chamber, a parallel plate slit-flow chamber was chosen (GlycoTech Corp., Gaithersburg, MD, USA). This chamber was constructed with an acrylic top, a glass microscope slide bottom, a silicon gasket in-between, and ports for inlet, outlet, and vacuum sealing. The beam splitters were made in-house by coating microscope slides with a thin film of aluminium in a high-vacuum chamber. All other components were fabricated from 3D printed plastic or laser cut acrylic.

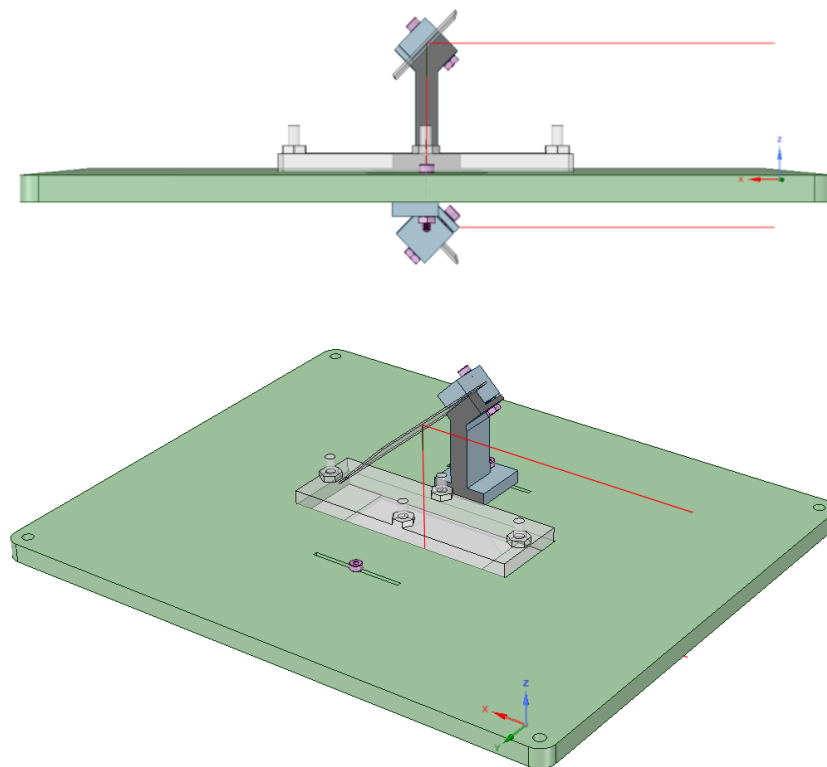


Fig. 21. Initial CAD design of the modular microscope stage insert that would add laser diffractometry to conventional bright-field microscopy.

Although it was planned that the initial design was to be operated in conjunction with extended focal length microscope objectives, when the stage was initially fitted to the microscope, to obtain the necessary angle of the beam splitters, adequate clearance for objective focal depth could not be obtained. Thus, the initial design was modified to implement a non-axial design that passed the laser through one end of the chamber, and white-light through the other end (Fig. 22). Bright-field visualisation was recorded with the CMOS camera (optiMOS, QImaging Corp., Surrey, CA), and laser diffraction patterns were generated onto a projector screen with a camera focused on the screen for capture.

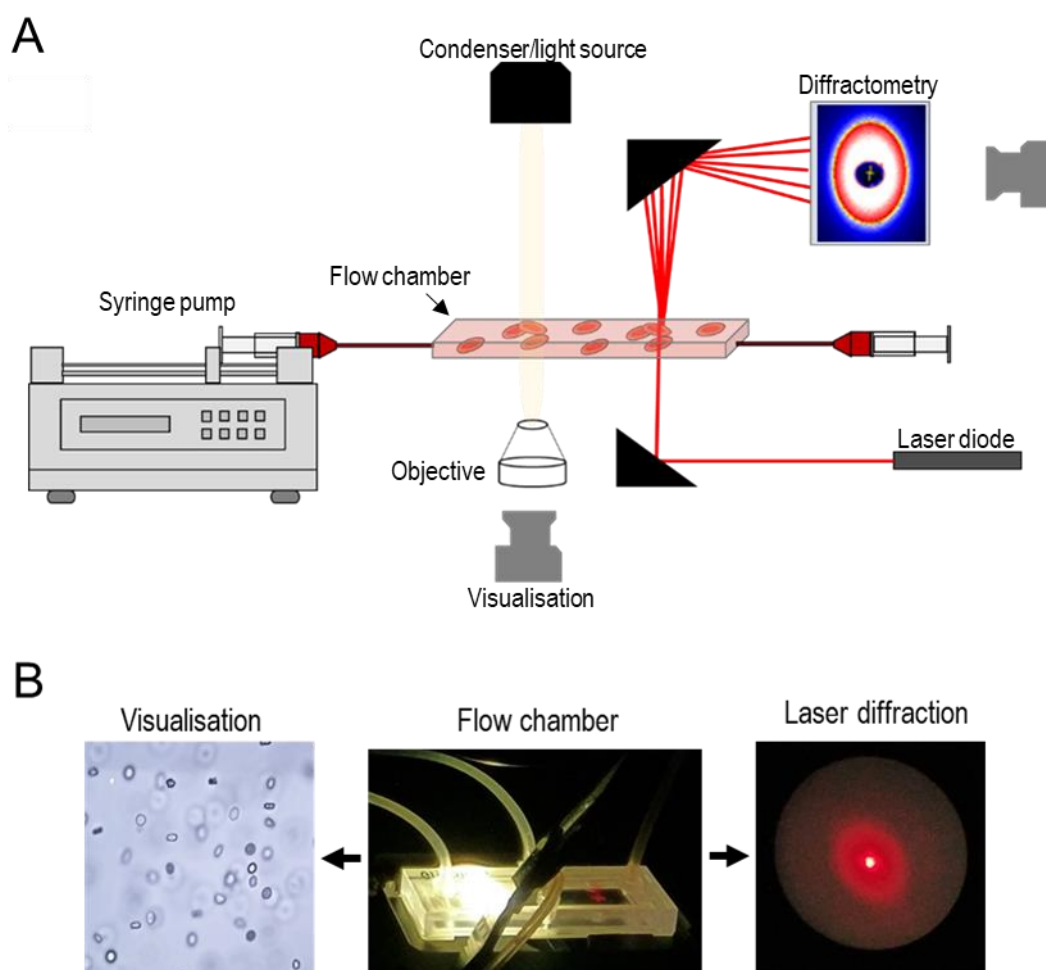


Fig. 22. Initial (non-axial) system schematic (A) and data (B) used for the optimisation of the combined rheometry-ektacytometry technique.

If blood cells behaved uniformly in response to a shear stimulus, all fully-developed flow regions within the shear chamber would yield relevant data that could infer the relationship between low-shear ektacytometry and single cell dynamics. However, preliminary testing with the non-axial system identified that real-time data often 'flickered' in the diffraction patterns as cell subpopulations responded non-uniformly. The preliminary testing rig was thus concluded to need redesigning into a colinear system, independent of an existing microscope. This would require a standalone rail system for development, with the capacity for bright-field high-speed visualisation (replacing the need for the commercial microscope). Rather than using a projected diffraction pattern, extra lenses were also included in the rail setup for focusing the diffraction patterns onto the CMOS sensor. Once columnated, the additional lenses allowed for lower laser light intensities with a longer light path to be used, providing more room for extra optics/additions.

Final design and deployment

The redesigned colinear system was built as an independent rig that could capture single cell dynamics and low-shear diffractometry with the quality and resolution of existing commercial systems for microscopy and ektacytometry (Fig. 23). This system enabled the concurrent visualisation of a single area of a blood shearing chamber with laser-diffractometry imaging from ektacytometry *and* optical cell visualisation from bright-field microscopy.

The shearing/visualisation chamber was constructed with acrylic in a simple slit-flow clamped rheometer design. The pressure head in the chamber was generated by dual reciprocating syringe pumps with a stepwise increasing shear protocol (0.3-5 Pa). The pump control system was automated and synchronised to the other data acquisition devices. The coaxial design was achieved by aligning bright-field visualisation microscopy with co-localisation of an epi-illuminated laser light source. The two imaging systems were overlapped coaxially using 50:50 beam splitters, and the light

intensities of the laser and white-light sources were balanced with a variety of neutral density (ND) filters in either light path to optimise the captured image clarity and compensate for backscatter, cross-illumination, and ambient light contamination. Small-scatter diffraction patterns generated from the blood sample were columnated through the condenser lens and subsequently focused onto the CMOS sensor. Bright-field microscopy and laser-diffractometry visualisations were recorded and exported to image analysis software for further inspection.

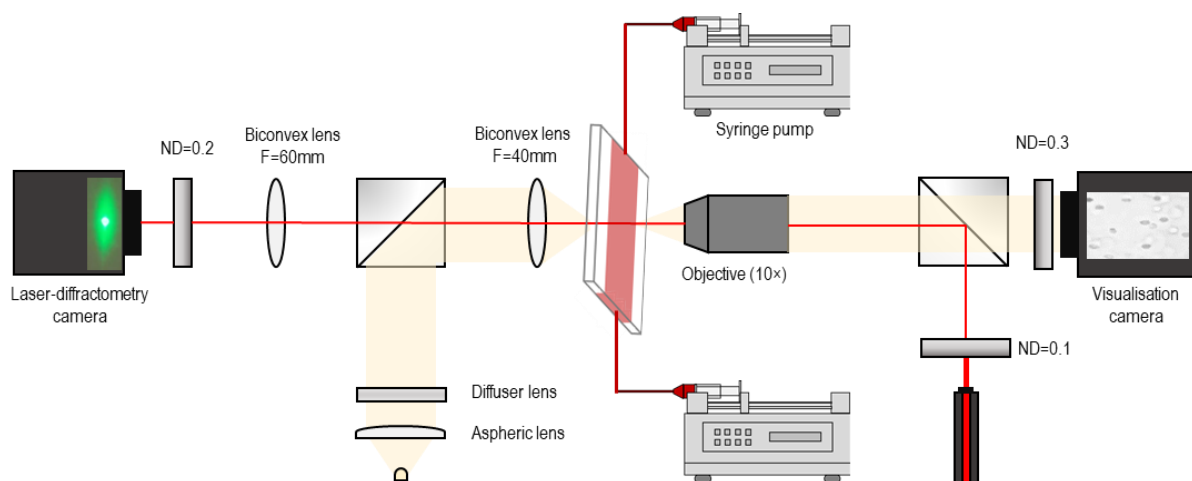


Fig. 23. Design schematic for the custom-built combined slit-flow rheometer ektacytometer (i.e., the 'ektacytoscope'). The designed system facilitated coaxial assessment of blood cells in shear flow with high-speed visualisation and small-scatter laser-diffractometry.

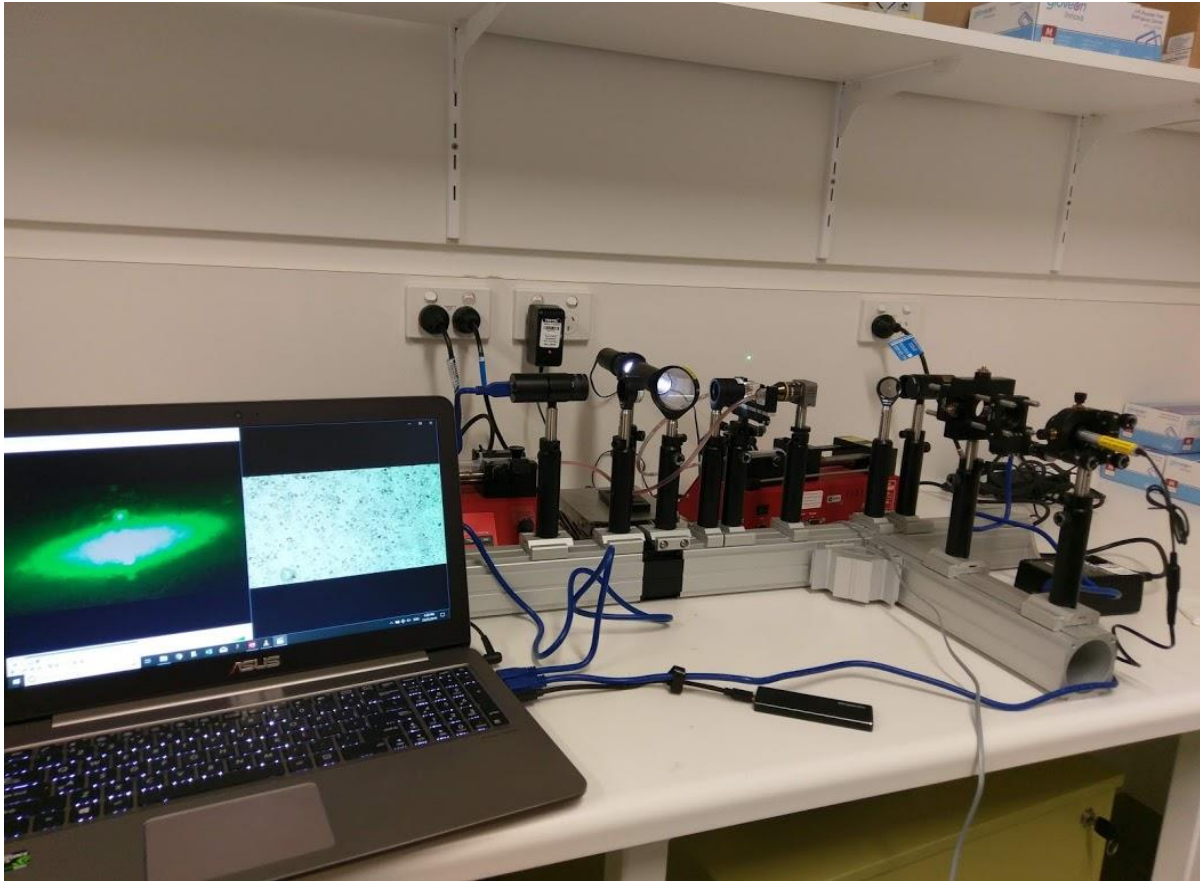


Fig. 24. Final optimisation stages of ektacytoscope construction.

Analysis software

Image analysis was performed in open source software (ImageJ, National Institutes of Health, Bethesda, USA) with independent routines being created to analyse the captured Fraunhofer diffraction patterns and visualised blood cells. Each image analysis routine was constructed from a similar hierarchy: initial filtering was performed to enhance signal-to-noise ratio; each image was binarised; automatic edge detection and selection was performed; and, each region of interest (ROI) was analysed for length, width, area, and orientation. Image analysis code was confirmed with manual inspection of random frames.

Micropipette aspiration system

In the current thesis, the changes in cell mechanics were investigated with micropipette aspiration to obtain values of membrane shear modulus and investigate *ex vivo* capillary transit time. The micropipette aspiration technique is a single cell manipulation tool that has extensive biomedical application, ranging from investigations of microinjection, *in vitro* fertilisation, and removal of cell nuclei (i.e., denucleation). Previously, micropipette aspiration methods have been deployed to investigate the mechanical and adhesive properties of blood cells⁶⁷, as it allows for the inspection of the RBC membrane of single cells with piconewton (pN) resolution. While commercial micropipette aspiration systems do already exist, due to lack of accessibility, to achieve Aim 2 and Aim 3 of the current thesis (inspecting RBC membrane mechanics, deformability, and capillary transit velocity), a low-cost micropipette aspiration system was constructed that could assess single blood cells following exposure to sublethal mechanical stresses.

Design specifications

To create a micropipette aspiration system to study RBC mechanics, multiple subsystems were required; and four major elements were needed to be developed:

1. A system to fabricate glass micropipettes with an inner diameter of 1-3 μm .
2. A system to micromanipulate the glass pipettes on a microscope for precise control.
3. A system for pressure regulation control with single pascal resolution.
4. Image analysis software for higher throughput data processing.

Micropipette fabrication and forging

For the inspection of RBC membrane mechanics, several micropipettes with an inner-diameter of 1-3 μm first needed to be fabricated. To repeatably create micropipettes

with the desired diameter, it was determined that glass capillary tubes needed to be melted and pulled into long tapered tips with less than 500 nm inner diameter, before being cut back to the desired size specific for the type of measurement to be performed. Borosilicate glass capillary tubes were obtained from Sutter Instrument Company (Novato, CA), and had an initial inner diameter of 0.5 mm and a length of 100 mm; the length allowed a single capillary tube to fabricate two identical micropipettes. The capillary tubes were pulled into the long taper micropipettes using a commercial micropipette puller (P-1000, Sutter Instrument Company, Novato, CA). Newly fabricated micropipettes were produced in large batches and transported in hard plastic containers with moulded slots for safe storage.

Prior to a testing day, the micropipettes needed to be cut to the desired size required for the type of experiment, and the cut tip needed to be perpendicular and have smooth walls. Due to the small size of the micropipette tips needed, the common method of cutting the micropipette tips by scoring and bending with a ceramic tile was insufficient for the present study. Instead, similar to the methods described by Engström and Meiselman⁶⁸, a microforge capable of cutting micropipettes with inner diameters of 0.8-4 μm needed to be constructed. Briefly, this method advances a micropipette into a melted glass bead, before it is left to cool, harden, and break away from the remaining micropipette. This system is highly successful due to the different melting points between the type of glass used for the micropipette, and the type of glass used for the microbead (typically an ultra-low melting point glass, e.g., solder glass). When obtaining the components that could be built into a microforge, due to budget restraints, solder glass was unable to be obtained, thus a slightly varied method using a microbead of borosilicate glass was developed.

The constructed microforge utilised a small length of high-resistance nichrome wire attached to heat resistant porcelain terminals, which were connected to a regulated DC power supply (Fig. 25). Due to the high-resistivity of the nichrome wire, exposure to small electric currents resulted in large heat generation, producing temperatures in

excess of the softening temperature of borosilicate glass (i.e., $>525^{\circ}\text{C}$). The microforge was built onto an inverted microscope, and the micropipette was connected to an x, y, z micromanipulator array, facilitating controlled movement of the glass pipette relative to the microbead.

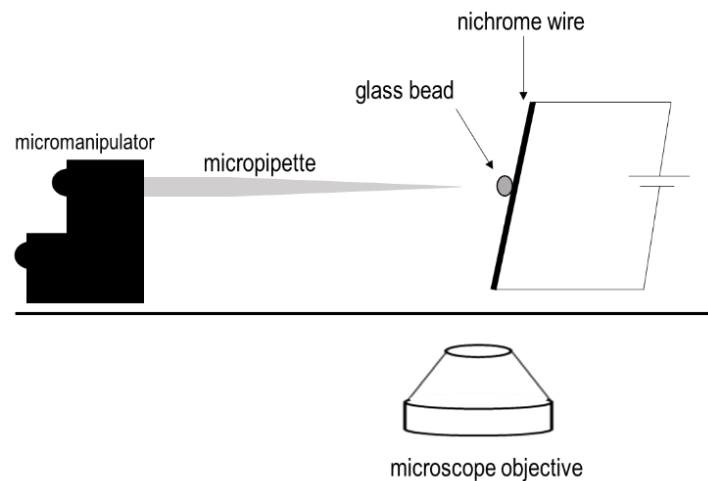


Fig. 25. Schematic of the constructed microforge used for cutting and shaping micropipettes.

Given the borosilicate glass bead and micropipette tip softened at the same temperature, a new procedure was determined for cutting the micropipette tips. Initially, the microbead was heated beyond the softening point, and the micropipette tip was advanced into the microbead to the desired cutting diameter. To yield a smooth perpendicular tip, it is important to align the advancement of the micropipette with the axial portion of the microbead. Once advanced to the required depth, the micropipette was rapidly withdrawn from the microbead and moved away from the nichrome wire. The electric current through the nichrome wire was then stopped, allowing the micropipette, microbead, and wire filament to cool and harden. Once all components were hardened, the micropipette was advanced into the microbead with a single hard fast action. The mechanical shock caused the micropipette to bend and

fracture at the point to which it was previously advanced into the softened bead (a visible impurity/weakness in the shape of the micropipette at this location could also be observed). If the micropipette did not fracture at the desired size or geometry, the procedure was repeated to produce a slightly larger tip. For larger holding pipettes, the microforge was also used for firepolishing by holding the micropipettes near the heated nichrome wire; longer duration exposure to the heated wire increased the smoothness of the tip and decreased the size of the pipette aperture.

The produced micropipettes were preserved between days of testing by priming and storing them similarly to the method as reported by Engström and Meiselman⁶⁸; however, rather than storing micropipettes in a buffer solution, an enzymatic cleaner was used. The micropipettes were thoroughly rinsed and primed with a 30-gauge needle prior to setup for measurement and experimentation.

Micropipette control system

Following construction of micropipettes with the desired diameter, the control system needed to be created. Given micropipettes need to be positioned at the cell membrane prior to the application of suction pressures, similar to the microforge, micromanipulation and microscopic observation were necessary to be combined in the system. A modular acrylic stage insert was created to be fit to an Olympus IX73 inverted microscope (Olympus, Melville, USA), with each micropipette being held by x, y, z micromanipulators. All imaging was performed using a 60× objective and a CMOS camera (QImaging Corporation, Surrey, Canada). The microscope and all fixed components were isolated from environmental vibration with a passively dampened table. All stage and micropipette manipulation systems were constructed with manual control, with the future ability to develop and implement motor control for an automated setup.

Pressure regulation

To perform micropipette aspiration, precise suction pressures (with single Pa resolution) must be applied to the cell membrane. To construct an adequate pressure regulation system, each micropipette was connected to a water column with a 30 mL fluid reservoir. To induce pressure changes, the height of the meniscus of the water column relative to the tip of the micropipette must be manipulated. Given pressure is regulated by changing the height of the meniscus, a larger fluid reservoir with an increased meniscus surface area, requires larger volume changes to yield equivalent differential pressures to smaller reservoirs. Thus, a 30 mL reservoir was implemented as it yielded less relative error in the system than smaller reservoirs, while also minimising the influence of evaporation

Each water column was connected to a computer controlled microfluidic syringe pump, where the volume changes were controlled to displace height (note: 1 mm height change in H₂O equates to ~9.98 Pa). Prior to each measurement, by assessing the movement of microparticles or cells, the height of the water columns were initially 'zeroed' for suction pressure. To minimise evaporation from the reservoirs throughout the duration of the experiment, the water columns were covered with pierced parafilm. Piercing the parafilm allowed for head-space pressure in the reservoir to remain constant when the water columns were manipulated.

Final design and deployment

The final design of a single micropipette system is displayed in Fig. 26 and Fig. 27. For the determination of the resistance to shear, the glass pipette was micromanipulated to be positioned at the surface of a single RBC. Using visual feedback of cell/microparticle movement as a guide, the pressure induced by the water column was again confirmed to be zero and level with the height of the stage. Using the syringe pump fluidics control, a small volume from the water column was added and

immediately removed to level the meniscus of the fluid and align the direction of syringe pumping to remove motor backlash; if the linear actuators and screw of the syringe pumps were left unchecked, motor backlash would induce erroneous results in the initial stages of the measurement. Suction pressure was then increased, ensuring that the aspirated portion of the cell (L_p) had stabilised and reached equilibrium before capturing the image for analysis at a given pressure (ΔP). Each frame was analysed for L_p , which was subsequently normalised for the radius of the pipette tip (r_p). Given ΔP and r_p were known parameters, the linear regression of L_p/r_p and the suction force (pN) was performed. The experimental determination of the slope gives the shear modulus (μ) for a single cell in units $\text{pN}\cdot\mu\text{m}^{-1}$.

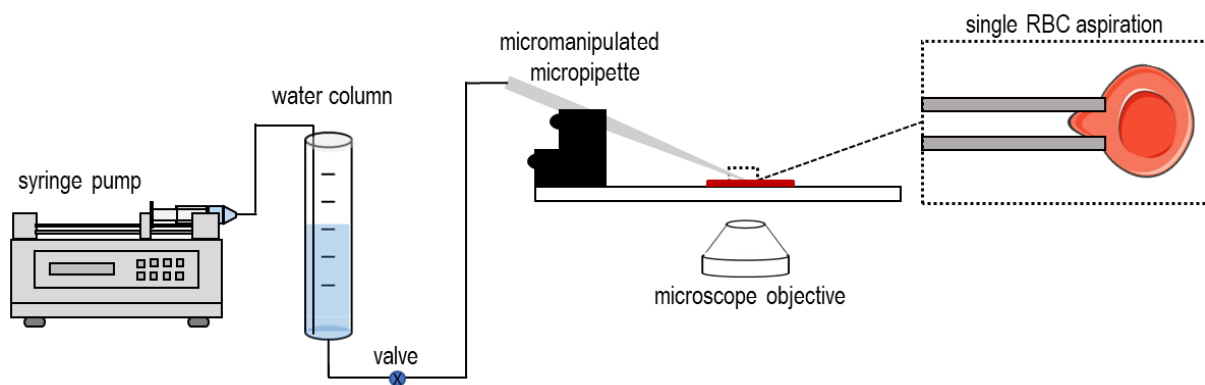


Fig. 26. Schematic of a single micropipette aspiration rig for the inspection of single RBCs.

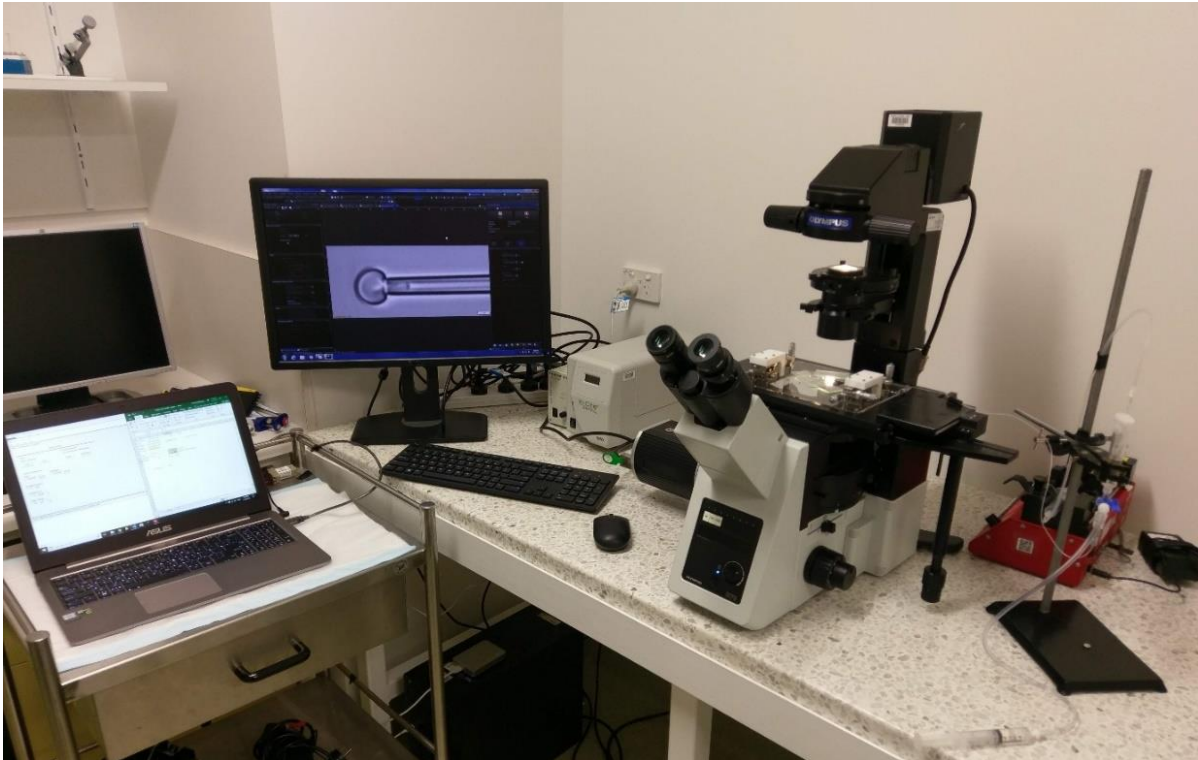


Fig. 27. Constructed single micropipette system performing single RBC aspiration.

The constructed system was able to be scaled into a rig that could support multiple micropipettes. For the experimentation performed in *Chapter 5*, the micropipette rig was assembled with dual micropipettes of different diameters for the measurement of shear modulus and capillary transit velocity.

Analysis software

While all micropipette image analysis in *Chapter 5* was performed manually, using open source software (ImageJ, National Institutes of Health, Bethesda, USA), an automated image analysis code was also created as a part of the current thesis. This image analysis software required initial pre-processing with the camera to induce a minor blur to soften the exposure of the captured images to assist post-processing. The image analysis code (*described in Appendix I*) leveraged image binarisation, edge detection, and grey value intensity plots to detect the inner walls of pipette, calculate its inner diameter, and automatically detect the cell tongue length, and generate a data output table.

Chapter III.

Sublethal mechanical trauma alters the electrochemical properties and increases aggregation of erythrocytes

Antony P. McNamee, Geoff D. Tansley, Michael J. Simmonds

The following Chapter contains a published co-authored journal article. I contributed with: the experiment concept and design, conduction of the experiment, data analysis and interpretation, contributed to reagents/materials/analysis tools, and wrote the manuscript. All authors reviewed and approved the manuscript.

Bibliographic details: McNamee AP, Tansley GD, Simmonds MJ. *Sublethal mechanical trauma alters the electrochemical properties and increases aggregation of erythrocytes.* Microvascular Research. 2018;120:1-7. Doi: 10.1016/j.mvr.2018.05.008. PubMed PMID: 29803580.

Abstract

Circulation of blood depends, in part, on the ability of red blood cells (RBCs) to aggregate, disaggregate, and deform. The primary intrinsic disaggregating force of RBCs is derived from their electronegativity, which is largely determined by sialylated glycoproteins on the plasma membrane. Given supraphysiological shear exposure – even at levels below those which induce haemolysis – alters cell morphology, we hypothesised that exposure to supraphysiological and subhaemolytic shear would cleave membrane-bound sialic acid, altering the electrochemical and physical properties of RBCs, and thus increase RBC aggregation.

Isolated RBCs from healthy donors (n=20) were suspended in polyvinylpyrrolidinone. Using a Poiseuille shearing system, RBC suspensions were exposed to 125 Pa for 1.5 s for three duty-cycles. Following the first and third shear duty-cycle, samples were assessed for: RBC aggregation; the ability of RBCs to aggregate independent of plasma (“aggregability”); disaggregation shear rate; membrane-bound sialic acid content, and; cell electrophoretic mobility.

Initial shear exposure significantly increased RBC aggregation, aggregability, and the shear required for rouleaux dispersion. Sialic acid concentration significantly decreased on isolated RBC membrane ghosts, and increased in the supernatant following shear. Initial shear exposure decreased the electrophoretic mobility of RBCs, decreasing the electronegative charge from -15.78 to -7.55 mV. Three exposures to the shear duty-cycle did not further compound altered RBC measures.

A single exposure to supraphysiological and subhaemolytic shear significantly decreased the electrochemical charge of the RBC membrane, concurrently increasing cell aggregation/aggregability. The cascading implications of hyperaggregation appears to potentially explain the ischaemia-associated complications commonly reported following mechanical circulatory support.

Introduction

As blood circulates the vasculature, the ability of the red blood cells (RBCs) to form stacks of branched aggregates and three-dimensional structures (i.e., rouleaux) under low shear conditions facilitates important physiological processes that decreases resistance to flow (e.g., axial migration of formed elements), while concurrently augmenting low-shear viscosity¹³. The rate and amplitude of RBC aggregation is modulated by counteracting factors that may be clustered broadly as “pro-aggregating” and “disaggregating” processes. Pro-aggregating forces are largely due to the presence of large molecular weight plasma proteins⁶⁹ (e.g., fibrinogen), while disaggregating forces are principally generated by mechanical shear and cell-cell electrostatic repulsion¹⁶ (with negatively charged sialylated glycoproteins being the major determinant of such repulsion).

RBC sialic acids (primarily N-acetylneuraminic acids) are located on the plasma membrane within the glycocalyx, and account for up to 90% of the cell’s negative charge¹⁸. Distribution of sialic acids over the surface of the membrane are reported to influence morphology, cell deformability, oxygen carrying capacity, and distribution of intracellular hemoglobin¹⁷. With the normal ageing and senescence process of RBCs, the zeta potential (ζ) and the plasma membrane sialic acid content is decreased¹⁹. Removal of sialic acid from the glycocalyx of RBCs, using the enzyme neuraminidase, was reported to significantly increase cell aggregation²⁰.

The process of RBC aggregation is rapid, forming rouleaux within seconds, and is observed to occur *in vivo* in low shear regions, such as within post capillary flow^{15,69}. With sufficiently high shear, however, formed rouleaux are able to disperse and disaggregate, differentiating this reversible process from coagulation and agglutination⁷⁰. Despite wall shear flows being too high in arterial circulation for aggregates to form, the shear profile varies radially across the vessel, decreasing to a minimum in the central region of flow (axis), where aggregation may occur²⁸. This aggregation and axial migration of formed elements facilitates a partial phase-

separation, contributing to the existence of a cell-poor layer of plasma at the vessel wall³¹. The cell-poor region facilitates development of a boundary layer with decreased local viscosity and frictional resistance, minimising wall shear stress and endothelial stimulation. The cell-poor layer also facilitates a “plasma skimming” effect, where side branches of the vasculature principally receive plasma, significantly decreasing haematocrit to ~10% in some capillary networks³⁰, contributing to lower haemodynamic resistance, and thus also limiting oxygen-rich RBCs⁷¹.

Hyperaggregability of RBCs may alter flow distributions of cells and near wall conditions, specifically increasing leukocyte and platelet margination and attachment⁷². *Ex vivo* investigations have indicated that increases in aggregation (at maintained haematocrit) have correlated with low-shear viscosity and the non-Newtonian behaviour of blood, with speculation of these findings *in vivo* being negatively correlated with tissue perfusion⁷³. An *in vivo* animal model of chronic hyperaggregation observed decreased wall shear stress which diminished nitric oxide synthesis mechanisms, altering vasomotor tone⁷⁴. Moreover, given the importance of nitric oxide in the prevention of platelet activation and attachment, enhanced aggregation may increase thrombotic risk⁷⁰.

Mechanical circulatory support devices have evolved such that they adequately meet the functional demands of replaced organs, and achieve current haemocompatibility criteria⁷⁻⁹; however, several significant complications have been reported with long-term use that are suggestive of blood damage and malfunction, without remarkable haemolysis. This damage, which is due to blood-interaction with non-physiological environments (i.e., contact with foreign surfaces, elevated shear forces, turbulence and cavitation), can cause dangerous complications of altered perfusion and rheological properties of blood^{10,50,75,76}. The observed complications of haemorrhagic events, thrombotic events, tissue ischaemia and anaemia, leading to multi-system organ failure⁶, may be partially explained by altered RBC aggregation behaviour. Current investigations of blood trauma and mechanical circulatory support have found that

acute and chronic exposure may increase low-shear blood viscosity⁷⁷ and increase RBC aggregation in haemodialysis^{78,79}. Using light microscopy, increases in RBC aggregation have been observed in bovine animal models implanted with ventricular assist devices, with concurrent increases in low-shear viscosity and erythrocyte sedimentation rate⁸⁰.

Given that high shear environments, such as those present within mechanical circulatory support devices, have been identified to induce ultrastructural changes to RBCs, altering morphology⁵⁰, causing cell fragmentation⁵², and disrupting the lipid bilayer⁵⁴, it is likely that this sublethal mechanical trauma may cleave sialylated membrane glycoproteins responsible for the cells' electrostatic negative charge. The aim of the present study was thus to investigate the aggregation behaviour and biochemical/electrochemical properties of RBCs (with emphasis on membrane-bound sialic acid) following short-term exposure to sublethal magnitudes of shear stress.

Materials and methods

Experimental overview

The electrochemical and rheological properties of RBCs following exposure to acute high-shear environments typical of clinically-relevant mechanical circulatory support were explored in an *in vitro* experimental model of Poiseuille flow. Isolated human RBCs were exposed to 125 Pa for 1.5 s on three repeated duty-cycles; following the first and third duty-cycles, samples were collected to quantify the level of blood trauma. The experimental procedures were conducted and completed within 4 h of venesection. The experimental protocols were reviewed and approved by the Griffith University Human Research Ethics Committee (Protocol number: 2016/712), which conforms with the Declaration of Helsinki.

Subjects and sampling

Twenty healthy men (28 ± 8 yr) volunteered to participate in the present study. After informed consent was obtained, participants were interviewed to determine if they were free from haematological and immune disorders, metabolic or cardiovascular comorbidities, and were not using medications known to influence rheology. Blood was collected from a prominent vein in the antecubital region within 90 s of tourniquet application, using a 21-G needle and syringe, and then immediately transferred into tubes containing $1.8 \text{ mg}\cdot\text{mL}^{-1}$ of $\text{K}_2\text{-EDTA}$.

Cell preparation

Following blood collection, blood products were isolated by centrifugation at $1500 \times g$ for 10 min. Plasma was then aspirated into a separate microfuge tube and stored until required for RBC aggregation measures. To further isolate RBCs, packed cells were washed twice with isotonic phosphate buffered saline (PBS; pH = 7.40, $290 \text{ mOsmol}\cdot\text{kg}^{-1}$), with use of centrifugation at $1500 \times g$ for 5 min, each time to remove and discard supernatant.

Overcoming the non-Newtonian characteristics of blood is critical for the accurate calculation and quantification of shear stress in Poiseuille flow, thus isolated RBCs were resuspended in a 360 kDa polyvinylpyrrolidone solution (PVP; $4.93 \text{ mPa}\cdot\text{s}$, pH 7.4, $290 \text{ mOsmol}\cdot\text{kg}^{-1}$) at a decreased haematocrit of $0.15 \text{ L}\cdot\text{L}^{-1}$. The RBC-PVP solution adopted a final viscosity of $5 \text{ mPa}\cdot\text{s}$ and exhibited predominantly Newtonian properties, facilitating accurate shear stress calculation whilst still exhibiting viscosity typical of normal *in vivo* ranges. Viscosity was measured using a cone-plate viscometer with a temperature reflective of the specific assay/experiment requirements (0.5 DVII+ with CPE40 spindle, Brookfield Engineering Labs, Middleboro, MA). The resuspension of RBC in PVP facilitated investigation of shear damage independent of other factors that may compound cell aggregation (i.e., shear activation of platelets)⁸¹.

Application of shear stress

As shear stresses in current mechanical circulatory support devices are predicted to induce less than 150 Pa for residence times ranging 0.04–3.08 s (device dependent)^{50,82}, the wall shear stress magnitude-duration combination (125 Pa for 1.5 s) applied to RBC suspensions was specifically chosen to: i. avoid overt haemolysis, while ii. being representative of clinical blood pumps. Development of the shear stress magnitude and duration of exposure was achieved using a linear Poiseuille shearing system, constructed using a 0.94 m segment of 200 μm I.D. polyethylene tubing. This microtube system was pressurised by synchronised infuse/withdraw dual syringe pumps (NE-8000X, New Era Pump Systems Inc., New York, USA) at a continuous flow rate of $1.178 \text{ mL}\cdot\text{min}^{-1}$. The pumping of cell suspensions was continued until all cells had been exposed three times to the shearing condition. Through specific control of various design elements (i.e., flow rate, microtubing diameter, and solution composition/viscosity), the present design could investigate sublethal shear damage to the RBC independent of extraneous compounding forces also observed in current clinical devices (e.g., turbulence, cavitation, and recirculation).

Isolation after shear stress

Immediately following the first and third exposure to shear, RBCs were separated from PVP via centrifugation at $1500 \times g$ for 10 min, aspirating and storing the supernatant for determination of cleaved sialic acid. Given PVP suspensions are considered to be pro-aggregating⁸³, isolated RBCs were washed twice with isotonic PBS prior to suspension in the desired medium for assessment (i.e., autologous plasma, dextran, PBS); centrifugation was performed at $1500 \times g$ for 5 min.

RBC aggregation and disaggregation shear rate threshold

Isolated RBCs were resuspended in autologous plasma at a standardised haematocrit of $0.4 \text{ L}\cdot\text{L}^{-1}$ for measurement of RBC aggregation. Using the $0.4 \text{ L}\cdot\text{L}^{-1}$ blood sample,

1 mL was injected into a 300 μm gap of an annular Couette-type photometric rheoscope (LORRCA, MaxSis, Mechatronics, Hoorn, The Netherlands) operating at 37°C. Sylllectometry was used to obtain indices of RBC aggregation by measuring magnitudes of laser backscatter generated by blood samples illuminated by laser light from an emitting laser diode (670 nm, 4 mW).

Following the application of a disaggregating shear (500 s^{-1} for 5 s), laser backscatter was measured for samples at stasis over a 120-s period to generate a time-dependent intensity sylllectogram, where increased laser backscatter indicated a more disaggregated homogenous blood sample. Through parameterization of this curve, indices reflecting the amount of aggregation over the 120-s period (AI_{120}) and the time required for half-maximal aggregation ($T_{1/2}$) were calculated. AI_{120} was obtained by calculating the ratio of the area under the laser backscatter-time curve to the sum of the total area under and above the curve.

After the measurement of RBC aggregation, the magnitude of shear rate sufficient to prevent the formation of aggregates was detected (i.e., the disaggregation shear rate; γ_{thr}). Following shearing sufficient for complete disaggregation (i.e., 500 s^{-1}), laser backscatter intensity was recorded at 14 predefined shear rates between 40 s^{-1} and 800 s^{-1} . The difference between the laser backscatter intensity at a given shear rate and the high-shear period for disaggregation was calculated across all shear rates, and analysed for the local minima. The magnitude of shear at which the difference in laser backscatter was minimal indicated the critical level of shear rate that prevented RBC aggregation, and thus the disaggregation shear rate.

RBC aggregability

To examine the intrinsic tendency of RBCs to form aggregates independent of extrinsic plasma factors (i.e. RBC aggregability), RBCs were resuspended in a standard pro-aggregating solution (3% dextran 70 kDa in PBS) adjusted to 0.4 $\text{L}\cdot\text{L}^{-1}$ haematocrit. RBC

aggregability is typically measured using 50 μL of the RBC-dextran suspension injected into a cone-plate shearing system (Myrenne RBC Aggregometer, Myrenne GmbH, Roetgen, Germany) operating at room temperature (22°C)^{11,84}. The cone-plate shearing system generates shear by rotating a cone with an angle of 2° against a stationary glass plate. Following an initial disaggregating shear of 600 s^{-1} for 10 s, infrared light transmission was measured for samples at stasis over a 120-s period to produce a syllectogram. Similar to the laser backscatter-time curve, parameterisation of the light transmission-time curve provided indices of AI_{120} and $T_{1/2}$. Increased magnitudes and rates of aggregation were indicated by increases in AI_{120} and decreases in $T_{1/2}$, respectively.

RBC electrophoretic mobility

Determination of the change in zeta potential (ζ) and cell charge following exposure to shear required 5 μL of isolated RBCs to be suspended in 30 mL of PBS in a custom-developed electrophoretic mobility chamber. Using a regulated DC power supply (MP3087, Powertech Systems Equipment Corp., Hacienda Heights, USA) at 30 V and 80 mA, a field strength of $203\text{ V}\cdot\text{m}^{-1}$ was produced within the chamber between two platinum electrodes. Measurements were performed at room temperature (22°C), and the velocity at which RBCs travelled towards the cathode was recorded using an Olympus IX70 inverted microscope (Olympus, Melville, USA) with an optiMOS high-speed camera (Qimaging Corporation, Surrey, Canada) and standardised for optical viewing depth. The velocity was recorded for a minimum of 15 cells across a minimum of 20 s for a subset of randomly-selected subjects ($n=5$). Electrophoretic mobility was determined by the quotient of the measured velocity of a tracked cell ($\mu\text{m}\cdot\text{s}^{-1}$) for a given field strength ($\text{V}\cdot\text{cm}^{-1}$).

The zeta potential (ζ) of RBCs in each group was calculated using the Henry equation (Equation 2.7) with the Smoluchowski approximation:

$$\zeta = \frac{\eta \times u}{\varepsilon} \quad (2.7)$$

where η was the dynamic viscosity and ε was the dielectric constant of the buffer, and μ was the electrophoretic mobility of the cells.

Preparation of RBC ghosts

To isolate the red cell membrane from its cytosolic contents and haemoglobin, RBC ghosts were prepared for each experimental group. The protocol, previously described by Dodge et al.⁸⁵ requires isolated RBCs to be washed with a hypotonic phosphate buffer solution (sodium phosphate dibasic; Na₂HPO₄; prepared at a pH of 8) and centrifuged at 20,000 × g for 40 min. Following the initial centrifugation, the supernatant solution (containing released cytosolic components) was aspirated and removed before the RBC ghost pellet was washed twice with hypotonic buffer solution (centrifugation was at 20,000 × g for 20 min).

Determination of sialic acid content

Sialic acid concentration was measured using the modified spectrophotometric periodate-resorcinol method⁸⁶, before and after exposure to shear using 20 μL of isolated RBC membrane ghosts and 500 μL of the PVP supernatant (indicating cleaved sialic acid). After initial oxidation of total sialic acid with periodic acid (IO₄; 0.04 M), samples were mixed with an acidic resorcinol solution containing resorcinol (0.06 % w/v), HCl (10 M), CuSO₄·5H₂O (0.1 M), and H₂O. Formation of the sialic acid chromophore was catalysed by heating samples to 98°C for 5 min; stabilisation was subsequently achieved via rapid cooling and addition of tert-butanol. Following stabilisation for 3 min at 37°C, light absorbance was measured against a sample blank at 625 nm using a microplate reader (FLUOstar Omega, BMG LABTECH, Offenburg,

Germany). Sialic acid concentration was determined using a calibration curve created from known standard solutions ranging 20-200 μM . To facilitate a comparison between amount of sialic acid removed from RBCs and gained in the supernatant, following determination of concentration of sialic acid, the absolute change in mass of sialic acid was calculated and reported.

Statistical analyses

Data were confirmed to be parametric using the Shapiro-Wilk test. All data were investigated with a one-way ANOVA with repeated measures applying Bonferroni corrections. Statistical analyses were performed using Prism 7 (Graphpad Software Inc., San Diego, USA), where significance was determined at an alpha of 0.05. Unless otherwise stated, data are presented as mean \pm standard error.

Results

RBC aggregation and RBC aggregability

Indices obtained from syllectometry that characterise the magnitude and rate of RBC aggregation at stasis for RBCs previously exposed to shear are presented in Fig. 28. Following exposure to 125 Pa for 1.5 s, the magnitude of RBC aggregation in plasma measured over 120 s (i.e., AI_{120} ; Fig. 28A) significantly increased ($F=33.35$, $p<0.001$). The rate of RBC aggregation in plasma also significantly increased following shear exposure, as indicated by decreased $T_{1/2}$ (Fig. 28B; $F=33.77$, $p<0.001$). Congruent with the RBC aggregation in plasma, RBC aggregability in a standardised plasma-free solution (3% dextran 70 kDa in PBS) significantly increased with initial exposure to shear (Fig. 28C; $F=13.01$, $p<0.001$). The rate of RBC aggregability also increased, indicated by a significantly decreased aggregation halftime (i.e., $T_{1/2}$; Fig. 28D; $F=15.94$, $p<0.001$). For all measures, no additional changes were observed subsequent to the initial exposure to shear.

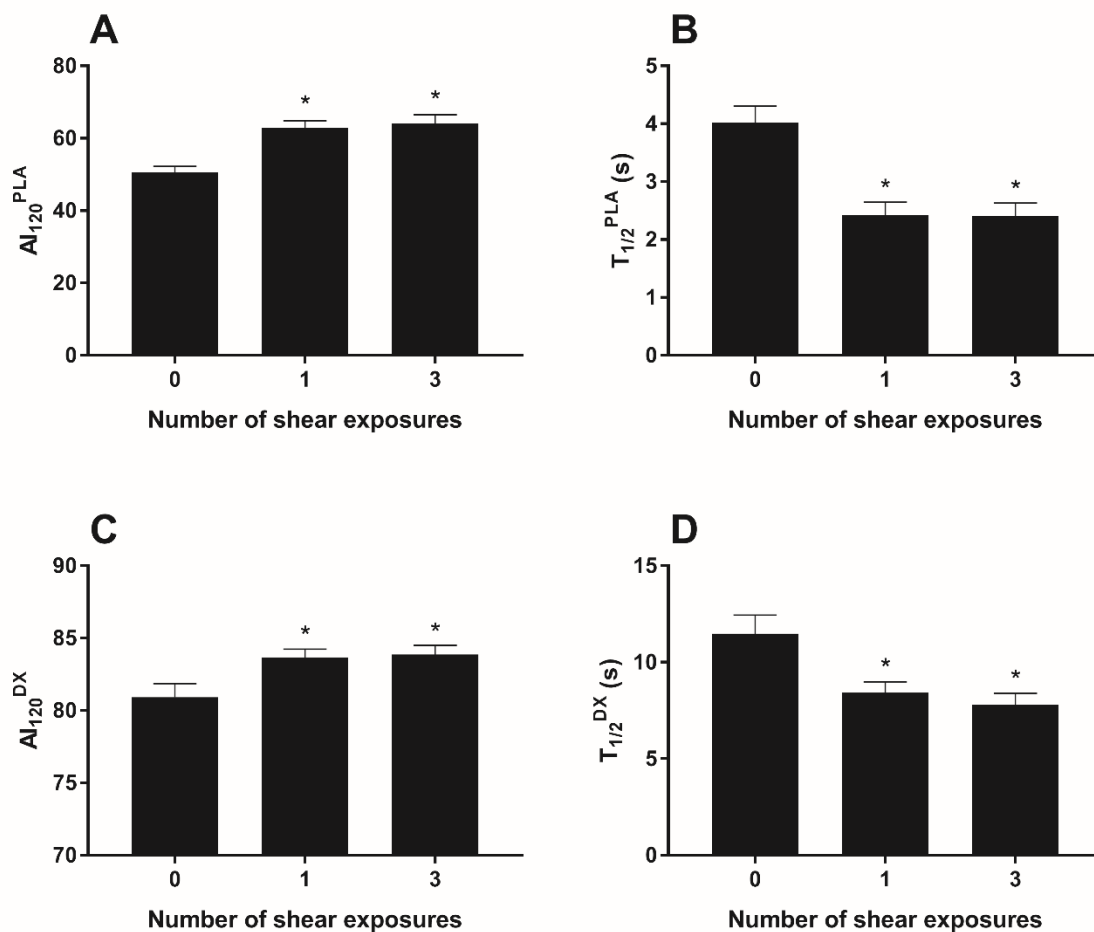


Fig. 28. Aggregation of red blood cells (RBCs) resuspended in autologous plasma (PLA), and a plasma-free medium (DX), at a standardised haematocrit ($0.4 \text{ L}\cdot\text{L}^{-1}$) following exposure to shear (125 Pa for 1.5 s). The magnitude of RBC aggregation in plasma measured at stasis over 120 s (AI_{120} ; Panel A) significantly increased following exposure to shear, while the halftime for aggregation in plasma ($T_{1/2}$; Panel B) significantly decreased. Exposure to shear increased the magnitude of RBC aggregability in a plasma-free medium measured over 120 s (i.e., AI_{120} ; Panel C), while the measured halftime significantly decreased (i.e., $T_{1/2}$; Panel D). *, significantly different to unsheared control (i.e., “0” shear exposures), $p < 0.05$.

RBC disaggregation shear rate threshold

The critical level of shear rate required to induce disaggregation (γ_{thr}) of blood samples previously conditioned with 125 Pa for 1.5 s, is presented in Fig. 29. Following exposure to shear, the disaggregation shear rate significantly increased ($F=8.93$, $p < 0.001$) from 158.7 ± 25.1 to $240.0 \pm 23.0 \text{ s}^{-1}$ (one exposure) and $242.7 \pm 19.2 \text{ s}^{-1}$

(three exposures). Subsequent to the initial change following exposure to shear, successive exposures to shear did not significantly alter the disaggregation shear rate.

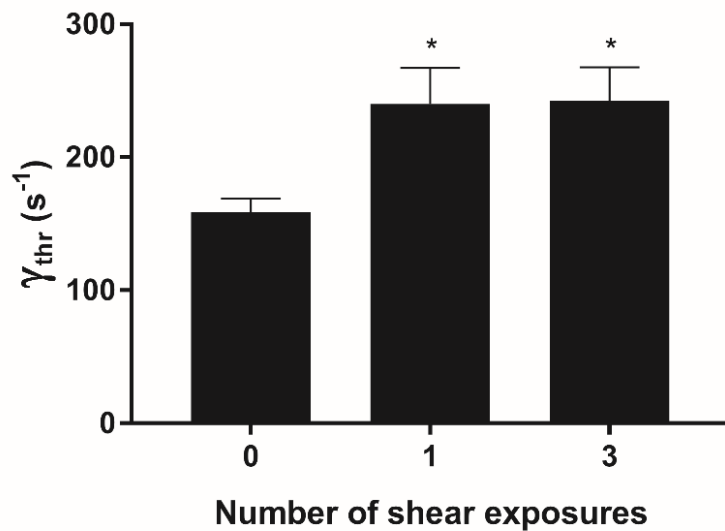


Fig. 29. The critical level of shear rate required to induce disaggregation (γ_{thr}) of red blood cells (RBCs) determined for blood samples exposed up to three times to conditioning shears (125 Pa for 1.5 s). *, significantly different to unsheared control (i.e., “0” shear exposures), $p < 0.05$.

Bound and unbound sialic acid

The concentration of sialic acid (SA) for 20 μ L of RBC membrane ghosts (Fig. 30A) and cleaved into 500 μ L of the supernatant (Fig. 30B) is presented following shear exposure. To facilitate comparison, calculated changes in mass of SA relative to control (ΔSA) are displayed in Fig. 30C for RBC bound SA (SA_{RBC}) and unbound SA in the supernatant ($SA_{unbound}$). The concentration of membrane-bound sialic acid (i.e., SA_{RBC}) significantly decreased with exposure to 125 Pa for 1.5 s ($F=12.38$, $p < 0.001$), while the concentration of SA measured in the shearing supernatant (i.e., $SA_{unbound}$) significantly increased ($F=37.18$, $p < 0.001$). No significant changes were detected between the first and third exposure to shear.

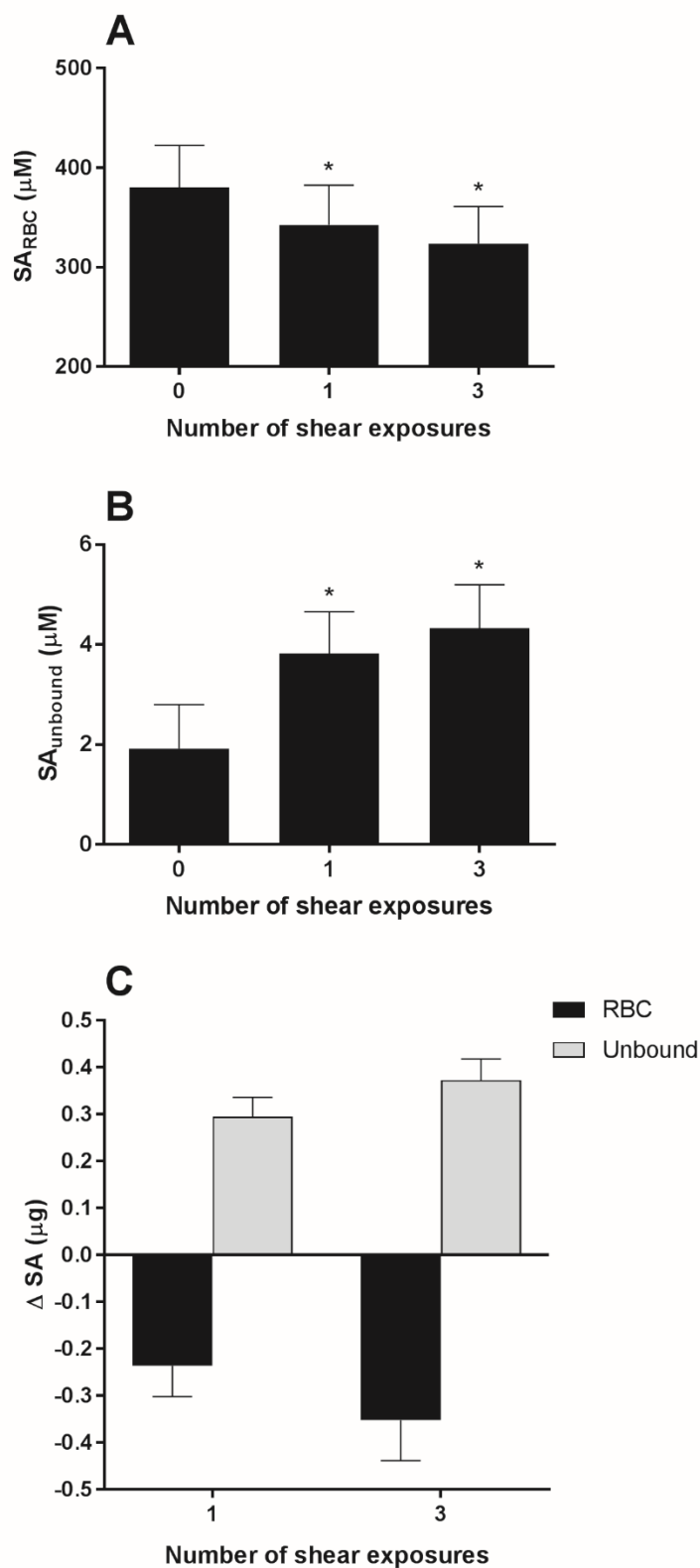


Fig. 30. The concentration of sialic acid (SA) measured in 20 μL of isolated red blood cell (RBC) membrane ghosts (SA_{RBC}; Panel A) and released into 500 μL of shearing supernatant (SA_{unbound}; Panel B) following exposures to 125 Pa × 1.5 s. Panel C reports the change in mass of SA following exposure to shear. *, significantly different to unsheared control ("0"), p<0.05.

Electrophoretic mobility and zeta potential

The electrophoretic mobility (EPM) of RBCs exposed to shear is illustrated in Fig. 31. EPM significantly decreased following first exposure to shear ($F=331.3$, $p<0.001$). The calculated mean zeta potential was -15.78 ± 0.31 mV for unsheared control RBCs ("0" number of exposure); one exposure to shear induced a significantly less negative zeta potential of -7.55 ± 0.21 mV. Following this initial change, subsequent exposures to shear maintained the less electronegative zeta potential (-7.52 ± 25 mV); however, no further cumulative effect was detected.

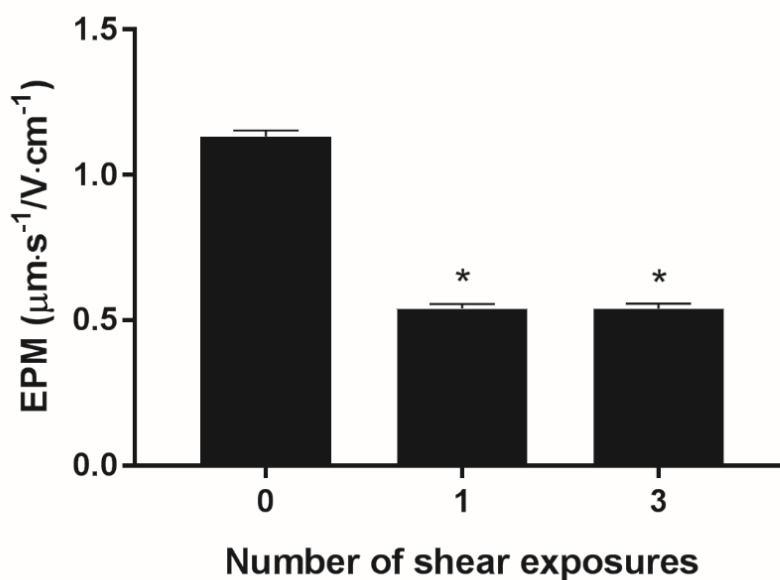


Fig. 31. The electrophoretic mobility for red blood cells (RBCs) suspended in PBS following exposure to shear (125 Pa for 1.5 s). Data collected from a subset of randomly-selected subjects ($n=5$). *, significantly different to unsheared control ("0"), $p<0.05$.

Discussion

The salient findings of the present study indicate that exposure of RBCs to shear stress, representative of that observed in mechanical circulatory assist devices, induces: i. increased magnitude and rate of RBC aggregation; ii. increased tendency of RBCs to aggregate in a standardised plasma-free medium (i.e., aggregability); iii. increased amount of shear required to disaggregate formed rouleaux; iv. cleaved membrane-bound sialic acid into the surrounding media; and, v. lowered electrostatic charge of RBCs (observed via decreased electrophoretic mobility), and thus also the cells' zeta potential. The collective findings present, for the first time, evidence that supraphysiological shear exposure may remove membrane-bound sialic acid from the glycocalyx of RBCs, leading to increased cell aggregation. Given that RBC aggregation and disaggregation are important parameters for the regulation of microcirculatory blood flow, these results may explain, in part, the elevated incidence of secondary complications leading to multi-system organ failure in patients receiving mechanical circulatory support.

Recent investigations of subhaemolytic damage to blood have predominantly focused on morphological changes, rather than alterations to the physical and electrochemical properties which explain cell behaviour in various environments (micro- and macro-vascular circulation). The present study, for the first time, reports that supraphysiological, subhaemolytic shear stress exposure (representative of the transit within mechanical circulatory support devices) increased the magnitude and rate of RBC aggregation. These novel findings are congruent with clinical data, which highlight that circulatory support-induced blood trauma increases low-shear blood viscosity, and erythrocyte sedimentation rate^{77,80}; RBC aggregation is a primary determinant of these clinical markers (for a review, see Simmonds et al.¹⁹). The present investigation extends beyond these prior studies, however, by shearing RBCs in a

medium independent of plasma and other formed elements, which facilitated our investigation into the discrete responses of RBCs to the specific flow conditions.

While isolated RBCs were sheared prior to being resuspended in autologous plasma, the increased cellular aggregation in the present study may originate from decreased disaggregating factors intrinsic to the sheared cells (i.e., surface charge density), or increased pro-aggregating factors resulting from interactions of sheared blood cells with other unsheared formed elements. It is plausible that damaging stimuli (such as shear exposure), for example, may cause the translocation of phosphatidylserine to the RBC surface membrane, altering subsequent interactions of RBCs with leukocytes and platelets⁸⁷. To determine whether interactions between RBCs and other formed elements of blood may explain the present findings, we also investigated the tendency of RBCs to aggregate independent of plasma factors, and observed similar trends of increased RBC aggregability following shear exposure. These findings suggest that factors intrinsic to RBCs, independent of extrinsic factors, are altered following supraphysiological shear stress exposure and thus explain shear-induced promotion of cell aggregation.

Standard methods of assessing RBC aggregation typically examine laser backscatter-time curves while cells are at stasis. Using the same hardware, the disaggregation shear rate threshold was explored by measuring changes in laser backscatter in shear flow, from 40 – 800 s⁻¹. As displayed in Fig. 29, the magnitude of shear required to disaggregate formed rouleaux (without augmenting cellular deformability) significantly increased following initial shear exposure, and was maintained for subsequent exposures to shear. These data indicate that exposure to subhaemolytic magnitudes of shear stress increases the amount of aggregation in shear flow, and the magnitude of subsequent shear required to sufficiently disaggregate formed rouleaux. If aggregates fail to disperse in circulation, the resistance of cells entering smaller vessels may increase, propagating a heterogenous distribution across capillary beds⁸⁸. While increased aggregation increases the likelihood of RBC stasis in smaller

capillaries, blood flow can be preserved via rerouting RBCs via thoroughfare/preferential channels (i.e., capillaries with larger diameter)⁸⁹, partially bypassing smaller capillaries and thus potentially disturbing local tissue oxygenation.

In the present study, the electrophoretic mobility of RBCs significantly decreased following exposure to conditioning shear, indicating a decreased negative cell charge (i.e., less negatively charged). As electrostatic repulsion of RBCs is a primary disaggregating force², this finding likely explains the increased aggregation, aggregability, and shear required for disaggregation observed following the conditioning shear. One of the primary contributors to the negative charge of the RBC is the abundant distribution of sialic acid across the cell surface¹⁸, accounting for ~90% of the cell's net negative charge and hydrophobicity⁹⁰. High shear environments have been reported to induce ultrastructural changes to RBCs, causing changed morphology⁵⁰, cell fragmentation⁵², and disruption of the lipid bilayer⁵⁴. Given the significant surface alterations that occur to the cell membrane of RBCs with subhaemolytic trauma, it is likely that supraphysiological shear stress cleaved sialic acid from the cell membrane, decreasing the electrostatic surface charge and thus also the disaggregating force intrinsic to the glycocalyx.

The removal of sialic acid from the RBC membrane has previously been correlated with normal cell ageing/senescence processes resulting in decreased negative surface charge of the cell^{19,91}; this process may be accelerated with the enzyme neuraminidase²⁰. While shear stress has not previously been reported to cleave sialic acid, Fig. 30 presents that shear exposure decreased RBC membrane-bound sialic acid, and increased sialic acid content in the suspending media. Fig. 30C confirms that, when concentrations of sialic acid are standardised as mass lost/gained, the change in sialic acid content in the supernatant matches the amount removed from the RBC membrane. These data indicate that membrane-bound sialic acid can be removed in high shear conditions and thus may explain some of the physical changes in RBCs following supraphysiological shear exposure.

The impact of shear removal of membrane-bound sialic acid content may also explain the decreased RBC deformability and increased membrane rigidity observed in other studies^{25,50,51,75,76}. As sialic acid is negatively ionised, and cytosolic haemoglobin is positively charged, membrane-bound sialic acid is proposed to be an important regulator of haemoglobin distribution in the cytoplasm, thus also playing a role in maintaining the oxygen carrying capacity of RBCs¹⁷. Moreover, as sialic acid is bound to band 3, it has been observed to influence cell morphology and membrane deformability¹⁷. Further studies will elucidate the role of sialic acid in maintaining cell morphology, and will contribute to the development of numerical models of the dynamic balance between pro-aggregating and disaggregating forces.

While the present study demonstrates that RBC sialic acids can be removed with a single exposure to supraphysiological sublethal shear, no further compounding of this effect was observed during repeated exposures. Of note, similar trends of increasing RBC aggregation/aggregability (Fig. 28) and decreasing cell electrophoretic mobility (Fig. 31) were observed, providing a secondary confirmation of the sialic acid change in response to shear exposure. Collectively, these data indicate that the accumulation of blood trauma may occur rapidly (i.e., < 1 s duration), causing the cells' charge to significantly decrease to half of its initial level. Given enzymatic (neuraminidase) treatment may remove up to 90% of cell charge¹⁸, the initial decrease in charge (followed by a plateau) appears to indicate: i. further shear accumulation is required to remove the remaining sialic acid, or ii. the remaining sialic acid is less sensitive to shear damage (i.e., possibly located within the cytosol, or the inner monolayer of the RBC membrane, thus "protected" from shear). Although sialic acids are ubiquitous in many tissues of the body, its presence within the cytosol or on the inner monolayer of the RBC membrane remains to be identified. Moreover, while sialic acids are predominantly located on glycophorin A (~75 %), they are also located on band 3, glycolipids and other glycophorins of the cell membrane⁹², which may vary in junctional attachment sites. The findings of the present study, may suggest that the

relative strength of the sialic acid junctional attachments, or the integrity of the O-linked and N-linked oligosaccharides containing sialic acid is varied⁹³, with some attachments being more susceptible to shear.

The collective findings of the present study indicate that RBCs' electrochemical charge and aggregation behaviour are altered following the initial exposure to supraphysiological shears. The present magnitude-duration combination of shear exposure, while being below the haemolytic threshold, supports previous estimates of the threshold shear required for sublethal damage⁵¹. Given accumulation of sublethal damage occurs rapidly (i.e., during the first exposure to high shear), these data bear substantial implications for patients acutely receiving mechanical circulatory support. Irrespective of short-duration transits, blood passing through mechanical circulatory support devices may rapidly become damaged. The implications for post-surgical tissue perfusion are of interest, given that even once "off-pump", the continued circulation of sublethally damaged RBCs and associated impaired blood fluidity is likely to persist until complete cell turnover (up to 120 days). The hyperaggregation of RBCs and associated sluggish low-shear blood flow may cause increased leukocyte and platelet margination/attachment⁷², diminished nitric oxide synthesis altering vasomotor tone⁷⁴, and increased thrombotic risk⁷⁰; potentially contributing to the prevalence of complications (e.g., haemorrhage, thrombosis, tissue ischaemia, anaemia, etc.) that ultimately lead to multi-system organ failure and death⁶. Given patients indicated for mechanical circulatory support are typically at elevated risk of altered blood fluidity (due to comorbid chronic disease and inflammation), future mechanical circulatory support should be designed to limit magnitudes of shear exposure to levels that do not alter the electrochemical and other physical properties of blood cells.

The present study was designed specifically to explore the effects of elevated shear stress on RBC physiology in the absence of other factors known to influence cell viability typical of rotary blood pumps – e.g., complex and turbulent flow – thus

caution is required for extending the present experimental insights to clinically-utilised blood pumps and current clinical practice. Moreover, the present study design sheared RBCs in PVP to facilitate cell properties to be explored following shear exposure, independent of other blood cells (platelets, leukocytes) and plasma factors; while it is predicted that high shear would have similar effects in plasma, the magnitude of such an effect may be lessened due to the so-called “protective” qualities of plasma⁹⁴. Nevertheless, the findings of the present study may assist the development of current numerical models of blood damage, assisting the advancement of circulatory support device design. Moreover, the present findings emphasise that further investigation of RBC aggregation and blood damage is warranted in clinical populations receiving mechanical circulatory support.

Chapter IV.

Exposure to sublethal and supraphysiological shear stress alters erythrocyte dynamics in subsequent low-shear flows

Antony P. McNamee, Tom Fitzpatrick, Geoff D. Tansley, Michael J. Simmonds

The following Chapter contains a co-authored manuscript submitted for publication. I contributed with: the experiment concept and design, conduction of the experiment, data analysis and interpretation, contributed to reagents/materials/analysis tools, and wrote the manuscript. All authors reviewed and approved the manuscript.

Abstract

Blood is a non-Newtonian and shear-thinning fluid owing to the physical properties and behaviours of red blood cells (RBCs). Under increased shear flow, pre-existing clusters of cells disaggregate, orientate with direction of flow, and deform. These essential processes enhance fluidity of blood, although accumulating evidence suggests that sublethal trauma to blood – induced by supraphysiological shear exposure – paradoxically increases the deformability of RBCs, but only when examined under low shear conditions. Some propose that rather than actual enhancement of cell mechanics, these observations are “pseudo-improvements” and possibly reflect altered flow and/or cell orientation leading to methodological artefacts, although direct evidence is lacking. The present study thus sought to explore RBC mechanical responses in shear flow using purpose-built laser diffractometry in tandem with direct optical visualisation to address this problem.

An annular Couette shearing system exposed freshly-collected RBCs to a mechanical stimulus known to drastically alter cell deformability (i.e., Prior Shear Exposure to $100 \text{ Pa} \times 300 \text{ s}$; “PSE”), while samples not previously exposed to shear served as a reference (“Con”). Samples were subsequently transferred to a custom-built slit-flow chamber that combined laser-diffractometry with direct cell visualisation. Cell suspensions were sheared in a stepwise manner (0.3, 0.6, 0.9, 1.2, 1.5, 1.8, 2.1, 2.4, 2.7, 3.0, 4.0, and 5.0 Pa), with each step being maintained for 15 s. Deformability and cell orientation indices were recorded for small-scatter Fraunhofer diffraction patterns and also visualised RBCs.

RBCs in the PSE condition had significantly decreased visualised cellular deformability, when compared with Con ($p < 0.001$). In subsequent flow studies, laser derived indices also indicated that PSE had decreased capacity to elongate at any given shear stress, when compared with Con ($p = 0.001$). Novel observations demonstrated that PSE RBCs had increased heterogeneity of optically-derived

orientation with flow vector at any shear, when compared with Con ($p < 0.001$). Further, PSE cells had poor alignment (i.e., steeper) equilibrium in 5 Pa flow.

The present findings indicate that prior shear exposure and stress-strain history can alter subsequent behaviour of RBCs in physiologically-relevant low-shear flows. These findings may yield insight into microvascular disorders in recipients of mechanical circulatory support and individuals with haematological diseases that alter physical properties of blood.

Introduction

As blood flows through the varied geometries of the cardiovascular system, its viscous properties dynamically respond to fluctuating shear rates imposed by fluid-wall interactions. Given red blood cells (RBCs) constitute 36-50% of blood and ~99% of the formed elements, the movement and biophysical properties of single RBCs largely dictate the fluid stability and viscous behaviour of blood¹². At the cellular scale, rheology is primarily dependent on RBC deformability and orientation relative to tangential shear stresses; further, these properties are vital for alignment and entry of RBCs (~8 μm) into the smallest apertures of the vasculature (~3 μm inner diameter)⁹⁵. The ability of RBCs to orientate and deform is predominantly governed by the cell's physical properties: including elasticity and stability of the surface membrane and connected cytoskeleton, the viscosity of the haemoglobin-dominant cytosol relative to that of the surrounding media, and a biconcave morphology that yields a favourable surface area relative to cell volume. Thus RBCs exhibit a unique elastic range without exceeding plastic limits and/or surface rupture (for review see Chien⁹⁵).

In higher shear flow, single cells adopt an elastic drop-like behaviour, where the surface membrane freely rotates around the cytosol in a 'tank-treading' motion^{96,97}. This tank-treading movement has been identified to be an important attribute that facilitates energy dissipation of external work across the membrane, transferring tangential stresses to the inner fluid, allowing maintenance of a steady shape and orientation with the flow vector⁹⁸. Tank-treading acts to decrease hydraulic resistance in cell transit of the microcirculation and across axial regions of larger vessels with higher concentrations of cells (i.e., increased haematocrit)²; tank-treading is thus imperative for optimal blood fluidity.

The rate of tank-treading is highly dependent on external factors (i.e., applied shear rates and velocity of the fluid) and internal cellular factors (i.e., cell membrane viscosity and morphological characteristics that influence hydrodynamics of the

cell)⁹⁹. Goldsmith and Marlow¹⁰⁰ observed RBC tank-treading, elliptocyte morphology, and orientation with flow in shears ≥ 1.2 Pa. In flow where shear was < 1.2 Pa, however, tank-treading was still observed, although cells did not elongate, and the resting biconcave morphology was maintained. In very low-shears, cells were observed to flip and tumble in an unsteady motion. Fedosov et al.¹⁰¹, highlighted that large deformations and membrane 'buckling' are necessary to facilitate the transition of cells from tumbling to tank-treading motions, and that rigid cells requiring larger forces for buckling also needed increased shears to facilitate this dynamic transition. Thus, if RBCs' sensitivity to mechanical stimuli (particularly membrane material properties) is altered with pathological processes, flow homeostasis may be compromised, causing interruptions in local fluid stability, and possibly hindering the ability of RBCs to uniformly access and traverse the microcirculation.

The material properties of the RBC membrane are susceptible to shear-rigidification prior to complete rupture with accumulated exposure to shear stresses that are supraphysiological yet sublethal. Recent investigations that manipulated RBC stress-strain history to induce sublethal mechanical damage of the cell membrane identified that sublethal shear exposure induces: shear-rigidification^{62,102}; remodelling of the membrane biochemistry altering cell electronegativity¹⁰³; and, morphological alterations⁵⁰ possibly indicating instability of junctional attachments of spectrin to the lipid bilayer. Given strong membrane deformations are required to transition from tumbling to tank-treading, RBCs that have been exposed to sublethal mechanical trauma are likely to have altered cell dynamics, may become trapped in tumbling motions, and require greater shear rates to transition to tank-treading¹⁰¹.

Prior exposure of RBCs to supraphysiological shear stresses may also produce an unexpected *increase* in cellular deformation when measured under lower shears, despite obvious decrement of cellular deformation at moderate-to-higher shear stresses⁶². Specifically, laser-diffractometry techniques typically employed in these studies are useful for assessing the mean RBC deformability for an entire sample; as

RBCs increasingly deform, laser-diffraction patterns become more ellipsoidal in shape and thus indirectly provide cell mechanical information. Given this technique is an indirect population measurement, “pseudo-improvements” in cellular deformability in low-shear flows may actually reflect biophysical properties other than solely cell deformability. Bull et al.⁶⁶ identified (with secondary confirmation in a rheoscope) that cell morphology and orientation data influences low-shear ektacytometry, with different orientated elliptocytes producing ‘hazy’ diffraction patterns. An adjunct observation also reported that cell orientation is an important determinant of low-shear ektacytometry values¹⁰⁴, with paradoxical low-shear increases in diffraction elongation indices likely representing increased heterogeneity of cell populations rather than ‘true’ deformation¹⁰⁵. Given a single diffraction pattern is the product of light-scattering from millions of blood cells, different cell subpopulations (e.g., young and old) contribute to the entirety of the output, being overlaid with varying intensity¹⁰⁶. A paradoxical elevated low-shear diffraction elongation index has been observed in blood cells obtained from: clinical populations (i.e., sickle cell anaemia⁶⁵); with morphological alterations⁶⁶; that were glutaraldehyde hardened¹⁰⁷; and, following exposure to sublethal shear damage^{42,50,62-64,108}. Numerous authors hypothesise that low-shear increases in RBC deformability in such conditions known to decrease cell mechanics is likely due to non-alignment of RBCs in flow, and excessive cell tumbling, although conclusive evidence is lacking.

The present study thus examined the behaviour of blood flow for RBCs that had previously been exposed to sublethal and supraphysiological shear stresses, with particular interest in cell orientation to flow. It was predicted these data might elucidate the paradoxical low-shear “increases” in cellular deformability as determined via laser-diffractometry in conditions known to cause impaired cell mechanics.

Materials and Methods

Blood sampling and preparation

Blood was collected from healthy men (age: 27 ± 8 yr; $n = 10$) via routine venepuncture of a prominent vein in the antecubital region of the upper limb using a 21-gauge needle and syringe; the syringe draw was performed slowly to minimise shearing during collection. Immediately following collection, the blood was transferred into a tube containing $1.8\text{mg}\cdot\text{mL}^{-1}$ K₂-EDTA and thoroughly mixed. All experimental procedures were completed within 4 h of initial blood collection. The present study protocol was reviewed and approved by the Griffith University Human Research Ethics Committee (reference number: 2016/712), which conforms with the Declaration of Helsinki.

Experimental design

To investigate the influence of RBC shear-rigidification on subsequent low-shear cell orientation behaviour, the present study employed three experimental stages: i. while previous literature has begun elucidating thresholds that delineate RBC sublethal damage⁶², *Experiment One* sought to confirm magnitudes of sublethal shear stress that induce cell rigidification; ii. using the identified shear magnitude from *Experiment One* that induced the largest cell rigidification, *Experiment Two* sought to examine the magnitude-duration interaction required to alter laser diffractometry and cell mechanics at 0.3 Pa; iii. *Experiment Three* employed the shear magnitude-duration combination of *Experiment Two* that *most* altered low-shear diffractometry at 0.3 Pa to rigidify fresh RBCs before transferring them into a custom built device that enabled concurrent laser diffractometry and optical visualisation during flow at various low-shear stresses. Resultant data were analysed for cellular deformability and cell orientation.

Experiments One & Two: shear magnitudes that rigidify RBCs

In preparation for ektacytometry investigations, fresh RBCs were suspended at 1:200 in a viscous solution (PVP-PBS: 5% polyvinylpyrrolidone in 0.1 mol·L⁻¹ phosphate buffered saline; 290 mOsmol·kg⁻¹, 7.4 pH, 29.9 mPa·s), and 1 mL was injected into the gap of a commercial annular Couette shearing system and ektacytometer (Laser-assisted Optical Rotational Cell Analyser, Mechatronics, Hoorn, The Netherlands) operating at 37°C ± 0.2°C. As previously described⁵⁰, the rotational velocity of the outer cup was manipulated to induce discrete magnitudes and durations of shear exposure (i.e., 1-100 Pa, and 1-300 s) for shear-conditioning and standard RBC deformability tests. A low-powered laser (655 nm, 3 mW) was emitted briefly through the RBC suspension to yield small-scatter diffraction patterns. Diffraction patterns are typically circular for cells at rest (due to their random orientation) and become more ellipsoidal as RBCs deform (and align with flow). An elongation index (EI) was determined across a discrete range of specifically-chosen shear stresses (0.3-3 Pa) by fitting an ellipse to the diffraction patterns using the equation: $EI = (A - B) / (A + B)$, where A is the long axis, and B is the short axis of the ellipse. A mechanical sensitivity index was also calculated using the method previously described in detail⁶², where increases in this index reflect rigidification and heightened susceptibility to subsequent mechanical trauma. For the shear stress magnitude that induced the largest increase in mechanical sensitivity in *Experiment One*, the impact of increasing duration of exposure (5, 10, 60, 300 s) were investigated in *Experiment Two* by inspecting EI-shear stress relationships for *pseudo-improvements* in low-shear deformability. The sample that displayed the largest increase in low-shear EI was chosen as the shear condition to be used in *Experiment Three* of the study.

Development of the ektacytoscope

Investigating single cell dynamics with low-shear ektacytometry required the development and deployment of a custom-built device that combined laser diffractometry and optical visualisation (i.e., ektacytometer and rheometer – “ektacytoscope”) with coaxial design (Fig. 32). This system enabled the concurrent visualisation of a single area of a blood shearing chamber with laser-diffractometry imaging from ektacytometry *and* optical cell visualisation from bright-field microscopy. The shearing/visualisation chamber was constructed with acrylic in a slit-flow rheometer design. The pressure head in the chamber was generated by dual reciprocating syringe pumps with a shear protocol that increased shear stress in a stepwise manner (0.3-5 Pa). The pump control system was automated and time synchronised with the data acquisition devices. The coaxial design was achieved by aligning bright-field visualisation microscopy with co-localisation of an epi-illuminated laser light source. The two imaging systems were overlapped coaxially using 50:50 beam splitters, and the light intensities of the laser and white-light sources were balanced with a variety of neutral density filters in each light path to optimise the captured image clarity and to compensate for backscatter, cross-illumination, and ambient light contamination. Small-scatter diffraction patterns generated from the blood sample were columnated through the condenser lens and subsequently focused onto a complementary metal-oxide-semiconductor (CMOS) sensor. Bright-field microscopy and laser-diffractometry visualisations were recorded and exported to image analysis software for further inspection.

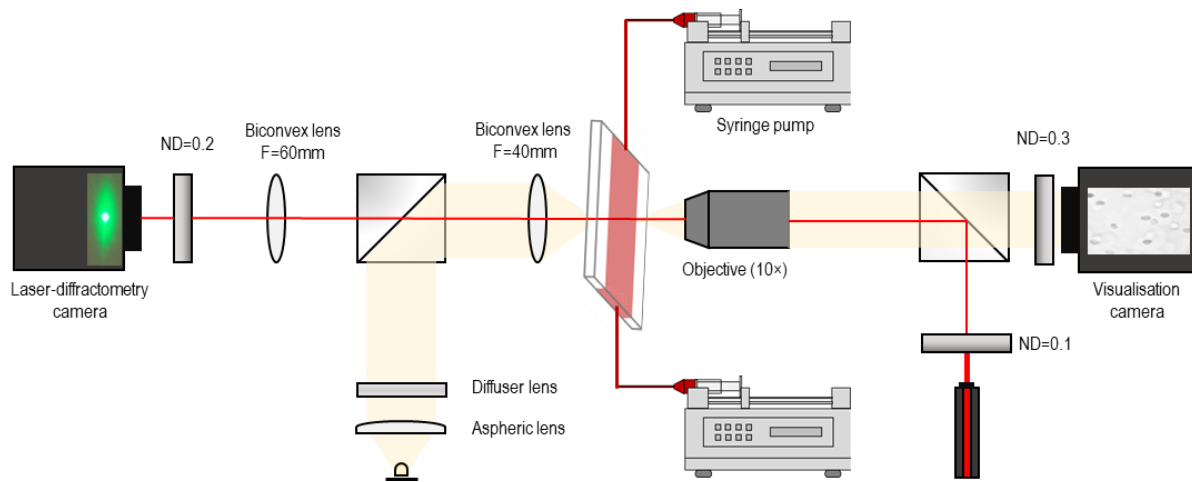


Fig. 32. Design schematic for the custom-built combined slit-flow ektacytometer-rheometer (i.e., the “ektacytoscope”). The designed system facilitated coaxial assessment of blood cells in shear flow with high-speed visualisation and small-scatter laser-diffractometry. ND: neutral density. F = focal length.

Experiment Three: RBC treatment phase and ektacytoscope assessment

Following identification of the shear magnitude-duration combination that yielded low-shear EI increases in *Experiment Two*, fresh RBCs were suspended in the PVP-PBS solution at 6% haematocrit, and 1 mL was then injected into the annular Couette shearing system. The suspension was sheared at 100 Pa for 300 s, and then 600 μL was recovered and transferred into a tube containing 2.4 mL of fresh PVP-PBS (final haematocrit: 2%). This ‘Prior Shear Exposure’ (PSE) RBC suspension was subsequently transferred to the ektacytoscope, using 1 mL to slowly prime the tubing and slit-flow chamber. Once primed and free from air bubbles, flow velocity was confirmed to be zero via visualisation and laser-diffractometry. The syringe pumps were subsequently activated, and velocity was manipulated to achieve peak shear magnitudes that started at 0.3 Pa and increased to 3 Pa in 0.3 Pa increments, followed by two further steps of 4 and 5 Pa. Each shear magnitude was sustained for 15 s, with the last 10 s of each stage being extracted for subsequent analysis; this ensured transitional flow periods were avoided during subsequent data analyses.

Data analysis

Data obtained from traditional ektacytometry in *Experiments One and Two* were analysed with a one-way ANOVA with repeated measures, with emphasis on *post-hoc* comparisons applying the Bonferroni correction to examine low-shear differences. Correlation analyses were performed between markers of cell rigidity (i.e., mechanical sensitivity index) and the EI value at the lowest measured shear (i.e., 0.3 Pa) for all data from *Experiments One and Two*; the mechanical sensitivity index displays cell rigidity as percentage change in deformability relative to unsheared baseline (as previously described elsewhere^{42,50,62}). Video data from *Experiment Three* were captured for visualised cells and laser-diffraction patterns, and subsequent image analysis was performed using custom software routines written in open source software (ImageJ, National Institutes of Health, Bethesda, USA). Following image processing, data were analysed for EI (deformability), angle of orientation, and ellipse fit area. As the visualisation images yielded >300 cells/frame, histograms of the EI distribution were generated to examine population differences between non-sheared (Con) and PSE RBCs. For visual orientation analyses, an ellipse was fitted to each cell in every frame, and cells that had a calculated EI above 0.2 were assessed for orientation relative to the flow vector (0°). Orientation data were grouped into 10° bins for frequency counts and assessed for total frequency and relative differences between PSE and Con RBCs. All statistical analyses were conducted using commercial software (Prism 7; Graphpad Software Inc., San Diego, USA). Significance was determined at an alpha of 0.05. Unless otherwise stated, data are presented as mean ± standard error.

Results

Experiment One: confirmation of shear magnitudes that rigidify RBCs

The mechanical sensitivity index obtained from ektacytometry following RBC treatment with varied magnitudes and durations of shear stress is illustrated in Fig. 33. Exposure to ≥ 5 s of 100 Pa or 75 Pa, or 60 s of 50 Pa significantly increased mechanical sensitivity and RBC rigidity ($p < 0.001$). For any matched duration, 100 Pa shear stress yielded the most pronounced increases in cell mechanical sensitivity.

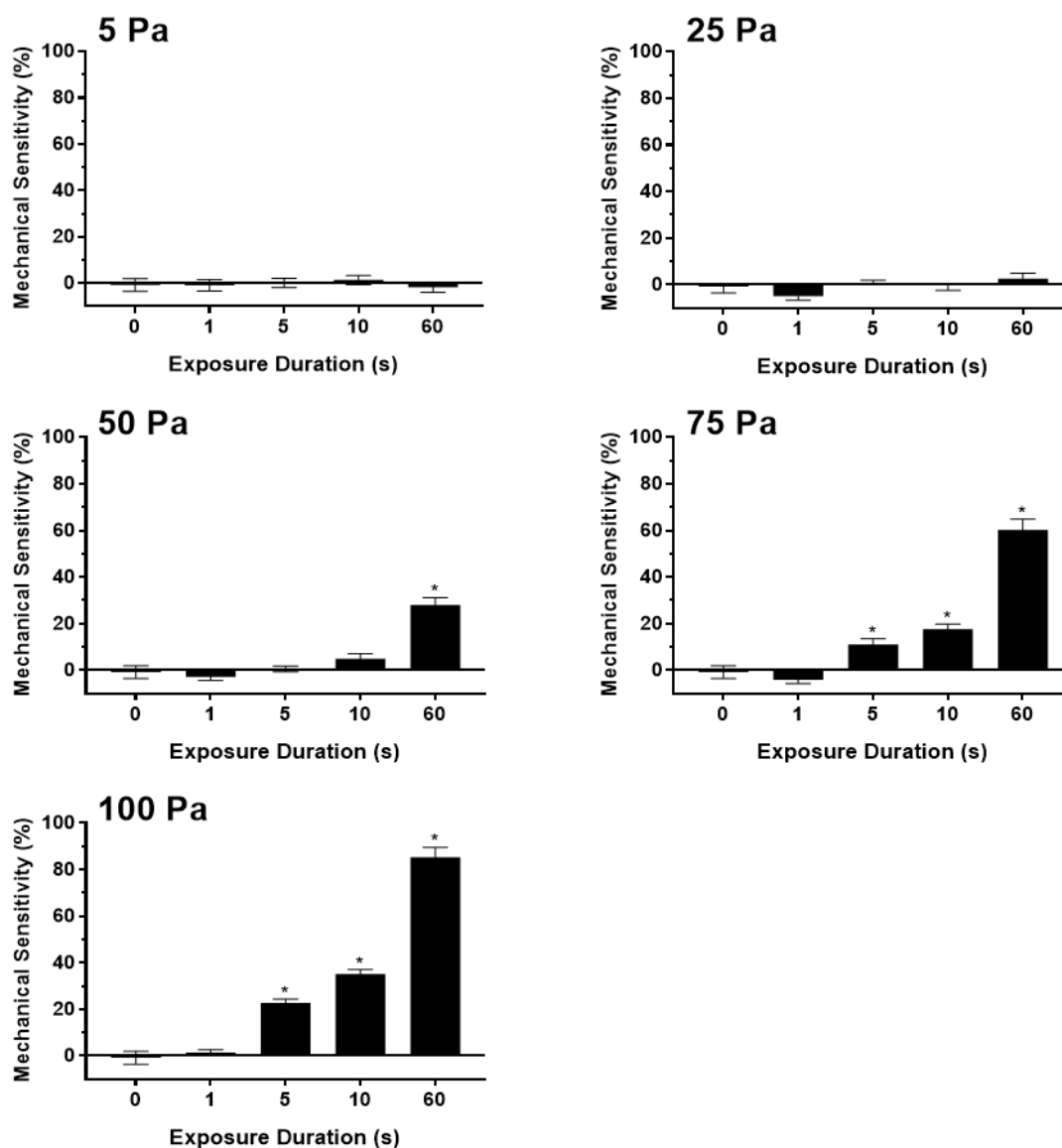


Fig. 33. Mechanical sensitivity (i.e., related to cell rigidity) of fresh red blood cell suspensions exposed to varied magnitude and duration of non-lethal shear stress. *, significantly different to unsheared '0' sample, $p < 0.05$.

Experiment Two: RBC rigidity and low-shear EI

The EI-shear stress ektacytometry curves are illustrated in Fig. 34A for unsheared Con, and RBCs previously exposed to varied durations of 100 Pa. While Con displayed a typical deformability response to shear, at shears ≥ 1 Pa all RBCs prior exposed to 100 Pa required significantly more shear to attain the same level of deformability ($p < 0.001$). Below 1 Pa, however, increased exposure to prior shear augmented low-shear EI values in a dose-response manner, with 100 Pa \times 300 s of prior shear displaying the largest instantaneous EI value at 0.3 Pa.

Using the raw EI-SS curves in *Experiment One* and the data presented in Fig. 34A, Fig. 34B demonstrates a significant positive correlation between mechanical sensitivity (and RBC rigidity) and the instantaneous EI value at 0.3 Pa for grouped shear-magnitude combinations ($R^2 = 0.95$).

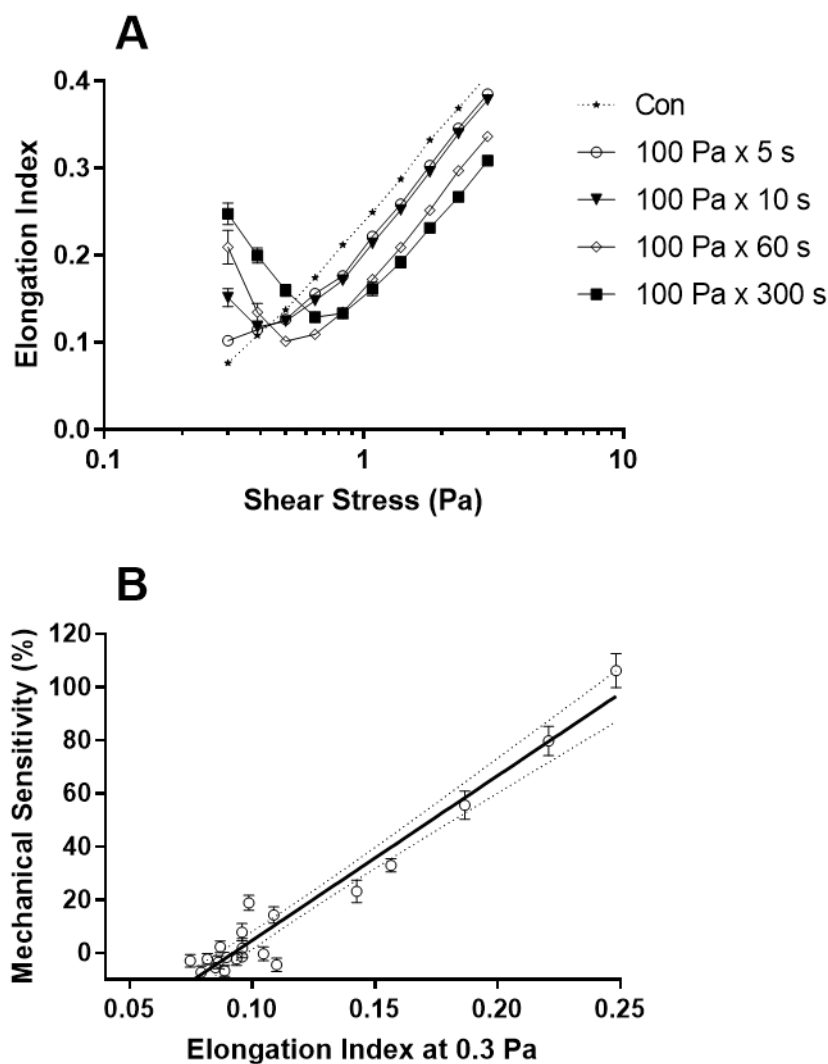


Fig. 34. (A) RBC ektacytometry deformability curves for unsheared Con and RBC suspensions previously exposed to increasing duration of 100 Pa. (B) Relationship of mechanical sensitivity index and the Elongation Index obtained from laser diffraction patterns at 0.3 Pa; $R^2 = 0.95$.

Experiment Three: coaxial ektacytometry and rheometry of RBC deformability

Ektacytoscope-derived deformability analyses of RBC suspensions are displayed in Fig. 35. For RBCs that had Prior Shear Exposure (PSE) to 100 Pa \times 300 s, the laser-derived deformability (Fig. 35A) was paradoxically and yet predictably (*as per Experiment Two data*) increased when measured at 0.3 Pa compared with Con. Further, PSE RBCs exhibited significantly decreased laser-derived deformability when measured at all shears >1 Pa compared with Con ($p=0.001$). Concurrent optically-

derived deformability (Fig. 35B) provided a similar general trend; however, no difference was detected at low-shears for PSE RBCs. Above 1 Pa, however, PSE RBCs exhibited significantly decreased optical deformability ($p < 0.001$); this was consistent with laser-derived analyses. Optical deformability responses less than 1 Pa were significantly elevated compared with laser deformability measures due to several RBCs in the visualisation plane being imaged when rotated away from the camera, thus capturing the side view of a RBC, where the long and short axes are recorded as $\sim 8 \mu\text{m}$ and $\sim 2 \mu\text{m}$ respectively.

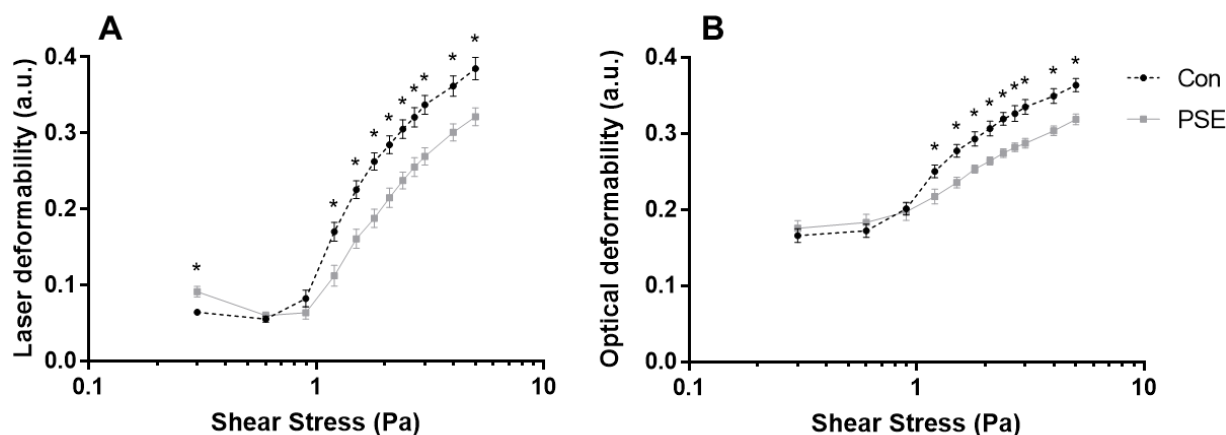


Fig. 35. Coaxial laser-diffractometry (A) and concurrent visualisation rheometry (B) for Con red blood cell suspensions and red blood cells prior exposed to shear (PSE). *, significantly different to Con, $p < 0.05$.

Experiment Three: histograms of RBC deformation

Typical approaches to estimating cellular deformability represent an averaged response for all cells within a given measurement period; however, in the present study a frame-by-frame approach was employed to assess all visible cells to yield a frequency histogram of cellular deformability for a given sample (Fig. 36). Data are presented for PSE cells, and also unsheared Con, under instantaneous exposure to

shears between 0.3 and 5 Pa. At all shears above 0.9 Pa, control RBCs generated increased EI values (i.e., increased deformability) at the modal response. At 0.9 Pa and below, no significant differences were detected between the distributions of measured EI values for unsheared Con and PSE RBCs.

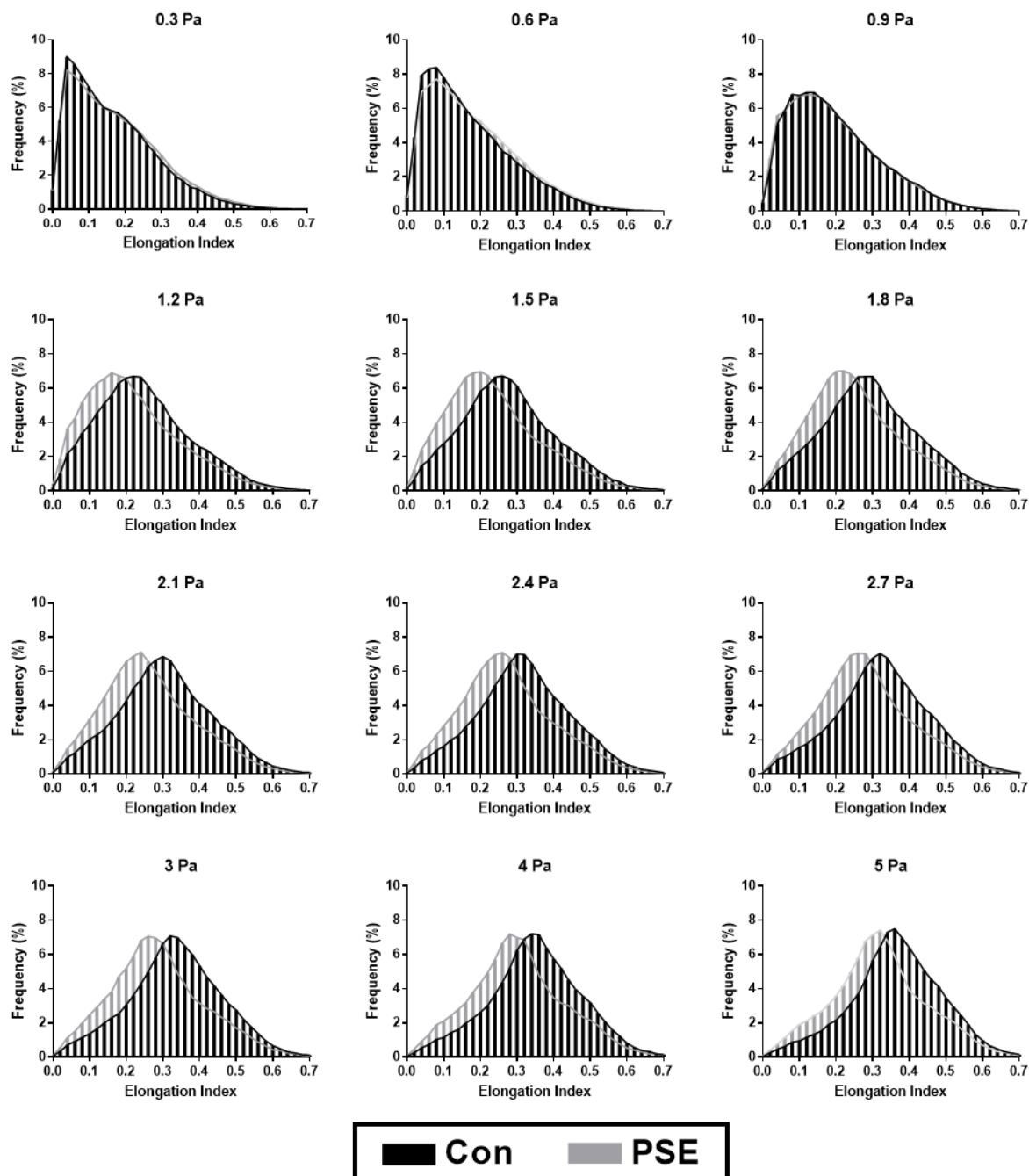


Fig. 36. Frequency distribution histograms of the elongation index of visualised flowing RBCs at discrete magnitudes of instantaneous shear stresses for unsheared Con, and for RBCs with prior shear exposure (PSE).

Experiment Three: RBC orientation at 0.3 and 5 Pa

Given differences in laser-derived deformability at 0.3 Pa could not be explained by concurrent optical deformability, RBC orientation data were compared between PSE and Con at 0.3 Pa (Fig. 37A and 37B) and 5 Pa (Fig. 37C and 37D). In 0.3 Pa shear flow, Con exhibited significantly more RBCs with greater alignment with the flow vector than PSE (i.e., the long axis closer to 0°; $p < 0.001$). This trend was also maintained in 5 Pa shear flow, where equilibrium of cell orientation was less aligned for PSE than Con ($p < 0.001$). The average equilibrium of cell orientation for Con was 9°, while PSE RBCs achieved an average orientation of 12°.

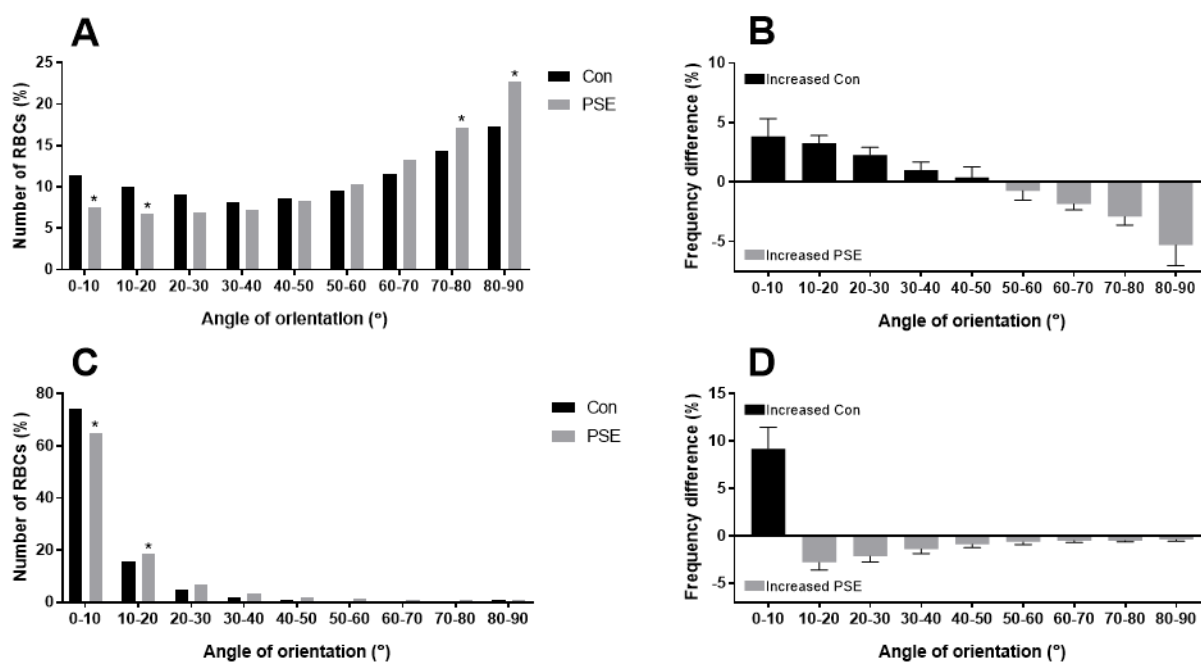


Fig. 37. Frequency of cell orientation for unsheared Con and PSE RBCs in 0.3 Pa (A, B) and 5 Pa (C, D) shear flows. *, significantly different to Con, $p < 0.05$.

Discussion

Since the advent of prosthetic heart valves and the emergence of mechanical circulatory support, there has been avid interest in the effects of supraphysiological shear stresses on blood. While prior works centred on understanding the processes involved in overt blood trauma (e.g., haemolysis; for review, see Olia et al.¹⁰⁹), recent attention has shifted towards more sensitive markers of *functional* blood trauma. The primary objective of the present study was to investigate how exposure of RBCs to sublethal shear stress alters cellular dynamics (especially cell orientation) when those cells are subsequently in low-shear conditions. A secondary aim was to elucidate the observed, but to date unexplained, paradoxical low-shear increase in elongation index (EI) that is derived from laser-diffractometry for RBCs that are previously exposed to high shears. The salient findings of the present study were that following prior high shear exposure: i. RBC deformability was confirmed to significantly decrease; ii. orientation of RBCs with the mean flow vector was significantly less aligned; iii. maximum alignment of RBCs was achieved at a steeper angle; and iv. the heterogeneity of RBC populations increased, with relatively fewer cells maintaining ability to elongate appropriately. Further, it was observed that a marker of RBC rigidity (i.e., mechanical sensitivity index) was correlated paradoxically with elevated EI values at low-shears, following prior exposure of RBCs to high shears. Collectively, the present findings indicate that shear-rigidification and membrane material fatigue alters the behaviour of blood at flow rates that are physiologically relevant. It is further postulated that when RBCs are exposed to high shear stresses, upon entry into lower shears, greater energy is required for orientation and alignment with the mean flow vector. These findings may yield insight into the microvascular dysfunction reported for recipients of mechanical circulatory support and individuals with haematological conditions that alter the biophysical properties of blood.

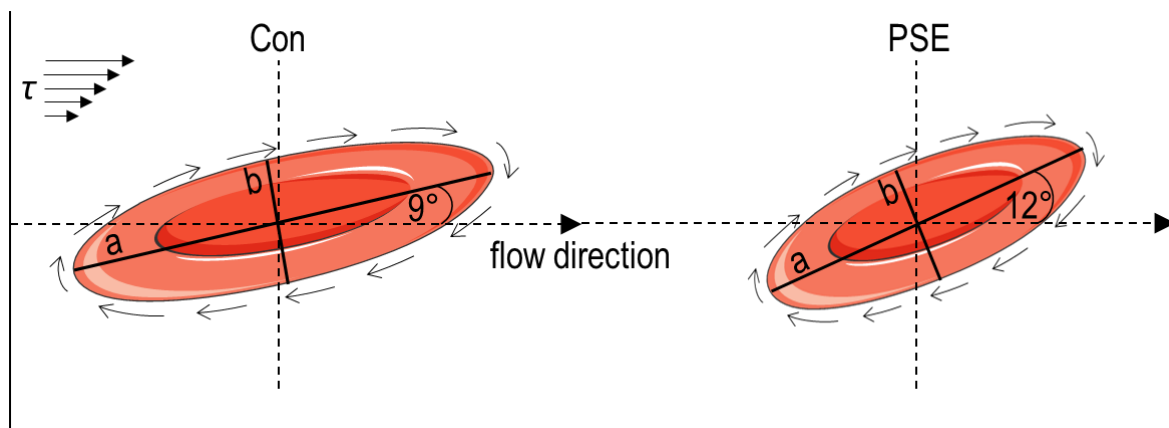


Fig. 38. Schematic of red blood cell dynamics in 5 Pa shear flow for Con and red blood cells with sublethal trauma from prior shear exposure (PSE). PSE red blood cells are less deformable and are less able to align with the flow vector.

In the present study prior exposure to sublethal shear stress significantly decreased RBC deformability *and* hindered the ability of RBCs to orientate in flow. Cellular deformability of RBCs was recently demonstrated to be significantly decreased following prolonged exposure to >38 Pa, and short-term exposure to ~80 Pa⁶². The present findings are consistent with this notion; RBC deformability was impaired in a stepwise fashion with shear stress exposures >50 Pa, but no effect was observed for cells exposed to ≤ 25 Pa (Fig. 33). The results extend the prior literature by identifying that while PSE cells were less deformable, PSE cells also required greater flow velocity to achieve substantial orientation (i.e., 0.9 Pa for shear-rigidified RBCs *versus* 0.5 Pa for Con). The current data supports the hypothesis presented by Fedosov et al.¹⁰¹ that more rigid (less deformable) cells require increased shear flows to facilitate the dynamic transition of tumbling-to-tank-treading movements.

The biophysical properties of RBCs have been demonstrated to significantly impact flow through microchannels of various sizes, with particle deformability and orientation being mediators of wall friction forces and hydraulic resistance in passage

through the microcirculation². In the present study, once a majority of the blood cells had achieved substantial orientation and elongated in higher shears, cells that had been previously exposed to the sublethal shear had steeper angles of misalignment with flow. Given tank-treading movements facilitate energy dissipation of tangential shear stresses to maintain steady shape elongation and orientation with the flow vector⁹⁸, it is likely that in addition to shear-rigidification causing altered transitional movements of tumbling-to-tank-treading, shear-rigidified RBCs may also have diminished ability to tank-tread and dissipate energy in *all* shear flows, thus orientating differently to healthy RBCs. Previous works that employed *in vivo* microcirculatory rat models, identified that infusion of biochemically rigidified RBCs decreased blood flow velocity through capillaries, diminished the number of available perfusion pathways in tissue beds by plugging vessels, and even led to stasis of flow^{110,111}. It is thus plausible that the findings of the present study suggest that shear-induced hinderances in the ability of RBCs to orientate and deform would also likely yield consequences for microcirculatory blood flow and tissue oxygenation.

In the present study, exposing RBC suspensions to sublethal shear stress decreased average cell deformability, yet increased the heterogeneity of the cell populations, indicating that subpopulations of RBCs respond differently to shear. In our recent investigation⁶⁴, it was highlighted that different subpopulations have varied tolerance to sublethal damage, with older (more dense) subpopulations being more susceptible to mechanical trauma than younger cells. It is plausible that the present increases in histogram distribution is resultant of diverse subpopulations with varied mechanical susceptibility; qualitative observations identified varied cell morphologies following exposure to shear. Curiously, while the deformability of most cells decreased, a few cells remained unaltered in their ability to deform and align. Given all cells contribute to the generated diffraction pattern, further inspection into the varied intensities of the captured image might facilitate more rapid discrete subpopulation detection.

Identifying and isolating cells that do not accumulate shear damage would be of value for elucidating potential cellular protective mechanisms.

The present study provides direct optical evidence, for the first time, indicating that low-shear laser-diffractometry measurements of rigid RBCs are mis-reporting the artefact of poor cell alignment and heterogeneity as pseudo-improvements in cellular deformability. While numerous authors have commented on the abnormal low-shear ektacytometry values with conditions that alter cell biophysics^{42,50,62-66,107,108}, without confirmation by visual inspection, many investigations have strategically excluded this data from the analysis processes¹¹². In the design of the present study, with the development of the ektacytoscope, direct investigation of the parallel variables of laser diffractometry and bright-field microscopic visualisation could be performed. The findings elucidate that when low-shear EI values were elevated, cell populations had greater heterogeneity of orientation responses, and required greater shear to achieve substantial orientation (i.e., 0.9 Pa for shear-rigidified RBCs and 0.5 Pa for control).

In the present study, while the elevated low-shear EI value was correlated with marked changes in cell tumbling, morphological characteristics and shape recovery may also contribute to this pseudo-improvement/measurement artefact. No differences were detected in visualised RBC EI values at 0.3 Pa between PSE and Con cells; however, congruent with other reports^{50,59,113}, qualitative observations of shear induced aberrant cell morphologies were noted. Wen et al.¹¹⁴ partly characterised low-viscosity ektacytometry, and identified that cell relaxation responses have fast and slow responses, with the slow variation being required for shape memory and complete morphological recovery. Artmann et al.¹¹⁵ deployed classical micropipette techniques to induce morphological alterations to RBCs, and identified that shear-induced echinocytosis could return to biconcave morphology, albeit the required recovery times were beyond 30 min. Using recovery times similar to that in the present study to transfer between systems, Kuck et al.⁶³ identified shear-rigidification as 'physiologically irreversible'. It is thus possible that in addition to the shear-induced

changes in orientation and tumbling contributing to low-shear EI increases, heterogeneity of cell morphology with aberrant shape modifications may also play a role.

Conclusions

The collective findings elucidate that exposure of RBCs to supraphysiological sublethal shear stresses change cell biophysics in a manner that affect cell dynamics when subsequently in low-shear flow. This finding may illuminate some of the microvascular associated complications in individuals with diseases that alter RBC biophysics, or in individuals receiving high-shear mechanical circulatory support. Further inspection of the small-scatter laser-diffractometry with combined visualisation diffractometry may provide valuable data that can yield new clinical insights for the assessment of subtle rheological disturbances.

Chapter V.

Sublethal mechanical shear stress increases the elastic shear modulus of red blood cells but does not change capillary transit velocity

Antony P. McNamee, Geoff D. Tansley, Michael J. Simmonds

The following Chapter contains a co-authored manuscript submitted for publication. I contributed with: the experiment concept and design, conduction of the experiment, data analysis and interpretation, contributed to reagents/materials/analysis tools, and wrote the manuscript. All authors reviewed and approved the manuscript.

Abstract

The extent to which red blood cells (RBCs) may deform is unique among cells and represents the morphological response to an external mechanical stimulus. Cellular deformability is essential for passage of RBCs through the smallest apertures of the body; decreases in this capacity may lead to ischaemia within dependent tissues. Blood exposure to supraphysiological shear stress within mechanical circulatory support is suspected of reducing cellular deformability, and potentially being primal in several secondary complications in recipients of mechanical circulatory support. Supporting evidence is limited, however, given that no prior works have explored RBC dynamics with the resolution required to determine the shear elastic modulus, and/or cell transit time within capillaries, following exposure to such mechanical stresses. RBCs from healthy donors were thus exposed to 0, 5, 50, and 100 Pa shear stress in an annular Couette shearing system. For comparison, blood was also exposed to heat treatment – a known method that predictably increases RBC membrane shear modulus. Shear modulus assessment required aspiration of RBCs through narrow micropipettes at a known suction force. Cell transit velocities were measured within micro-channels in a region of fully-developed flow. Supraphysiological shear stress significantly increased the elastic shear modulus by 39% and 69% following exposure to 50 and 100 Pa, respectively. Cell transit velocity, however, was unaffected by prior shear exposure. Differences observed were consistent with our internal control (heat treatment), supporting that cell mechanics are significantly impaired following supraphysiological and sublethal shear stress exposure. Given mechanical circulatory support operates at shear stresses consistent with the present study, it is plausible that these devices induce fundamental impairment to the material properties of RBCs.

Introduction

Mechanical circulatory support is commonly used to assist (or replace) the function of native organs during acute surgical interventions and/or chronic organ failure. Over the past half-century, these devices have been continually improved; however, significant complications continue to plague recipients, with “blood trauma” being implicated^{34,46,49}. Blood interactions with foreign surfaces, excessive turbulence, and mechanical stresses can cause dangerous complications of altered blood rheology and organ perfusion (for review, see Nemeth et al.¹¹⁶).

The capability of red blood cells (RBCs) to deform is vital for successful blood circulation and fluidity. The human RBC has a resting diameter of $\sim 8 \mu\text{m}$, and must be able to reversibly stretch, fold, and deform through the smallest capillaries of the body ($< 3 \mu\text{m}$ lumen) to facilitate gas exchange and tissue perfusion¹². The unique capacity of RBCs to endure large deformations and subsequent recovery is predominantly determined by a few key attributes: unlike most cells, RBCs are anuclear and have no organelles; RBCs have a biconcave morphology with a large surface-area-to-volume ratio ($\sim 40\%$ larger than a sphere of the same volume); the RBC membrane is comprised of a highly elastic lipid bilayer connected to a stable latticed protein cytoskeleton; and, RBCs contain a cytosol (principally comprised of haemoglobin) that is more viscous than the extracellular plasma, facilitating energy/force dissipation across the cell membrane. While a RBC is well equipped to repeatedly traverse circulation during its 120-d lifespan, alterations to the cell membrane, cytoskeleton, and cytosol may greatly impact cellular deformability and thus its ability to transit the microvasculature⁹⁵.

Particle deformability is an important determinant of wall friction forces, and thus transit velocity through a tube. The different biophysical properties of RBCs have been demonstrated to significantly impact flow through microchannels of various sizes, where cell geometry (e.g., volume and surface area) predominantly govern entry into

small pores/capillaries ($\sim 3 \mu\text{m}$), and cell viscosity factors (i.e., intracellular *and* membrane viscosity) dictate entry into larger pores/vessels ($\sim 7 \mu\text{m}$)¹¹⁷. The rigidity of the RBC membrane in response to shear stress (i.e., the shear elastic modulus) largely influences RBC-wall friction forces, and transit times while cells traverse smaller vessels¹¹¹. In a recent microfluidic investigation of cancer cells, this notion was reaffirmed as evidenced by stiffer cells traversing more slowly through artificial channels due to stronger friction forces at the wall¹¹⁸. Driessen et al.¹¹⁹, and Lipowsky et al.¹¹⁰, employed *in vivo* rat models to identify that infusion of partially-hardened RBCs (with increased shear moduli) decreased blood flow velocity through capillaries, diminished the number of available perfusion pathways in tissue beds by plugging vessels, and even led to stasis of flow. Further, hardened RBCs were observed to be shunted through large thoroughfare channels, thus skimming past smaller vessels, supporting the notion that blood flows through pathways of least resistance, and especially when cellular deformability is impaired. It follows that ensuing malperfusion of the microcirculation would lead to increased likelihood of localised ischaemic events.

Recent advances in characterising mechanically-induced blood damage identified that shear stress magnitudes that are supraphysiological, yet non-lethal, can negatively impact RBC structure and function as evidenced through: i. aberrations to cell morphology⁵⁰; ii. decreased cellular deformability⁴²; iii. altered cell electronegativity and cell surface chemistry and thus thresholds for cell aggregation/disaggregation¹⁰³; and iv. cell fragmentation⁵⁹. The extent to which these alterations influence *in vivo* haemodynamics remain to be elucidated, although it is hypothesised that altered RBC mechanobiology may propagate malperfusion and/or flow stagnation that lead to poor tissue oxygenation^{110,120}. Despite recent advances in understanding how RBCs are functionally affected by sublethal shear stresses, it remains unknown whether the cell membrane mechanical properties *per se* are affected. The current study thus examined whether a vital material property – the shear elastic modulus – is altered following

RBC exposure to sublethal shear stress, to elucidate the mechanisms underlying altered RBC behaviour.

Materials and Methods

Blood sampling and preparation

In the present study, healthy men (i.e., free from cardiovascular and metabolic comorbidities, and haematological/immune disorders) were recruited to donate blood samples via venepuncture from a prominent vein in the antecubital region using a 21-G needle and syringe; the syringe method was employed with an aspiration rate of $\sim 0.5 \text{ mL}\cdot\text{s}^{-1}$. Once collected, blood was immediately transferred into tubes containing $1.8 \text{ mg}\cdot\text{mL}^{-1}$ K₂-EDTA anticoagulant which were gently mixed for ~ 10 s. Using a haematology analyser (DxH 600, Beckman Coulter, Brea, USA), RBC parameters were subsequently inspected with complete blood cell analysis and confirmed to be within normal ranges. All experimental procedures were completed within 4 hours of initial blood collection. The experimental protocols of the present study were reviewed and approved by the Griffith University Human Research Ethics Committee (reference number: 2016/712), which conforms with the Declaration of Helsinki.

Experimental design

To investigate the influence of sublethal shear stress exposure on RBC shear modulus and subsequent capillary transit velocity, the current study design comprised three main steps: 1. treatment phase – exposing blood samples to discrete magnitudes of shear stress; 2. shear modulus determination via cell aspiration through a minimally-tapered glass micropipette with an inner diameter of $1.2 \mu\text{m}$; and 3. for the cells that had been examined in Step 2, capillary transit velocity and volume measurements were performed immediately after Step 2 with a different minimally-tapered glass micropipette, this time having an inner diameter of $3 \mu\text{m}$.

RBC preparation and treatment phase

Following blood collection, to facilitate accurate shear/viscosity control, the non-Newtonian properties of blood were overcome by diluting the sample ~200 times with a standard-viscosity suspending medium (360 kDa polyvinylpyrrolidone in 0.1 M phosphate buffered saline; viscosity = 29.9 mPa·s, pH = 7.4, osmolality = 291 mOsmol·kg⁻¹). Subsequently, samples were separated into seven groups: 1 × untreated control (Con); 3 × shear conditioned at 5, 50, and 100 Pa; and 2 × heat treatment at 48°C for 5- and 10-min. Shear conditioning was performed in a commercial annular Couette shearing system (LORRCA MaxSis, Mechatronics, Hoorn, Netherlands) operating at 37 ± 0.2°C. Following blood exposure to the experimental condition, 10 µL of the diluted blood sample was mixed into 500 µL of PBS containing 2% w/v bovine serum albumin. Samples were then placed atop of a glass coverslip and transferred to the microscope rig for subsequent analyses.

Micropipette aspiration: rig design

The micropipette aspiration rig used in the present study was retrofitted to an inverted microscope (IX73, Olympus, Melville, USA). As depicted in Fig. 39, the micropipette aspiration rig was constructed of three primary components: micromanipulated glass micropipettes, semi-automated water column pressure control, and microscopic cell imaging using a 60× objective and a CMOS camera (QImaging Corporation, Surrey, Canada). The minimally-tapered glass micropipettes were initially fabricated from borosilicate glass capillary tubes using a micropipette puller (P-1000, Sutter Instrument Company, Novato, USA). To cut the pipettes to an inner diameter (I.D.) suitable for the measurements of the present study, a custom-made microforge was constructed with nichrome wire and a borosilicate glass microbead. Given the micropipette and microbead consisted of the same material properties, a variation of the method described by Engström and Meiselman⁶⁸ was deployed to cut the tips. Briefly, the microbead was heated beyond its softening point before the micropipette

tip was advanced into the microbead to the desired cutting diameter. Once advanced to the required depth, the micropipette was rapidly withdrawn from the microbead and the electric current through the nichrome wire was stopped, allowing the micropipette, microbead, and wire filament to cool and harden. Once all components were hardened, the micropipette was rapidly advanced into the solid microbead with a single action, where the mechanical shock caused the micropipette to bend and fracture at the point which it was previously advanced into the softened bead; a visible impurity/weakness in the shape of the micropipette could be observed at this location.

For the current study, the micropipette rig was constructed with dual micropipettes of different diameters, with the same two micropipettes being used for the entirety of the study (1.2 μm I.D. for shear modulus assessments, and 3 μm I.D. for capillary transit velocity). To preserve the micropipettes between days of testing, each was primed and stored similar to the method reported by Engström and Meiselman⁶⁸, except rather than storing in buffer solution, an enzymatic cleaner was used. The micropipettes were thoroughly rinsed prior to priming with a 30-G needle. During each measurement, precise suction pressure was controlled with the use of water columns constructed with 30 mL fluid reservoirs connected to computer controlled microfluidic syringe pumps. Prior to each measurement the height of the water columns was initially 'zeroed' for suction pressure (note 1 mm of water equates to ~ 9.98 Pa) by ensuring they caused no movement of microparticles or cells near the micropipette tip. To minimise evaporation from the reservoirs throughout the duration of the experiment, the water columns were covered with pierced parafilm.

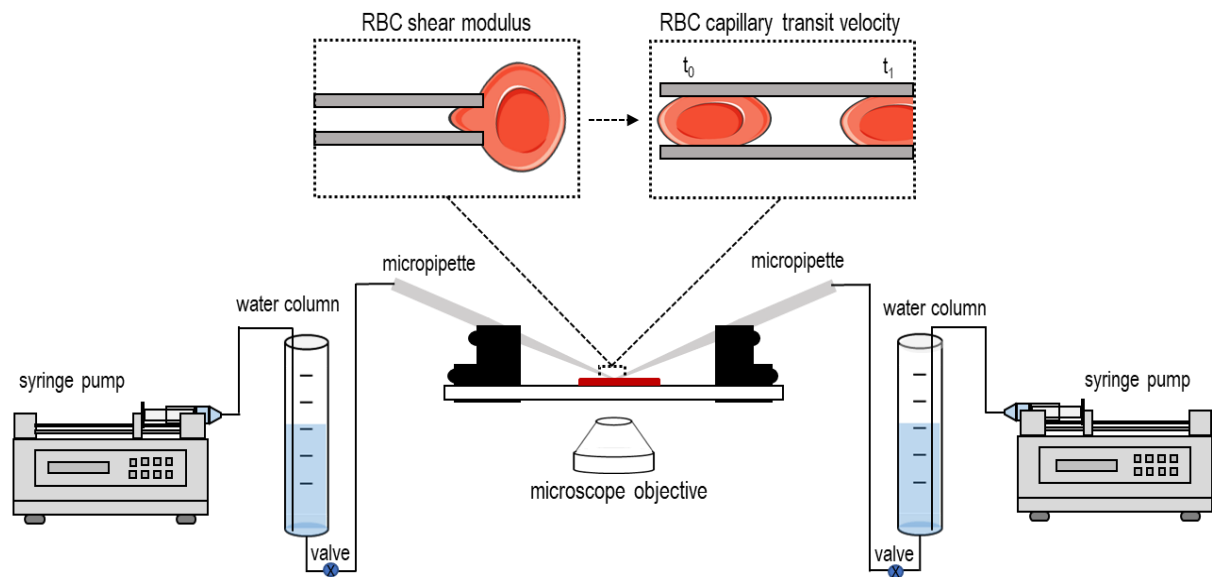


Fig. 39. Schematic of the dual micropipette aspiration rig that was developed for assessment of mechanics and transit velocity of blood cells.

Micropipette aspiration: shear elastic modulus

For the determination of the shear elastic modulus, the smaller 1.2 μm glass pipette was manipulated to be positioned at the surface of a single cell. Using visual feedback of cell/microparticle movement as a guide, the pressure induced by the water column was again confirmed to be zeroed and level with the height of the stage. Using the syringe pump fluidics control, 200 μL was removed and subsequently replaced in the water column to level the meniscus of the fluid and align the direction of pumping to remove motor backlash (if unchecked, this would induce erroneous results in the initial stages of the measurement). Suction pressure was then increased in 5 Pa increments to 50 Pa (or until “cell folding” occurred); this pressure range facilitated measurement of a cell’s shear elastic modulus without inducing hysteresis and shear-hardening. At each pressure increment (ΔP) it was ensured that the aspirated portion of the cell (L_p) had stabilised and reached equilibrium prior to capturing the micrograph image for analysis. Each micrograph frame was analysed for L_p , which was subsequently normalised for the radius of the pipette tip (r_p). Given ΔP and r_p

were known parameters, $L_p \cdot r_p^{-1}$ was linearised against the suction force (pN); suction force was determined by calculating the ΔP exerted across the area of the micropipette tip ($\pi \cdot r_p^2$). The experimental determination of the slope gives the shear modulus (μ) for a single cell in units $\text{pN} \cdot \mu\text{m}^{-1}$.

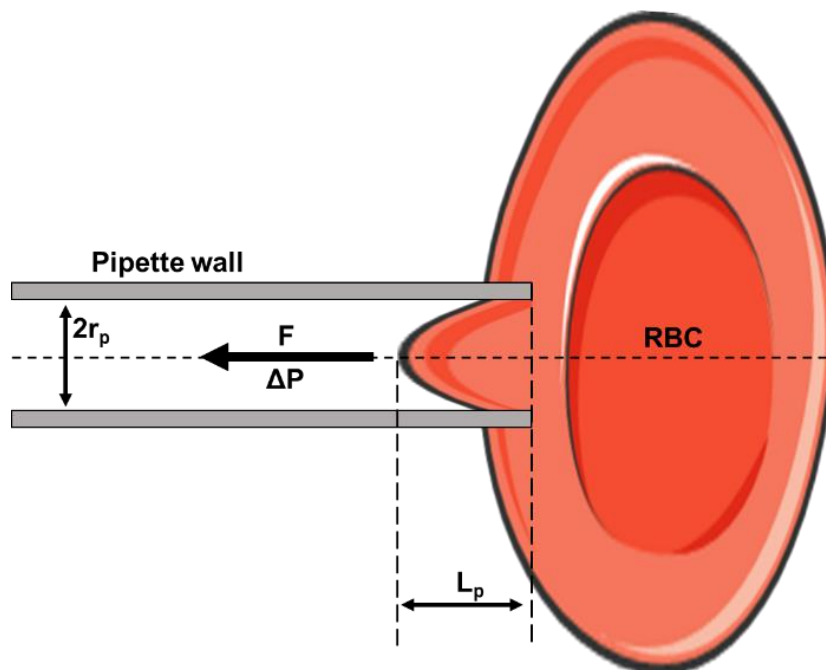


Fig. 40. Micropipette aspiration principle for determining the shear modulus (μ) of single red blood cells. Step 1: the micropipette was manipulated to the surface of the cell membrane. Step 2: aspiration pressure (ΔP) was applied to the inside of the pipette. Step 3: the length of aspirated portion of the cell at the centre of the pipette (L_p) was normalised for r_p and plotted as a function of suction force ($F = \Delta P \cdot \pi \cdot r_p^2$).

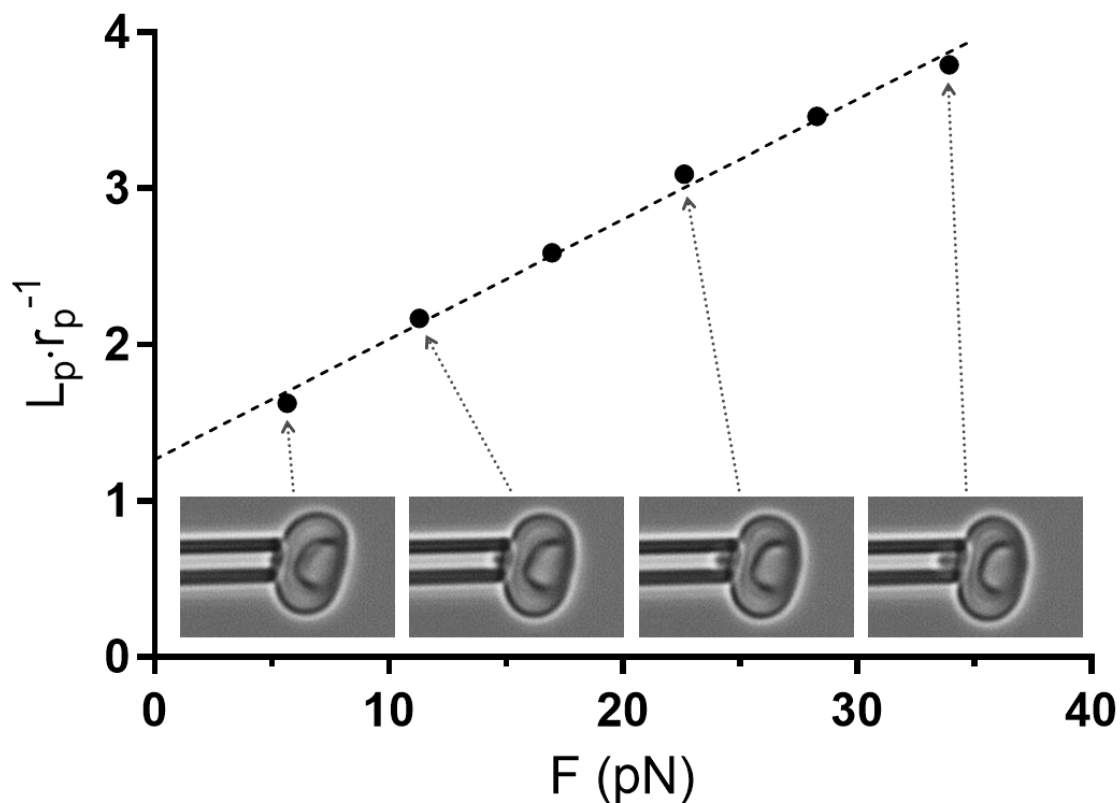


Fig. 41. Aspiration of a red blood cell into a micropipette with a 1.2 μm inner diameter. The reciprocal of the gradient of the line of identity yields the shear modulus (μ), and the y-intercept represents the bending modulus of the membrane.

Micropipette aspiration: volume and capillary transit velocity

After measurement of a cell's shear modulus, the larger glass micropipette (i.e., 3 μm I.D. tip) was used with the micropipette aspiration rig to estimate cell volume and assess capillary transit velocity. Following the initial zeroing of the pressure water column, the larger micropipette was also manipulated to the cell membrane, and 30 Pa of suction pressure was applied to the system. Following entry of the entire cell into the micropipette, micrograph images were captured at 1 Hz. In each captured frame, the length of the cell was measured, and cell volume was estimated by calculating cylindrical volume (assuming excess volume due to curvature at the ends of the cell would account for the fold in the biconcave region). Cell transit velocity (v)

was determined by $d(x)/d(t)$ of RBC centroids (Fig. 42). Given Chien⁹⁵ reported that cell volume is an extremely important determinant of passage through narrow capillaries, velocity data were normalised for individual cell volume.

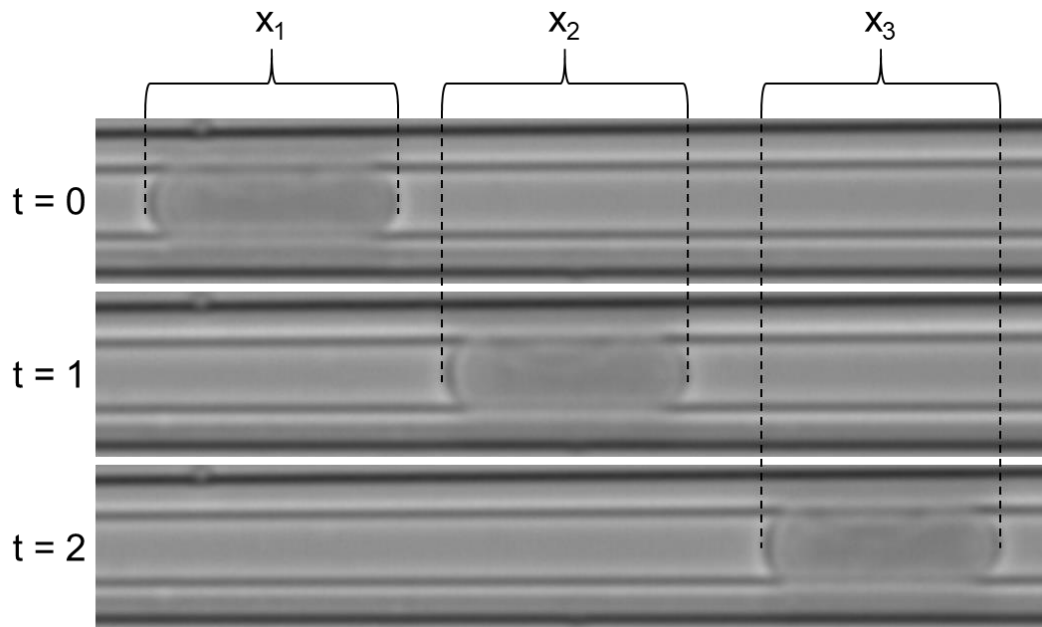


Fig. 42. Identification of RBC $d(x)/d(t)$ for capillary transit velocity (v) measurement.

Statistical analysis

For each individual cell in each experimental condition, shear modulus (μ ; the gradient of $L_p \cdot r_p^{-1}$ vs F), cell volume, and capillary transit velocity (v) were determined. Following confirmation of normality with Shapiro-Wilk test and investigation of Q-Q normality plots, Pearson's correlation and regression analysis were performed. Data (shear modulus, volume, and velocity) from each experimental condition were grouped and compared using a one-way ANOVA with matched repeated measures applying the Geisser-Greenhouse correction where required, and the Bonferroni post-hoc analysis. Significance was determined at an alpha of 0.05. Unless otherwise stated, results are presented as mean \pm standard error.

Results

Haematology

Relevant clinical haematology values are presented in Table 1. All parameters were confirmed to be within normal references ranges for healthy individuals.

Table 1. Relevant haematology results obtained from complete blood count test.

		Normal Range ¹²¹
RBC count ($\times 10^{12}\cdot\text{L}^{-1}$)	4.93 ± 0.12	4.5 – 5.6
Haemoglobin ($\text{g}\cdot\text{L}^{-1}$)	154 ± 3	137 – 172
Haematocrit ($\text{L}\cdot\text{L}^{-1}$)	0.45 ± 0.01	0.40 – 0.50
MCV (fL)	90.3 ± 0.7	83 – 98
MCH (pg)	31.3 ± 0.3	28 – 33
MCHC ($\text{g}\cdot\text{L}^{-1}$)	347 ± 3	320 – 360

RBC: red blood cell. MCV: mean corpuscular volume. MCH: mean corpuscular haemoglobin. MCHC: mean corpuscular haemoglobin concentration.

Cell volume

The volumes of the discrete cells analysed in the present study are illustrated in Fig. 43, clustered for experimental group. Typical values for apparently healthy donors were observed in the untreated (Con) cells, with the average measured volume comparing favourably with the MCV values determined using a commercial cell analyser (Table 1). Significant decreases in cell volume were detected following exposure to 50 and 100 Pa shear stress, and also after heat treatment (HT) – a known

mediator of impaired cell mechanics. Qualitative microscopy observation of the cells (Fig. 44) supported the measured change in cell volume, noting increased prevalence of echinocytes, stomatocytes, and crenated cells following exposure to 100 Pa shear stress, and also after 5 and 10 min of HT.

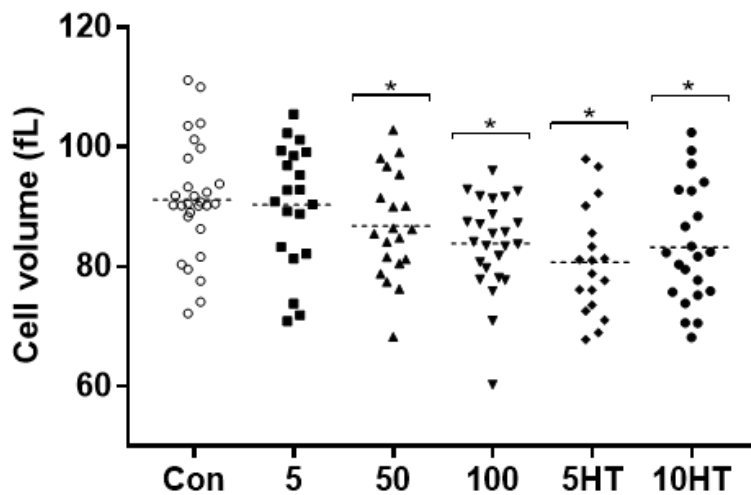


Fig. 43. Cell volume of individual RBCs derived from the micropipette aspiration technique. Shear exposure at 50 and 100 Pa, and heat treatment (HT) for 5 and 10 min, altered the mean and range of cell volume. * significantly different to Con, $p < 0.05$.

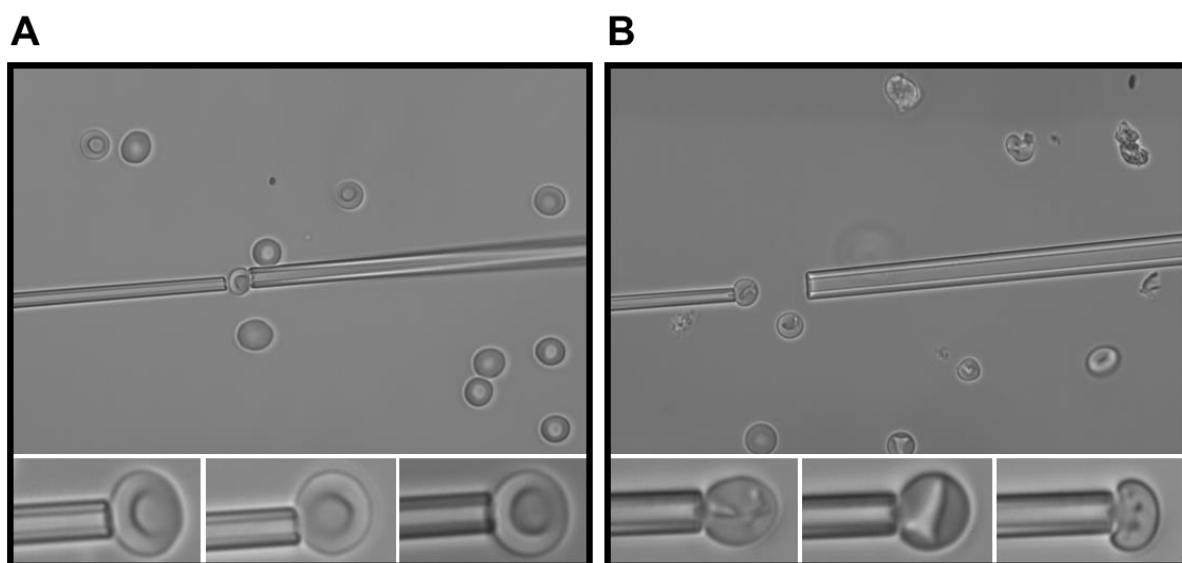


Fig. 44. Micrograph of RBCs undergoing micropipette aspiration for unsheared Con RBCs (A) and RBCs following exposure to the 100 Pa shear condition (B).

Shear elastic modulus ($\text{pN}\cdot\mu\text{m}^{-1}$)

The calculated shear modulus values for individual and grouped cell responses to each experimental condition is presented in Fig. 45. The rigidity of the RBC membrane significantly increased with accumulated shear exposure as well as heat treatment conditions ($F=65.07$, $p<0.001$). All shear conditions (except 5 Pa) increased shear modulus when compared with untreated Con. The heterogeneity of shear modulus values – that is, the spread – increased following experimental treatment incorporating either of shear or heat.

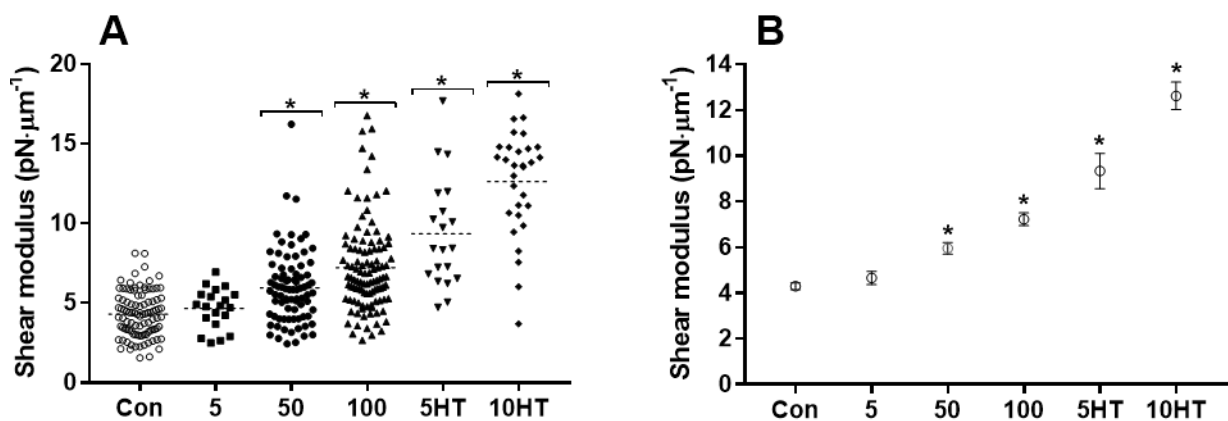


Fig. 45. Individual (A) and grouped (B) shear modulus (μ) of red blood cells determined by micropipette aspiration technique following exposure to varied magnitudes of shear stress or duration of heat treatment (HT; positive control). * significantly different to Con, $p < 0.05$.

Normalised capillary transit velocity

Capillary transit velocity was normalised for individual cell volume and reported for each experimental condition (Fig. 46A); correlations with shear modulus were also examined (Fig. 46B). No significant differences were detected between groups for

normalised capillary transit velocity, nor for correlation with shear modulus values. That is, shear modulus did not dictate capillary velocity in the developed flow region of the defined geometry employed in the present study. Qualitative observations indicated that cells with larger shear modulus values required a longer duration to enter the 3 μm micropipette; e.g., a few extreme cases were observed in the 10HT condition, where complete cell entry into the microchannel required greater than 60 s

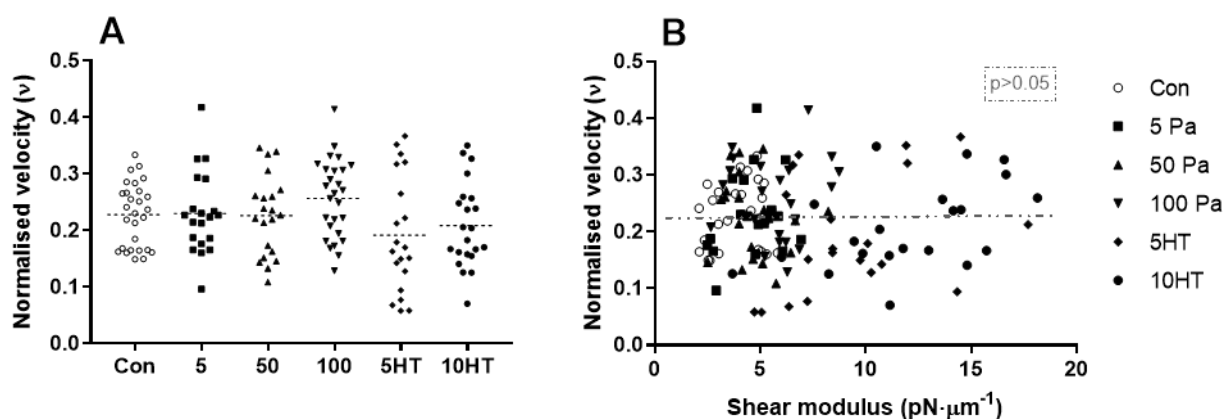


Fig. 46. Normalised capillary transit velocity (A) and correlation of normalised velocity with shear modulus (B) did not significantly change between untreated (Con), shear, and heat treatment (HT) conditions.

Discussion

The salient findings of the present study indicate that when RBCs are exposed to dose-increases of shear stress in a step-wise manner: i. cell volume is decreased; ii. membrane shear modulus and cell rigidity are increased; and iii. cell capillary transit velocity remains unaltered. It was also noted that considerable heterogeneity was observed within each cell suspension – i.e., individual RBCs responded differently to shear stimuli. The collective findings of the present study indicate sublethal mechanical trauma can alter the physical and morphological properties of

RBCs that influences cell entry into small capillaries. Upon cell entry into small apertures, however, transit velocity was unaffected by rigidity and/or deformability. The potential for impaired cell entry into small apertures typical of the microcirculation, and thus also the subsequent challenge to oxygen distribution across the microvascular beds is likely to propagate profound complications. It is possible that these results may explain, in part, the heightened risk of ischaemic complications observed following surgical interventions that expose blood to high-shear environments, such as mechanical circulatory support.

Cell volume significantly decreased following exposure to discrete shear stresses (50 and 100 Pa) that were supraphysiological, yet below the haemolytic threshold (i.e., sublethal domain of shear stress); this was not observed when cells were exposed to physiological shears (5 Pa). Changes in cell volume induce several effects that alter the mechanical properties of RBCs. At a morphological level, direct imaging of cells demonstrates that exposure to increased shear stress is associated with an increased frequency of echinocytes, stomatocytes, and crenation^{46,50,115}; this was confirmed in the present study. These observations of aberrant morphology are associated with increased surface-area-to-volume-ratio, which is consistent with our observation of decreased cell volume following high shear exposure (Fig. 43). Intracellular viscosity of RBCs may also increase following high shear exposure, given cytosolic viscosity is largely dependent upon the concentration of haemoglobin¹²²; efflux of fluid in the absence of membrane rupture results in a relatively increased haemoglobin concentration. While the underlying mechanism of a shear-mediated cytosol loss remains to be determined, it is plausible that fluid-shifts may occur due to passive development of 'leaky' membrane pores, or active mechanotransductive pathways, with evidence supporting Piezo and Gardos channel involvement^{95,123}. Both surface area-to-volume ratio, and cytosolic viscosity, are primary determinants of RBC deformability, and thus the present data suggest these physical properties contribute to cell rigidification following exposure to sublethal shears. The implications of altered

cell properties on blood flow are complex, given that while increased cytosolic viscosity bares negative implications for cell deformability and thus fluid properties, Chien⁹⁵ reported that decreased cell volume may be beneficial for cell transit through narrow capillaries due to decreased wall friction forces.

Exposure of blood to supraphysiological shear stresses, below haemolytic levels at which cell rupture is induced, alter the physical and electrochemical properties of RBCs by remodelling the membrane, denaturing cytoskeletal proteins, and thinning the glycocalyx^{103,124-126}. A number of recent reports have identified that exposure of RBCs to sublethal mechanical trauma also decreases RBC deformability as measured using laser diffractometry^{41,42,50,62}. While laser diffractometry provides high-throughput assessment of the ensemble-average response for RBC suspensions, it lacks single cell resolution which facilitates interrogation of cell subpopulations and cannot provide absolute measurements of cell rigidity (e.g., shear modulus) that are essential for discrete mathematical modelling.

The present study employed classical micropipette aspiration techniques to yield high-resolution data, for the first time in this context, to quantitatively measure the change in membrane shear modulus of RBCs exposed to sublethal shear stress. Exposure to physiological shear stress (i.e., 5 Pa) did not alter the shear elastic modulus of RBCs; however, when RBCs were exposed to sublethal shear stresses (i.e., 50 and 100 Pa), the shear elastic modulus significantly increased by >50% (Fig. 45B). Indeed, a step-wise increase in cell rigidity was observed when RBCs were exposed to 50 and 100 Pa, when compared with unsheared samples, towards levels approaching heat treatment at 48°C for 5 min – a “classic” model of experimental cell rigidification¹²⁷. To our knowledge, this is the first definitive measurement of the cell mechanical properties of RBCs following exposure to sublethal shears, and demonstrates that in addition to cell dehydration induced by mechanical stimulation, cell membrane rigidity is independently increased. Decreases in cellular deformability following exposure to sublethal shears are thus caused by both intracellular and

extracellular alterations, which may be caused by cross-linking of cytoskeletal proteins¹²⁴, formation of pores in the RBC membrane¹²⁸, and spectrin fragmentation^{125,129}.

The current findings also demonstrated that when RBCs are exposed to treatments that increase membrane rigidity, a considerable heterogeneity may be observed in the magnitude of change in the shear elastic modulus (Fig. 45A). When RBCs were exposed to sublethal shear stress, for example, it was clear that while the bulk of cells (and thus the average response) presented with augmented shear elastic modulus, some cells appeared to remain unaffected. A similar response was even observed for a handful of cells that were heat treated at 48°C for 10 min – an extreme treatment used to induce rigidification. The present data thus highlights that blood cells do not respond uniformly to “damaging” interventions, including sublethal mechanical stresses. This heterogenic response for the shear elastic modulus of single RBCs following exposure to sublethal mechanical stress has not been previously reported, and precise mechanisms dictating (non)response to shear damage remain to be elucidated. Recent work⁶⁴ presents a plausible explanation, however, for such disparity in the present individual cell responses: subpopulations that arise due to physiological “aging” respond differently to mechanical shear, where the most dense RBCs (older cells) accumulate shear rigidification at more than twice the rate of the less dense counterparts (younger cells).

Particle deformability has consistently been identified to be an important determinant of wall friction forces, and thus transit velocity. In a recent microfluidic investigation of cancer cells, this notion was reaffirmed with stiffer cells flowing slower due to stronger friction forces at the wall¹¹⁸, with the membrane viscous interface likely being more important than the elasticity of the particle itself¹³⁰. In contrast to prior studies^{111,119,120} which observed that diamide rigidified RBCs had reduced flow velocity and even resulted in irreversible clogging of small apertures, no changes in cell capillary transit velocity were observed in the present study. It is plausible that the

changes in cell volume following shear-rigidification resulted in reduced wall contact, compensating for increased friction forces, and thus yielding no net change in transit speed. Moreover, given tube geometry is a primary determinant of flow, the interaction between cell membrane mechanics, cell volume, and capillary geometry needs to be considered, with our present findings being representative of similar (i.e., $\sim 3 \mu\text{m}$) rigid tubes. It was directly observed, however, that despite transit velocities being unaffected by shear modulus, the most rigid cells in the present study required longer duration to orientate and *enter* the micropipette at a given suction force. It is plausible that this novel observation may have more profound implications for biological function than cell transit velocity itself: if cells do not orientate with flow or are margined in bulk flow due to altered cell mechanics, malperfusion and/or flow stagnation may propagate in smaller vessels that lead to poor oxygen delivery within the vascular bed, and potential localised ischaemic events^{110,120}.

The findings of the present study are meaningful given the increased reliance on mechanical circulatory support in various forms of medical intervention. The shear stresses that exist within mechanical circulatory support, while low enough to avoid overt cell rupture, have been recently thought to negatively impact blood cell and plasma protein function¹⁰⁹. The present study provides direct evidence, for the first time, that sublethal shear stresses also increase the shear elastic modulus of RBCs. This finding has profound implications for microvascular function; if severely rigid cells remain in circulation and are not promptly sequestered or phagocytosed, sluggish/slow flow is likely to ensue and lead to localised ischaemic events. These findings thus also lend support for further evaluation of current medical pumps that exert supraphysiological stresses on blood, and the potential clinical complications that may be independent of the primary pathology itself. This knowledge will tangibly lead to improved blood compatibility and thus design of blood-contacting medical devices.

Chapter VI.

Oxidative stress increases erythrocyte sensitivity to shear-mediated damage

Antony P. McNamee, Jarod T. Horobin, Geoff D. Tansley, Michael J. Simmonds

The following Chapter contains a published co-authored journal article. I contributed with: the experiment concept and design, conduction of the experiment, data analysis and interpretation, contributed to reagents/materials/analysis tools, and wrote the manuscript. All authors reviewed and approved the manuscript.

Publication details: McNamee AP, Horobin JT, Tansley GD, Simmonds MJ. *Oxidative stress increases erythrocyte sensitivity to shear-mediated damage*. *Artificial Organs*. 2018. **42**(2): p. 184-192.

Abstract

Patients receiving mechanical circulatory support often present with heightened inflammation and free radical production associated with pre-existing conditions in addition to that which is due to blood interactions with non-biological surfaces. The aim of this experimental laboratory study was to assess the deformability of red blood cells (RBCs) previously exposed to oxygen free radicals and determine the susceptibility of these cells to mechanical forces.

In the present study, RBCs from 15 healthy donors were washed and incubated for 60 min at 37°C with 50 μ M phenazine methosulphate (PMS; an agent that generates superoxide within RBCs). Incubated RBCs and negative controls were assessed for their deformability and susceptibility to mechanical damage (using ektacytometry) prior to the application of shear stress, and also following exposure to 25 different shear conditions of varied magnitudes (shear stress 1, 4, 16, 32, 64 Pa) and durations (1, 4, 16, 32, 64 s).

The salient findings demonstrate that incubation with PMS impaired important indices of RBC deformability indicating altered cell mechanics by ~19% in all conditions (pre and post exposure to shear stress). The typical trends in shear-mediated changes in RBC susceptibility to mechanical damage, following conditioning shear stresses, were maintained for PMS incubated and control conditions.

We demonstrated that free radicals hinder the ability of RBCs to deform; however, RBCs retained their typical mechanical response to shear stress, albeit at a decreased level compared with control following exposure to PMS. Our findings also indicate that low shear exposure may decrease cell sensitivity to mechanical damage upon subsequent shear stress exposures. As patients receiving mechanical circulatory

support have elevated exposure to free radicals (which limits RBC deformability), concomitant exposure to high shear environments needs to be minimised.

Introduction

Oxygen free radicals are important for an array of normal physiological processes, including cell-cell signalling, immune defence and mitogenesis¹³¹: when unregulated, however, free radicals may contribute to the pathogenesis of numerous systemic disease states. Specifically, when reactive oxygen species, such as superoxide (O_2^-), hydroxyl radical (OH^\cdot), peroxy radical (OH_2^\cdot) and hydrogen peroxide (H_2O_2) overcome cellular antioxidant defence mechanisms (i.e. "oxidative stress"), damage to local tissue is observed which may precipitate various disease states¹³².

Throughout the circulatory system, red blood cells (RBCs) are susceptible to oxidative stress due to their direct exposure and interaction with large quantities of oxygen¹¹. In healthy individuals, reactive oxygen species are produced within RBCs by the oxidation and reduction of ferric (Fe^{3+}) to ferrous (Fe^{2+}) iron in the haem complex, which facilitates oxygen binding, transport, and unloading¹³³. While this reaction provides a continuous source of intracellular reactive oxygen species, the antioxidant defence system of the RBC is well equipped to prevent such oxidative stress¹¹. Extrinsic to the RBC, however, reactive oxygen species can be produced by glucose oxidation¹³⁴, biocompatibility issues with mechanical assist devices and extracorporeal circulation, and superoxide dismutase within mitochondrial oxidative phosphorylation^{135,136}. Given the continual free radical production from intra- and extracellular sources, any mismatch between the development of reactive oxygen species and their subsequent removal may overcome systemic antioxidant defence mechanisms, damaging cellular components and membrane surfaces, making them more susceptible to further damage³⁷.

Blood fluidity and organ perfusion are highly dependent upon the ability of RBCs to disaggregate and deform in response to mechanical forces¹⁹. Oxidative damage can

have an extensive influence on blood fluidity by altering the mechanical properties of RBCs¹³⁷ and diminishing endothelial function^{132,138}; to such an extent that oxidative stress has been identified to contribute to various circulatory diseases, such as diabetes, cardiovascular disease, and ischaemic stroke^{131,132,134,139}. Specifically, oxidative damage can contribute to alterations in the biochemical and mechanical properties of individual cells and thus the resultant bulk flow of blood by altering various properties of RBCs. The presence of reactive oxygen species can cause: digestion of the RBC surface membrane by cytoplasmic enzymes causing protein degradation and lipid peroxidation^{140,141}; direct quenching of nitric oxide, decreasing its bioavailability¹⁴²; and, physical rigidification of the RBC membrane via increased spectrin-haemoglobin crosslinking¹⁴⁰. Biochemical and mechanical changes to RBCs secondary to oxidative damage may result in hindered cellular function, particularly the capacity of the RBC to deform in response to shear stress, which may ultimately precipitate overt haemolysis⁷⁶.

Understanding the rheological functioning of blood and its response to shear stresses within, and superseding, the physiological range is of scientific and clinical interest for predicting an individual's response/success to the use of mechanical circulatory assist. Current investigations that test mechanical device biocompatibility and rheological damage, often investigate rates of RBC haemolysis subsequent to supraphysiological shear stress exposure, commonly studying blood obtained from healthy donors. Given that mechanical assist devices now have the capacity to minimise haemolysis (although they still operate in the supraphysiological domain of shear stress⁸²), and oxidative stress is highly prevalent in the diseases indicated for mechanical circulatory assist, novel methods are currently being explored to characterise and minimise blood damage associated with the combined exposure to shear stress and oxygen free radicals¹⁴³.

To investigate and describe the changes in RBC populations following exposure to subhaemolytic shear stress, Simmonds and Meiselman⁵¹ employed a standardised

method of assessing magnitude-duration effects of a conditioning shear stress on subsequent RBC deformability and Mechanical Sensitivity. The standardised method allowed for the: i. characterisation of shear-mediated changes in RBC sensitivity to mechanical stress; and, ii. identification of a “subhaemolytic damage point” – i.e. the critical point at which shear stresses induced mechanical damage to RBCs, significantly decreasing RBC deformability under subsequent shear exposure. Given the original method was developed using blood from healthy donors, it remains unknown whether factors known to alter RBC mechanics (e.g. oxidative stress) also influence the subhaemolytic damage point. The findings provided by such data could be further developed into future models to: i. predict individual patient mechanical assist device success; and, ii. provide a basis for new haemocompatibility criteria. The aim of the present study is to examine and characterise the shear-mediated changes in RBC deformability, and the subhaemolytic damage point, of RBC suspensions previously exposed to oxygen free radicals.

Materials and methods

Subjects and sampling

Fifteen healthy men (28 ± 8 yr) volunteered to participate in the present study. Inclusion criteria required that participants were free from: cardiovascular and metabolic comorbidities, or haematological/immune disorders. After informed consent was obtained, participants were invited to the laboratory facility to supply a blood sample. Blood was collected from a prominent vein in the antecubital region within 90 s of the application of a tourniquet, using a 21-gauge needle and syringe, and transferred into tubes containing the anticoagulant dipotassium ethylenediaminetetraacetate (K_2 -EDTA) at a concentration of $1.8 \text{ mg}\cdot\text{mL}^{-1}$. All experimental procedures were completed within 4.25 h of blood collection. The experimental protocols were reviewed and approved by the Griffith University

Human Research Ethics Committee (Protocol number: AHS/21/15/HREC), which conforms with the Declaration of Helsinki.

Experimental design

Changes in RBC deformability in response to varied duration and magnitude of shear stress exposure were explored using RBC suspensions incubated for 60 min with/without a free-radical generating agent – the samples incubated without a free-radical generating agent were considered to reflect normal “Control” responses to shear stress exposure. The experimental design involved three phases for each of these conditions: 1) determination of RBC deformability without prior exposure to shear stress (i.e. “unsheared”); 2) exposure of fresh RBCs to a conditioning shear for a specific duration at a discrete shear stress; 3) the subsequent and immediate measurement of deformability of the RBCs exposed to the conditioning shear (i.e. during “2”, above). To quantify the potential altered RBC mechanics due to *ex vivo* ageing (i.e., blood storage), RBC deformability of “unsheared” cells were repeated at the end of each experiment.

Sample preparation – oxidative stress

Following blood collection, whole blood samples were immediately centrifuged at 1500 g for 10 min and the plasma and the buffy white coat were aspirated from the sample, leaving isolated packed RBCs. RBCs were washed twice with phosphate buffered saline (PBS; pH = 7.40, 287 mOsmol·kg⁻¹), centrifuged at 1500 g for 5 min, and then resuspended at ~0.4 L·L⁻¹ haematocrit in a solution of 5 parts PBS and 1 part bovine serum albumin (BSA; 1% in PBS). RBC suspensions were subsequently incubated for 1 h at 37°C with 50 µM phenazine methosulphate (PMS) solution; an agent that generates superoxide within RBCs, thereby inducing oxidative stress¹³². The specific concentration of PMS solution allowed for significant production of superoxide anions without inducing alterations to normal cell morphology¹⁴⁴, which

was confirmed during development of the present experimental procedures. Blood samples from a subset of the cohort ($n = 9$) were treated in the same manner as described above, although following resuspension of the washed RBCs in PBS with BSA, PMS was not added. As these cells were not exposed to the free radical generating agent during incubation, collected data were considered to reflect normal “Control” responses to shear stress exposure.

Following incubation, RBCs were separated from supernatant by centrifugation at 1500 g for 5 min. RBCs were then washed twice with PBS and isolated RBCs were stored in a tube until immediately prior to the application of shear stress and deformability measures. Samples were prepared for shear stress exposure and deformability measurement by suspending 25 μL of RBCs at a haematocrit of 0.5% in 360 kDa polyvinylpyrrolidone (PVP; 29.6 mPa·s, pH = 7.30, 296 mOsmol·kg⁻¹). For the application of shear stress and ektacytometry, 1 mL of each RBC suspension was inserted into a Couette shearing system.

Application of conditioning shear stress

An annular Couette flow shearing system and ektacytometer (Laser-assisted Optical Rotational Red Cell Analyser; LORRCA MaxSis, Mechatronics, Hoorn, Netherlands) operating at $37 \pm 0.2^\circ\text{C}$ induced a controlled conditioning shear stress to RBC suspensions. Shear stress exposure varied in magnitude and duration, ranging from 1 Pa for 1 s to 64 Pa for 64 s. Twenty-five preconditioning shear stress conditions were thus employed in the present study – shear stress magnitudes were 1, 4, 16, 32 and 64 Pa, which were all applied for durations of 1, 4, 16, 32 and 64 s. Freshly prepared RBC suspensions were used for all investigations and were conditioned and analysed within 5 min of preparation.

RBC deformability measures

Immediately following RBC exposure to a specific conditioning shear stress, RBC deformability measures were conducted using low-power laser-light diffractometry to measure the diffraction pattern of RBC suspensions across a discrete range of shear stresses (0.3–50 Pa). The diffraction pattern was circular for cells at rest and became progressively ellipsoidal as RBCs deformed¹⁴⁵. The diffraction pattern was captured by an integrated digital camera and analysed in real-time by fitting an ellipse to a region of interest. An Elongation Index (EI) of the diffraction pattern, indicating the instantaneous morphology of the RBCs, was calculated:

$EI = (\text{length} - \text{width}) / (\text{length} + \text{width})$, based on the geometry of the ellipse.

Data analysis

The raw EI-shear stress data provided by the ektacytometer for deformability measures were transferred into analytical software (Prism 6, Graphpad Software Inc., San Diego, USA), and a non-linear curve of the Lineweaver-Burk equation was fitted to the raw EI data. To improve the goodness of fit to the EI-shear stress deformability curve, EI values below 0.94 Pa (which were atypically elevated following specific prior shear conditions) were excluded from the curve-fit analysis for all conditions²⁵. The non-linear curve-fitting algorithm enabled the determination of the value for: i. the maximum theoretical EI at an infinite shear stress (i.e. EI_{\max}), and; ii. the shear stress required to induce half maximal EI (i.e. $SS_{1/2}$). Decreased RBC deformability is associated with an increased $SS_{1/2}$ and decreased EI_{\max} . While these parameters describe the RBC deformability response, Baskurt and Meiselman¹⁴⁶ identified that these variables are not always in agreement for cells with abnormal mechanical behaviour; however, the ratio of $SS_{1/2}:EI_{\max}$ is a valid measure that provides a more robust parameter of RBC deformability when comparing various RBC populations. Increases in $SS_{1/2}:EI_{\max}$ are indicative of decreased RBC deformability, and *vice versa*.

Given impairments in RBC deformability lead to detrimental functional implications, including the diminished regulation of microcirculatory blood flow and the precipitation of complete cell destruction^{37,76}, an index of RBC susceptibility to mechanical damage was expressed by calculating the differences in $SS_{1/2}:EI_{max}$ relative to control measures (prior to shearing), as a percentage of the control value^{25,50}:

$$\text{Mechanical Sensitivity (\%)} = \frac{(SS_{1/2}n:EI_{max}n) - (SS_{1/2}Con:EI_{max}Con)}{(SS_{1/2}Con:EI_{max}Con)} \times 100$$

where n represented the specific level-duration of shear stress exposure, and Con represented the unsheared value.

Positive values of the Mechanical Sensitivity index indicate decreases in RBC deformability relative to control and thus functional impairments, while negative values correspond to enhancements in RBC deformability measures and functionality²⁵.

Mean Mechanical Sensitivity data for all subjects was collated into an x, y, z matrix, where the mean Mechanical Sensitivity measure was the z axis, and shear stress duration and magnitude were the x and y axis respectively (Origin, OriginLab Corp., Release 9, Northampton, USA). Thin-plate splines were employed to interpolate raw x, y, z values, and a surface mesh plot was overlaid to facilitate visual identification of the subhaemolytic threshold. The subhaemolytic damage point was considered to occur at the 95% confidence interval (C.I.) above the calculated mean of all samples not significantly different to control. If discrete experimental values were positive and > 95% C.I., impairments to RBC deformability were considered to have occurred. By contrast, if discrete negative values were measured and < -95% C.I., enhanced RBC deformability was considered to have occurred. All values between -95% and +95% C.I. of the control mean were considered to be unaltered by the conditioning shear stress protocol.

To assess changes in the shear-mediated responses of the Mechanical Sensitivity index between the surface mesh of the experimental PMS plot and the control plot, a delta Mechanical Sensitivity was determined by subtracting the control matrix from the PMS matrix. The calculated delta 64×64 matrix was also presented as a surface mesh to assist visual representation of shear induced changes in Mechanical Sensitivity of experiment samples (relative to control).

Statistical analysis

Normality of data were confirmed with Shapiro-Wilk test, with investigation of kurtosis and skewness of the data. Baseline changes in EI–shear stress curves were investigated using a one-way ANOVA with matched repeated measures applying the Geisser-Greenhouse correction where required. An independent samples *t*-test was applied to determine significant differences in the group mean of the $SS_{1/2}:EI_{max}$ data of PMS and control samples prior to shear stress exposure. Following shear stress exposure, however, the $SS_{1/2}:EI_{max}$ data were analysed using a multifactorial ANOVA with repeated measures and post hoc tests using the Bonferroni correction. Significant variations in the $\Delta SS_{1/2}:EI_{max}$ were analysed relative to the mean using a one way ANOVA with repeated measures (applying the Bonferroni correction). Significance was determined at an alpha of 0.05. Unless otherwise stated, results are presented as mean \pm standard error.

Results

RBC deformability prior to conditioning shear stress

The EI at given shear stresses of RBCs incubated for 60 min in the presence/absence of PMS, prior to the exposure to conditioning shear stresses (i.e. unsheared), are illustrated in Fig. 47. The EI (indicating RBC deformability) exhibited a typical sigmoidal response across the varied and discrete shear stresses of 0.3–50 Pa. The maximal theoretical EI (EI_{max}) was 0.648 ± 0.002 for PMS and 0.644 ± 0.002 for Con, and the amount of shear stress required to induce half of EI_{max} (i.e. $SS_{1/2}$) was 2.00 ± 0.03 for PMS and 1.67 ± 0.02 for Con. A significant main effect for condition was detected ($F = 19.29$, $p < 0.001$). The EI was significantly decreased in the PMS condition at low shear values of 0.53, 0.94, 1.65 and 2.91 Pa ($p < 0.05$). No significant differences between conditions were detected at higher shear stresses.

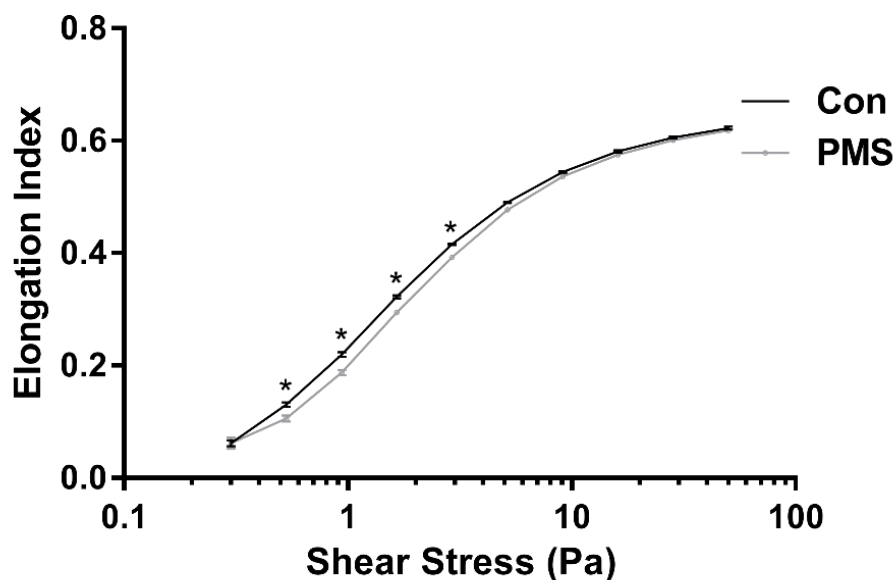


Fig. 47. The Elongation Index (i.e. deformability) of RBC suspensions previously incubated for 60 min with PMS, and without (Con), across a discrete range of shear stresses (0.3–50 Pa), before exposure to conditioning shear stresses. Significantly different between Con and PMS *, $p < 0.05$.

The ratio of $SS_{1/2}:EI_{max}$ for RBC suspensions incubated for 60 min either in the presence/absence of PMS prior to the application of a conditioning shear stress is illustrated in Fig. 48. Samples incubated with PMS display significantly increased $SS_{1/2}:EI_{max}$ when compared to Con ($t = 6.23, p < 0.001$).

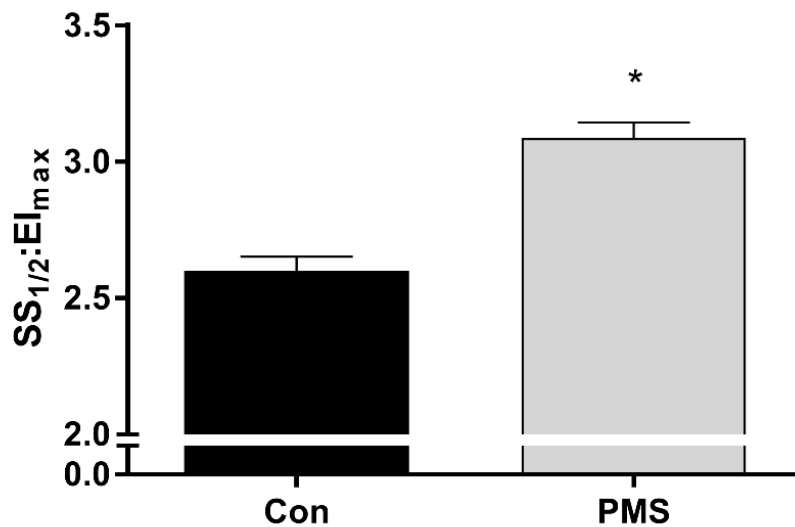


Fig. 48. $SS_{1/2}:EI_{max}$ parameterisation of RBC deformability for Con and PMS incubated samples, prior to conditioning shear stress exposure. Significantly different *, $p < 0.05$.

Effects of prior conditioning shear stress exposure on RBC deformability

The $SS_{1/2}:EI_{max}$ (i.e. deformability) for RBC suspensions exposed to 25 discrete shear stress magnitude–duration combinations are presented in Fig. 49 for Con and PMS. PMS-treated RBCs displayed significantly increased $SS_{1/2}:EI_{max}$ compared with Con RBCs, reflecting decreased RBC deformability for all magnitudes and durations of shear stress ($F = 84.03, p < 0.001$). While PMS-treated RBCs exhibited significantly less deformability than Con, relative to unsheared PMS-treated RBCs, PMS-treated RBCs sheared at 64 Pa for ≥ 16 s observed a significant increase in $SS_{1/2}:EI_{max}$. Conversely, following combinations of 32 Pa for 32 s, 16 Pa for ≥ 16 s, and 4 Pa for ≥ 32 s, the $SS_{1/2}:EI_{max}$ of PMS-treated RBCs significantly decreased relative to its matched unsheared PMS incubated sample (i.e., indicating relative improvements in RBC

deformability). Despite improvements in RBC deformability relative to unsheared PMS-treated RBCs, relative to Con, incubation of RBCs with PMS decreased RBC deformability at all combinations of magnitude–duration of shear stress.

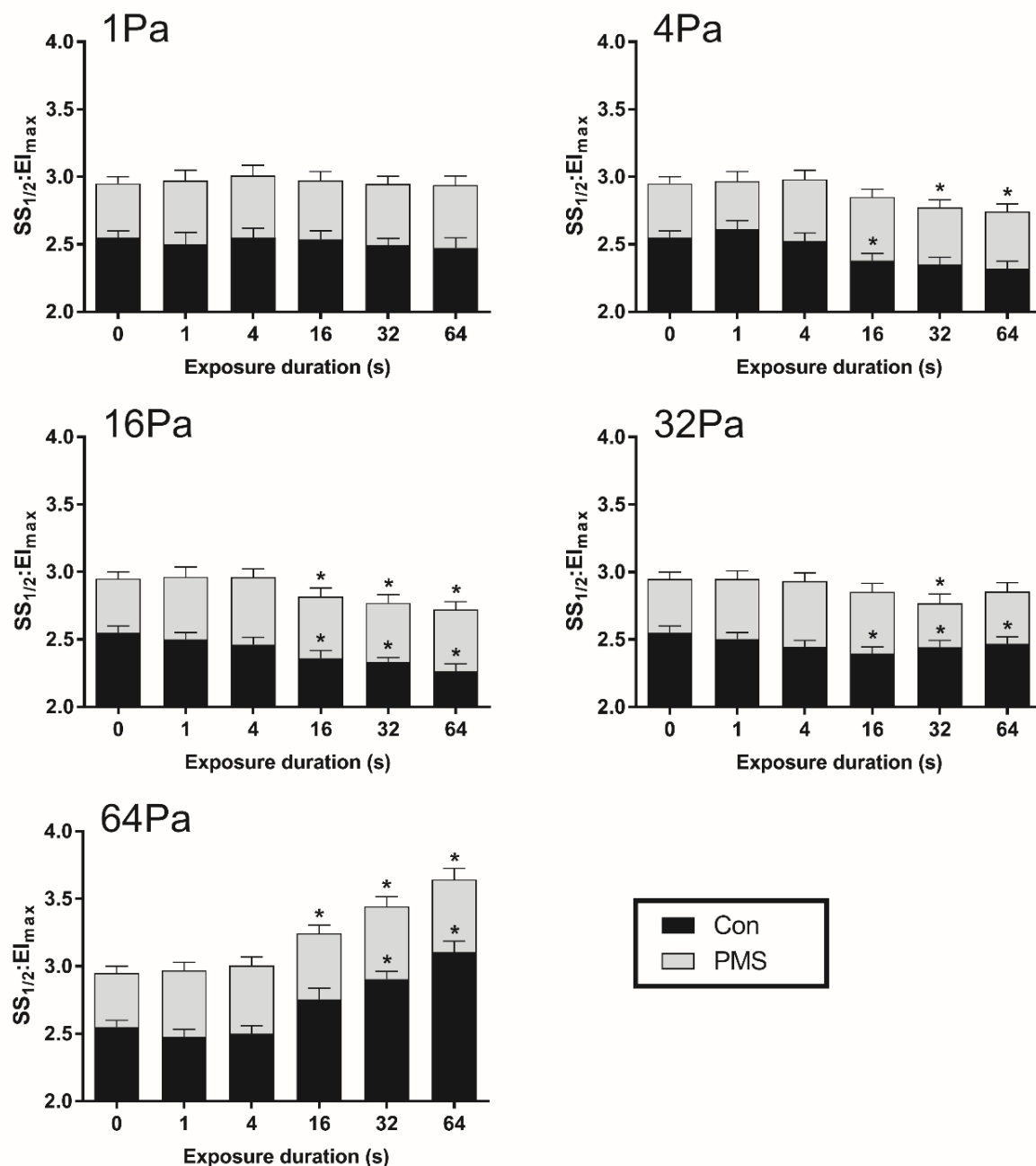


Fig. 49. $SS_{1/2}:EI_{max}$ parameterisation of RBC deformability measured for Con and PMS incubated samples following exposure to discrete magnitudes and durations of shear stress ranging 1–64 Pa for 0–64 s. All PMS incubated samples were significantly different to Con. *, conditioned sample significantly different from matched unsheared sample (0 s), $p < 0.05$.

A surface mesh of RBC susceptibility to subsequent mechanical damage (i.e. Mechanical Sensitivity) is illustrated in Fig. 50 for Con (Panel A) and PMS incubated samples (Panel B). The upper 95% C.I. for the Con Mechanical Sensitivity data index was found at 1.55%, indicating significant mechanical damage above this point. All Mechanical Sensitivity values of the PMS surface mesh were identified to be above the +95% C.I., indicating that PMS incubated samples, at all points, were more susceptible to mechanical damage than Con samples.

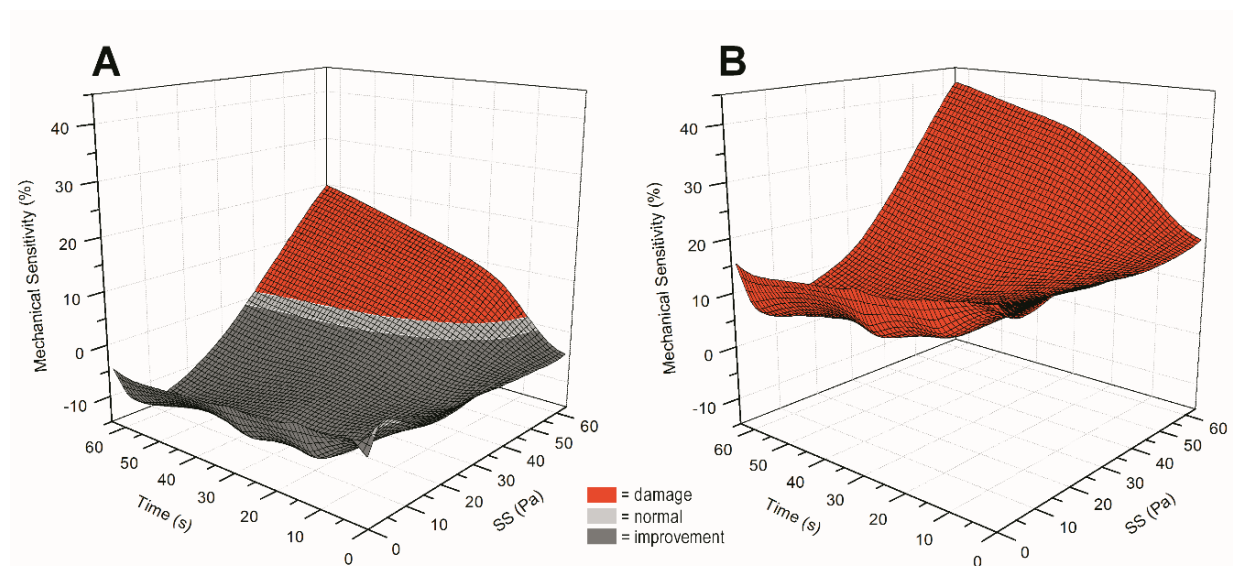


Fig. 50. A surface mesh of the RBC Mechanical Sensitivity (%) following shear stress exposure of varying durations and magnitudes for Con (Panel A) and PMS incubated samples (Panel B). The 95% C.I. are illustrated on the Con plot (Panel A), where the upper white line of the light grey region indicates the subhaemolytic damage point, where points above this line reflect combinations of duration and magnitude of shear stress exposure that induce significant mechanical damage. Conversely, all points below the lower white line of the light grey region are indicative of shear magnitude–durations that induce significant improvements to RBC deformability. All data points located within the surface mesh of the PMS incubated curve (Panel B) are greater than the +95% C.I. illustrated in Panel A.

To investigate the variances in the shear-mediated changes in RBC sensitivity to subsequent mechanical damage, the change in Mechanical Sensitivity (i.e., Δ Mechanical Sensitivity) between the matrices of PMS and Con conditions were determined. A visual representation and surface mesh of the calculated changes in Mechanical Sensitivity is presented in Fig. 51. The average calculated change in Mechanical Sensitivity was $19.0 \pm 2.0\%$. Varying the magnitude and/or duration of shear stress exposure did not significantly influence the Δ Mechanical Sensitivity for raw data points ($p = 0.159$). Post-hoc comparisons indicated that no significant differences were detected, for any of the data points, relative to the mean response for all shear magnitude duration conditions. Fig. 51 indicates that the shear-mediated changes between Con and PMS incubated samples are equivalent, despite the decreased deformability response at all time points (reflected via the vertical translation).

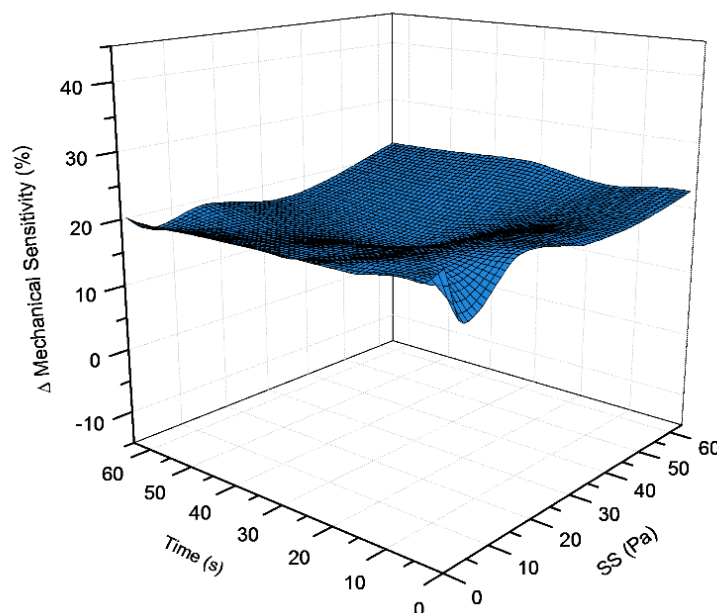


Fig. 51. Calculated differences of the Mechanical Sensitivity matrices between Con and PMS incubated samples following shear magnitude–duration interactions. This surface mesh is comparatively “flat” when compared to original Mechanical Sensitivity plots, indicating analogous shear-mediated changes between Con and PMS incubated samples, despite the vertical translation. No significant variances from the mean response were detected across the surface mesh.

Discussion

The salient findings of the present study demonstrate that RBCs, previously exposed to an intracellular superoxide generating agent, exhibit increased sensitivity to mechanical stress during subsequent exposures to shear. That is, the Mechanical Sensitivity of RBCs exposed to oxidative stress is impaired such that the magnitude and duration of shear stress required to damage RBCs is significantly decreased. Specifically, it was found that: i. RBC suspensions stimulated to generate intracellular superoxide exhibited significantly decreased cellular deformability under low shear conditions of ektacytometry prior to conditioning shear stress exposure (i.e. for “unsheared” samples); ii. when these rigidified RBCs were subsequently conditioned with varied durations and magnitudes of shear stress, important indices of RBC deformability were significantly impaired; iii. the general response of RBCs to shear stress was “typical” in trend for cells previously exposed to superoxide; however, there was a vertical transformation of this response ($19.0 \pm 2.0\%$), indicating that at all levels of shear stress exposure, impaired mechanical properties were observed. These findings collectively suggest that while the presence of intracellular superoxide decreases RBC deformability, RBCs retain the typical response to shear stress (i.e., shear-mediated changes), albeit at heightened risk for mechanical damage and microcirculatory dysfunction. Shear stress is thus a powerful stimulus that appears to induce predictable morphological responses in RBCs independent of prior mild exposure to superoxide.

Incubation of RBCs with PMS, stimulating the generation of intracellular superoxide anions, significantly altered baseline RBC deformability measures prior to shear stress exposure (Fig. 47). The effects of PMS-generated superoxide on the physical properties of RBCs has previously been well described to increase membrane stiffness and extensional rigidity, and decrease RBC deformability^{132,144,147}. Thus, the present observation that intracellular superoxide significantly decreased the Elongation

Indexes of RBCs under low shear stress (e.g. 0.53 – 2.91 Pa; Fig. 47) and significantly increased a global index indicative of impaired RBC deformability (i.e. $SS_{1/2}:EI_{max}$; Fig. 48), provides strong confirmation of these earlier reports. The present study, however, extends prior investigations by assessing the shear-mediated responses of RBCs previously exposed to intracellular superoxide generation.

The present study reports for the first time that RBCs previously exposed to intracellular superoxide generation, when subsequently conditioned with shear stress of a given duration and magnitude, exhibit significantly impaired RBC deformability beyond that which may be explained solely by oxidative stress (Fig. 49). Indeed unsheared PMS-treated RBCs displayed significantly increased $SS_{1/2}:EI_{max}$ (i.e., impaired deformability) compared with non-treated RBCs for all magnitudes and durations of shear stress. When PMS-treated RBCs were conditioned with 64 Pa for ≥ 16 s, however, the $SS_{1/2}:EI_{max}$ increased significantly relative to its matched unsheared PMS-treated RBCs. This observation indicates that exposure to mechanical forces compound the sublethal damage to RBCs induced by free radicals.

The current study also confirms evidence of the existence of a subhaemolytic threshold^{25,51,78}, with shear stresses far below the haemolytic threshold (and also that observed in mechanical assist devices) significantly decreasing RBC deformability, and increasing susceptibility to subsequent mechanical damage. PMS-treated samples of the present study exhibited an ~19% decrease in cell deformability before and after exposure to shear stress, with increases in Mechanical Sensitivity cumulating a further 42% following 64 Pa for 64 s (i.e. ~ 69% relative to unsheared Con). Given that the upper 95% C.I. determines the first occurrence of substantially impaired cellular deformability, all PMS samples were identified to be above the subhaemolytic threshold (Fig. 50). While mechanical forces compound the susceptibility to mechanical damage from free radicals, this finding indicates that the incubation of healthy RBCs with 50 μ M of PMS for 1 hour can induce subhaemolytic damage irrespective of exposure to shear stress, rendering RBC populations at a heightened

risk to mechanical and functional damage. Decreases in functional measures of RBC deformability will alter blood fluidity and may cause circulatory insufficiencies, impaired nutrient delivery, and propagate the development of disease¹⁴⁸.

Prior investigations have identified that oxidative stress can induce changes within the RBC cytoskeletal architecture by interrupting spectrin cross-bridges with adjacent membrane protein complexes, increasing membrane stiffness (measured through atomic force microscopy)^{149,150}. PMS-treated RBCs in the present study were observed to be at heightened risk of subsequent mechanical damage (Fig. 48); however, when normalising for the initial decreases in RBC deformability (caused by PMS), the shear-mediated responses for RBCs exposed to PMS (Fig. 50) were near identical to Con, albeit at an elevated level (i.e., more rigid than Con). When examining the changes in Mechanical Sensitivity (i.e., Δ Mechanical Sensitivity; Fig. 51) at matched shear magnitude–duration conditions, despite the vertical translation and elevated amplitude, the changes were not significantly different at any point (i.e., note Fig. 51 being horizontal). Curiously, this finding reveals that while oxidative stress decreases initial RBC deformability (increasing Mechanical Sensitivity; determining the vertical translation from baseline in Δ Mechanical Sensitivity), successive changes in RBC deformability are primarily governed/stimulated by shear stress.

When normalising the 19% increase in Mechanical Sensitivity of PMS-treated RBCs relative to Con, similar responses in the relative change under high shear (damage) and low shear (improvements) conditions were observed. Relative to unsheared PMS-treated RBCs, shear exposure to low-magnitude (4–32 Pa) longer-duration (16–64 s) combinations significantly increased RBC deformability and decreased the Mechanical Sensitivity index by ~5–10%. The finding that low-magnitude shear stresses can improve RBC deformability has recently been reported^{25,151}; however, unlike prior methods, the present study applied conditioning shear stress to already rigidified RBCs, damaged by free radicals, rather than healthy RBCs. The observed

enhancements of the present study suggest that low magnitude shear stress conditioning improves the capacity of RBCs to deform, independent of existing free radical damage. While the mechanism behind such process remains to be determined, it appears that low shear conditioning of blood can decrease subsequent mechanical damage.

While the subhaemolytic damage point could not be described for RBC suspensions incubated with PMS (as damage had already occurred), the findings of elevated sensitivity to subsequent mechanical damage provide important insights into mechanisms of shear-mediated changes in RBC deformability. The collective findings advocate shear stress as a powerful mechanical stimulus and determinant of RBC deformability, mediating both decrements and improvements, even in the presence of damaging free radicals. As patients receiving mechanical circulatory support are at elevated exposure to free radicals (thus limiting RBC deformability), concomitant exposure to high shear environments likely compounds the deleterious effects to important parameters that regulate microcirculatory blood flow. Thus, blood exposure to high shear environments should be minimised and the oxidative states of patients should be closely monitored or counteracted using antioxidants¹⁵². If blood were conditioned with low magnitudes of shear stress prior to mechanical circulatory support, however, RBC deformability may improve, Mechanical Sensitivity may decrease, and the consequential blood damage and its associated complications may be lessened. Further studies are planned to elucidate whether this improvement can be further enhanced in combination with antioxidant exposure, to decrease RBC mechanical damage below the subhaemolytic threshold, and whether free radical production during extracorporeal membrane oxygenation induces similar responses as observed in the present study.

Chapter VII.

Conclusion

The primary objective of the current doctoral thesis was to conduct works that contribute to gaining a more thorough understanding of the biophysical and functional changes that occur to red blood cells (RBCs) following exposure to discrete shear stresses that are supraphysiological and non-lethal, congruent with the shear environment that exists within current mechanical circulatory support systems. The thesis required the construction of multiple apparatus to investigate blood cells during shear flows at various scales – subcellular, single cell, cell-cell, and multi-cell clusters. This Chapter discusses the collective findings of the present dissertation, potential clinical implications of sublethal blood damage, relevant future experimental directions, and concludes the current dissertation.

Summary of findings

While artificial organs and mechanical circulatory support (MCS) systems (e.g., haemodialysis, cardiopulmonary bypass, ventricular assist devices) increase the lifespan of patients with end-stage chronic disease, many severe complications are still associated with their use. The precise mechanisms and processes that govern these secondary complications have to date been poorly understood; however, blood trauma related to blood-device interactions has been indicated, where artificial conditions (e.g., foreign materials, surfaces) and non-physiological fluid properties (e.g., excessive shears) are dominant. Non-haemolytic damage to blood has been observed in current clinical MCS devices, resulting in: altered blood cell morphology^{45,46}, augmented blood viscosity^{47,48}, and 'delayed anaemia' resulting from accelerated sequestration and a shortened RBC lifespan⁴⁹. The circulation of damaged blood may propagate sluggish flow or even complete flow-stasis, yielding negative implications for microvascular perfusion, and thus tissue oxygenation and nutrient delivery. Given the severity of perfusion associated complications, there remains a necessity to extensively characterise and elucidate the mechanisms of *functional* blood cell deterioration occurring from sublethal blood damage. Understanding the rheological function of blood and its response to shear stresses within, and superseding, the physiological range is of scientific and clinical interest, important for predicting an individual's response to MCS, and instigating further refinement of current haemocompatibility criteria. Thus, the primary objective of the current thesis was to conduct and include works that contribute to a more thorough understanding of the biophysical and functional changes that occur to RBCs following exposure to discrete shear stresses that are supraphysiological (but non-lethal), as found within the shear environment that exists within current MCS systems.

The current doctoral thesis was designed following completion of earlier works⁵⁰ which yielded curious findings regarding the breadth of RBC modifications following

exposure to sublethal shear stresses. Qualitative assessment of RBC micrographs indicated that sublethal damage dramatically altered cell morphology, increased aggregate formation, and induced cell fragmentation (even at levels reported to be 'non-lethal'). The sparse knowledge and understanding around RBC function with altered stress-strain history and mechanical damage required a collection of works to be generated; thus, the foundation for the present thesis was formed.

To adequately assess changes to RBCs, it was identified that new infrastructure with the capacity to assess the physical properties of blood at multiple scales was required to be constructed. A challenging, but important consideration of the system design and user requirement specification, was that, due to budget constraints, each machine needed to be developed for low-cost, without sacrificing the quality of macro/micro mechanobiological data generation. A suite of devices was developed to inspect single RBC membrane mechanics, electrochemistry, and deformability, while interrogating haemodynamics in low-shear and capillary flow.

The salient findings of the present thesis identified that when RBCs were exposed to supraphysiological sublethal shear stresses: the cell membrane was remodelled such that cell electronegativity was decreased (*Ch. III*), RBC aggregate formation kinetics/strength was increased (*Ch. III*), cells were rigidified (*Chs. IV, V, VI*), aberrant morphologies were produced (*Chs. IV, V*), an *ex vivo* chronic disease model (i.e., oxidative stress) further exacerbated shear-induced rigidification (*Ch. VI*), and haemodynamics in low-shear and capillary flows were altered (*Chs. IV, V*).

The collective findings support the accumulating body of evidence that indicates the existence of a sublethal damage: as RBCs are exposed to shears beyond elastic limits, cells undergo functional and morphological changes that are likely to upset subsequent blood rheology and homeostasis of systemic blood fluidity. Given MCS has been identified to induce shears within the supraphysiological sublethal domain, the findings of the current dissertation may, in part, explain the current clinical

complications associated with MCS use, possibly identifying rheological aetiologies for ischaemic complications, angiodyplasia, and the vascular related incidence of neurological complications. Thus, it must be emphasised that the current benchmark assessment of haemolysis to demarcate blood damage does not provide adequate resolution for sensitive pathological detection or assessments of device (mis)function.

General discussion

Sublethal damage and plastic deformation

The complete destruction of RBCs – i.e., haemolysis – is an easily comprehensible indicator of blood damage that remains the prominent focus of current haemocompatibility assessments. When RBCs are destroyed, cytosolic haemoglobin is released into the plasma causing toxic effects³⁵; hence haemolysis is an absolute endpoint damage that must be avoided. However, given shear stresses that exist within MCS are typically low enough to avoid overt cell rupture, the current thesis demonstrated that haemolysis as a haemocompatibility assessment tool is flawed due to its lack of sensitivity. As shown in this thesis, exposure of blood to supraphysiological shear stresses, below levels which induce cell rupture, alter the physical and electrochemical properties of RBCs (i.e., RBCs experience irreversible *functional* damage prior to their *lethal* haemolytic endpoint).

A primary outcome of the current thesis was to indicate that the accumulation of RBC sublethal trauma is similar to the accumulation of material fatigue observed in nonbiological materials. That is, RBCs are sensitive to levels of stress-strain history and can only recover full-functionality when stretched within elastic limits. Comparable with nonliving materials, when elastic limits are exceeded, the material damage of RBC membrane is irreversible. The novel findings of the current thesis indicated that when elastic limits of cell deformability are surpassed, which occurs at shear magnitudes below levels reported to induce haemolysis, RBCs undergo severe,

irreversible alterations in structure and function. In support of the results presented in the current thesis, other recent reports have also suggested that such mechanical membrane fatigue of the RBC precedes and occurs in the absence of haemolysis^{37,76,153}.

As materials surpass elastic limits of deformation, nonrecoverable increases in rigidity, loss of elasticity, and permanent distortions occur, which in the case of RBCs is biologically and rheologically undesirable. For RBCs, elastic deformability is imperative for their traverse of the miniscule apertures in the body's microcirculation to facilitate successful tissue perfusion. Blood flow, and consequential tissue oxygenation, is intrinsically-linked to the physical properties of the system, and is a highly sensitive homeostatic process², thus increases in cell rigidity can have catastrophic implications for the bulk flow of blood and systemic health.

Potential rheological and clinical implications

Shear stress is a powerful stimulus that affects blood at multiple scales, causing biochemical, physical, and structural alterations to RBCs. As evidenced in *Chapter III*, rapid exposure to sublethal shears can remodel key elements of the cell glycocalyx (i.e., membrane bound sialic acids), consequently decreasing cell electronegativity and altering hydrophobicity. Following electrochemical changes, *Chapter III* also provided evidence of increased cellular aggregation rates, adherence forces, and the magnitudes of shear required for disaggregation of RBCs. Alterations to the electrochemical properties of RBCs also have profound implications for material surface interactions and cell agglutination.

Chapter V reported that shear stress can also induce morphological alterations that have subsequent implications for RBC deformability. With exposure to sublethal shears, cell volume was identified to significantly decrease. While the precise mechanisms explaining the cell volume changes – whether it be active mechanotransduction or passive membrane pore formation – remains to be

elucidated, efflux of cytosolic fluid from RBCs may increase the concentration of cytosolic haemoglobin (and thus also cytosolic viscosity¹²²) and increase cell surface-area-to-volume ratio. An increase in cell-surface-area-to-volume ratio, in conjunction with potential protein denaturation of lipid bilayer-cytoskeleton junctional attachment sites, may contribute to localised membrane buckling, and thus also the presence of aberrant cell morphology (i.e., crenated RBCs). Given cytosolic viscosity is a primary determinant of RBC deformability, the decreases in RBC deformability observed in *Chapter VI* with shear exposure beyond tolerable elastic limits may be resultant of increased RBC membrane shear elastic modulus *and* increased cell cytosolic viscosity.

The modulations that occur to the physical properties of RBCs with sublethal shear bear rheological implications within all scales of circulation (i.e., large and small vessels). The hyperaggregation of RBCs and associated sluggish low-shear blood flow may cause increased leukocyte and platelet margination/attachment⁷², diminished nitric oxide synthesis altering vasomotor tone⁷⁴, and increased thrombotic risk⁷⁰. Increased RBC rigidity alters cell orientation and dynamics in shear flows, and increases friction and resistance to flow in the microcirculation². Increased hydraulic resistance in small vessels, increased cell-wall friction, and increased cell rigidity augments the likelihood of flow stagnation and flow stasis, leading to poor tissue oxygenation^{110,120}. With RBC aggregation being the primary determinant of low-shear blood viscosity, and RBC deformability predominantly dictating high-shear blood viscosity, we can hypothesise that accumulation of sublethal damage may also result in hyperviscosity of blood.

Given the alterations to rheological determinants of varied portions of circulation, it is plausible that shear induced alterations of RBCs potentially contribute to the MCS-related complications (e.g., haemorrhage, stroke, thrombosis, tissue ischaemia, anaemia, etc.) that may ultimately lead to patient multi-system organ failure and death⁶.

Even though MCS has been hypothesised to accelerate blood cell senescence, being associated with the early removal and sequestration of RBCs from circulation⁴⁴, the temporal component of blood damage and recovery poses substantial risk to vascular health the longer 'less-functional' cells remain in circulation. That is, even if exposure of RBCs to sublethal shears is extremely rapid (such as in acute treatments), irrespective of short-duration transits, the current thesis highlights that blood passing through MCS devices can rapidly become damaged. The implications for post-surgical tissue perfusion are of interest, given that even once a patient is "off-pump", the continued circulation of sublethally damaged RBCs, and associated impaired blood fluidity, is likely to persist until cell sequestration/lifecycle is complete⁴⁴.

Thresholds of sublethal damage

Throughout the course of the current doctoral program, a variety of shear magnitude-duration combinations were utilised to investigate its impact on the biophysical properties of RBCs. These shear magnitude-duration combinations, while varied, were specifically chosen as they represent values known to be below the reported haemolytic threshold, yet existent within the shear range computationally predicted in left ventricular assist devices and other MCS systems^{50,82}. To surmise the cumulative demarcations of tolerable levels of shear and the shear that induces sublethal damage, the results from each Chapter of the thesis have been summarised and combined in Table 2 displaying if shear magnitude-duration combinations cause sublethal damage (red), or are tolerable (yellow). Of note, the first identified shear combinations that induced sublethal damage to healthy RBCs are: 50 Pa × 60 s, 64 Pa × 32 s, 75 Pa × 5 s, 100 Pa × 4 s, 125 Pa × 1.5 s. While this is in congruence with earlier reports^{62,154}, further examination of these datapoints may yield higher resolution data and more accurate approximations of the sublethal damage threshold.

Table 2. Shear stress magnitude-duration combinations identified as (in)tolerable to RBCs.

t (s)	Shear stress (Pa)											
	1	4	5	16	25	32	50	64	75	100	125	
1	-	-	-	-	-	-	-	-	-	-	-	
1.5												*
2										⊗		
3												*
4	-	-		-		-		-		⊗	*	
5			-		-		-		*	*		
10			-		-		-		*	*		
16	-	+		+		+		-				
32	-	-		+		+		*				
60			-		-		*		*	*		
64	-	-		+		+		*				
300			-				*			*		

Following the shear magnitude-duration combination RBC were: - unaltered, + biophysically improved, * biophysically impaired indicating sublethal damage; shear combination not examined. [⊗]corresponding data points for 100 Pa sourced from Horobin et al. ¹⁵⁴.

Future Directions

Throughout the course of the current doctoral program, in addition to generating novel findings regarding shear-induced physical and biochemical alterations to RBCs, new research questions have been identified that should be investigated further (i.e., the now “*known unknowns*”).

Chapters III and IV identified that sublethal shear damage can alter RBC orientation and tank-treading behaviours, while cleaving glycoproteins from the glycocalyx. Given the cell membrane freely rotates in shear to facilitate energy dissipation, understanding the mechanism and uniformity of membrane rigidification is important to model subsequent cell dynamics. Further studies should seek to deploy high resolution subcellular inspection to determine the localisation of this accumulated sublethal damage.

An important question that is continuously posed throughout each chapter of the current thesis, surrounds biochemical involvement in RBC susceptibility to mechanical damage. Given the present thesis observed shear-mediated volume changes, improvements in RBC deformability (even in the presence of oxidative stressors), and morphological changes, deeper inspection is required to elucidate the

contribution of relevant mechanotransduction pathways (i.e., Piezo channel activation, Gardos channel activation, nitric oxide mediated S-nitrosylation of cytoskeletal proteins). Further inspection of biochemical 'knock-out'/inhibition investigations would elucidate biochemical involvement in sublethal damage, and may also assist in identifying new targets for pharmacotherapy of blood damage.

The present thesis adopted a reductionist approach to isolate the RBC responses to shear and determine multiple scales of cell damage. To be able to translate the current data into recommendations that are meaningful to implement into clinical practice, further studies must be conducted into non-isolated blood, i.e., the entire blood tissue. Whilst it is likely that each individual formed element of blood will be affected by sublethal shear, it is also likely that interactions between the various formed elements, and between the formed elements and the vascular endothelium, will modify the observed effects of the applied shears.

Chapter II identified a need for the development of technical instrumentation for multiscale RBC inspection. The small-scatter laser-diffractometry with combined visualisation diffractometry (i.e., the ektacytoscope) has the potential to be developed into a portable standalone system that may function as a non-invasive blood damage detection device, while yielding new clinical insights for the assessment of subtle rheological disturbances. Moreover, while technological advances have facilitated new methods for RBC biophysical inspection (e.g., optical tweezers), the current doctoral program highlighted that micropipette aspiration is a technique that is not antiquated. The high-quality, high-resolution data yielded by the micropipette aspiration technique in this thesis demonstrates its continued importance to the field of rheology and the importance of further developing this technique to enhance its efficiency in experimental throughput and automation. Such investment and refinement of devices to assess cell function will likely lead to the development of real-time blood damage detection devices, which would enhance clinical management of rheological pathologies.

Conclusion

RBCs are well equipped to traverse circulation and be continually exposed to physiological magnitudes of shear. Beyond the physiological limits, however, RBCs are susceptible, and indeed sensitive to mechanical damage. Collectively the findings of the present thesis identify that exposure of RBCs to shear stresses that are supra-physiological and subhaemolytic can rapidly induce structural and functional alterations that may partly explain secondary complications associated with high-shear MCS. Undeniably, MCS devices are medical marvels that do enable complex surgical interventions where otherwise patient outcomes would be fatal. Over recent decades, patient survival has substantially increased due to the development of more blood-compatible devices, and improved surgical procedures.

Nevertheless, the novel findings of this thesis are apparent: as blood damage still occurs below shear levels required to induce haemolysis, a primary component of understanding haemocompatibility has been missing, and it has been difficult to fully explain clinically-observed complications. Functional assessments of the formed elements of blood must be taken into consideration; and as shown in this thesis, contrary to the neglecting international standards...

sublethal damage is not a myth.

Sublethal damage of RBCs is an observable phenomenon and a logical progression of their material properties when they are sheared beyond elastic limits. Sublethal damage must be considered for the continual refinement of MCS to further enhance device success.

Since the initiation of this dissertation, the discipline has begun accumulating a significant body of evidence that supports the unique cellular alterations that may occur with sublethal damage. Already thresholds of elastic limits of cell deformability, biochemical function, and reversibility have begun to be elucidated; however, deeper

understanding is still required to inform MCS device design and current clinical best-practice. Indeed, adoption of improved, more sensitive haemocompatibility criteria and changes to international standards and practices for better determination of the haemocompatibility of devices will yield clinical improvement. Moreover, with the implementation of sublethal damage markers to guide haemocompatibility, new innovations will be conceived, e.g., more sensitive real-time blood assessment devices – moving sublethal markers into clinic/surgery, new MCS device designs not currently conceptualised, and novel pharmacotherapies enhancing the pliability and strength of blood.

Given patients indicated for mechanical circulatory support typically already have elevated risk of altered blood fluidity and oxidative stress (due to comorbid chronic disease and inflammation), future mechanical circulatory support should be designed to limit magnitudes of shear exposure to levels that do not alter the electrochemical and other physical properties of blood cells.

The uptake and adoption of more sensitive markers of blood damage will provide new targets for device development, which will subsequently yield more rapid advancement, better understanding of current patient complications, and future interventions that will ultimately improve the wellbeing and survival of patients globally. As the collective conditions treated by MCS comprise the most prevalent and expensive disease populations in Australia, and continual population growth will further increase the demand for artificial organs into the future, there is a need to immediately invest in the development of these systems to enhance patient outcomes.

Based on the findings of the current thesis, sublethal blood damage cannot be underestimated or ignored.

International haemocompatibility criteria must be updated to include *form and function* of human blood, over merely *presence/absence* of cells.

References

1. Calzia, E., Iványi, Z., and Radermacher, P., *Determinants of blood flow and organ perfusion*, in *Functional hemodynamic monitoring*. 2005, Springer. p. 19-32.
2. Schmid-Schönbein, H., Rieger, H., and Fischer, T., *Blood fluidity as a consequence of red cell fluidity: flow properties of blood and flow behavior of blood in vascular diseases*. *Angiology*, 1980. **31**(5): p. 301-319.
3. Baskurt, O.K., *Mechanisms of blood rheology alterations*. Biomedical and Health Research-Commission of the European Communities then IOS Press, 2007. **69**: p. 170.
4. Australian Bureau of Statistics *Causes of Death, Australia*. 2017 [cited 2019 16/12]; Available from:
<https://www.abs.gov.au/ausstats/abs@.nsf/Lookup/by%20Subject/3303.0~2017~Main%20Features~Australia's%20leading%20causes%20of%20death,%202017~2>.
5. Rose, E.A., Gelijns, A.C., Moskowitz, A.J., Heitjan, D.F., Stevenson, L.W., Dembitsky, W., Long, J.W., Ascheim, D.D., Tierney, A.R., Levitan, R.G., Watson, J.T., Ronan, N.S., Shapiro, P.A., Lazar, R.M., Miller, L.W., Gupta, L., Frazier, O.H., Desvigne-Nickens, P., Oz, M.C., Poirier, V.L., and Meier, P., *Long-Term Use of a Left Ventricular Assist Device for End-Stage Heart Failure*. *New England Journal of Medicine*, 2001. **345**(20): p. 1435-1443.
6. Kirklin, J.K., Naftel, D.C., Pagani, F.D., Kormos, R.L., Stevenson, L.W., Blume, E.D., Miller, M.A., Baldwin, J.T., and Young, J.B., *Sixth INTERMACS annual report: a 10,000-patient database*. *The Journal of Heart and Lung Transplantation*, 2014. **33**(6): p. 555-564.
7. Crow, S., John, R., Boyle, A., Shumway, S., Liao, K., Colvin-Adams, M., Toninato, C., Missov, E., Pritzker, M., Martin, C., Garry, D., Thomas, W., and Joyce, L., *Gastrointestinal bleeding rates in recipients of nonpulsatile and pulsatile left ventricular assist devices*. *The Journal of Thoracic and Cardiovascular Surgery*, 2009. **137**(1): p. 208-215.

8. Piccione Jr, W., *Left ventricular assist device implantation: short and long-term surgical complications*. The Journal of Heart and Lung Transplantation, 2000. **19**(8, Supplement 1): p. S89-S94.
9. Zhang, P., Yeo, J.H., Qian, P., and Hwang, N.H., *Shear stress investigation across mechanical heart valve*. ASAIO Journal, 2007. **53**(5): p. 530-6.
10. Ruggeri, Z.M., Orje, J.N., Habermann, R., Federici, A.B., and Reininger, A.J., *Activation-independent platelet adhesion and aggregation under elevated shear stress*. Blood, 2006. **108**(6): p. 1903-1910.
11. Baskurt, O.K., *Handbook of hemorheology and hemodynamics*. Vol. 69. 2007: IOS press.
12. Baskurt, O.K. and Meiselman, H.J. *Blood rheology and hemodynamics*. in *Seminars in thrombosis and hemostasis*. 2003. New York: Stratton Intercontinental Medical Book Corporation, c1974-.
13. Baskurt, O., Neu, B., and Meiselman, H.J., *Red blood cell aggregation*. 2011: CRC Press.
14. Cokelet, G.R. and Meiselman, H.J., *Macro-and micro-rheological properties of blood*. Biomedical and Health Research-Commission of the European Communities then IOS Press, 2007. **69**: p. 45.
15. Cabel, M., Meiselman, H., Popel, A., and Johnson, P., *Contribution of red blood cell aggregation to venous vascular resistance in skeletal muscle*. American Journal of Physiology-Heart and Circulatory Physiology, 1997. **272**(2): p. H1020-H1032.
16. Rampling, M., Meiselman, H., Neu, B., and Baskurt, O., *Influence of cell-specific factors on red blood cell aggregation*. Biorheology, 2004. **41**(2): p. 91-112.
17. Huang, Y.X., Tuo, W.W., Wang, D., Kang, L.L., Chen, X.Y., and Luo, M., *Restoring the youth of aged red blood cells and extending their lifespan in circulation by remodelling membrane sialic acid*. Journal of cellular and molecular medicine, 2016. **20**(2): p. 294-301.

18. Eylar, E.H., Madoff, M.A., Brody, O., and Oncley, J., *The contribution of sialic acid to the surface charge of the erythrocyte*. *Journal of Biological Chemistry*, 1962. **237**(6): p. 1992-2000.
19. Simmonds, M.J., Meiselman, H.J., and Baskurt, O.K., *Blood rheology and aging*. *Journal of Geriatric Cardiology : JGC*, 2013. **10**(3): p. 291-301.
20. Jan, K.-M. and Chien, S., *Role of surface electric charge in red blood cell interactions*. *The Journal of General Physiology*, 1973. **61**(5): p. 638-654.
21. Tse, W.T. and Lux, S.E., *Red blood cell membrane disorders*. *British Journal of Haematology*, 1999. **104**(1): p. 2-13.
22. Neu, B., Sowemimo-Coker, S.O., and Meiselman, H.J., *Cell-cell affinity of senescent human erythrocytes*. *Biophysical Journal*, 2003. **85**(1): p. 75-84.
23. Bagge, U., Brånemark, P., Karlsson, R., and Skalak, R., *Three-dimensional observations of red blood cell deformation in capillaries*. *Blood Cells*, 1979. **6**(2): p. 231-239.
24. Muravyov, A.V. and Tikhomirova, I.A., *Role molecular signaling pathways in changes of red blood cell deformability*. *Clinical Hemorheology and Microcirculation*, 2013. **53**(1): p. 45-59.
25. Simmonds, M.J., Atac, N., Baskurt, O.K., Meiselman, H.J., and Yalcin, O., *Erythrocyte deformability responses to intermittent and continuous subhemolytic shear stress*. *Biorheology*, 2014. **51**(2): p. 171-185.
26. Simmonds, M.J., Detterich, J.A., and Connes, P., *Nitric oxide, vasodilation and the red blood cell*. *Biorheology*, 2014. **51**(2-3): p. 121-134.
27. Grau, M., Pauly, S., Ali, J., Walpurgis, K., Thevis, M., Bloch, W., and Suhr, F., *RBC-NOS-dependent S-nitrosylation of cytoskeletal proteins improves RBC deformability*. *PLoS One*, 2013. **8**(2): p. e56759.
28. Mazumdar, J., *Biofluid mechanics*. 1992: World Scientific.

29. Fedosov, D.A., Caswell, B., and Karniadakis, G.E., *A Multiscale Red Blood Cell Model with Accurate Mechanics, Rheology, and Dynamics*. *Biophysical Journal*. **98**(10): p. 2215-2225.
30. Klitzman, B. and Duling, B.R., *Microvascular hematocrit and red cell flow in resting and contracting striated muscle*. *American Journal of Physiology-Heart and Circulatory Physiology*, 1979. **237**(4): p. H481-H490.
31. Fåhræus, R. and Lindqvist, T., *The viscosity of the blood in narrow capillary tubes*. *American Journal of Physiology--Legacy Content*, 1931. **96**(3): p. 562-568.
32. Kirklin, J.K., Pagani, F.D., Kormos, R.L., Stevenson, L.W., Blume, E.D., Myers, S.L., Miller, M.A., Baldwin, J.T., Young, J.B., and Naftel, D.C., *Eighth annual INTERMACS report: special focus on framing the impact of adverse events*. *The Journal of Heart and Lung Transplantation*, 2017. **36**(10): p. 1080-1086.
33. Rose, E.A., Gelijns, A.C., Moskowitz, A.J., Heitjan, D.F., Stevenson, L.W., Dembitsky, W., Long, J.W., Ascheim, D.D., Tierney, A.R., and Levitan, R.G., *Long-term use of a left ventricular assist device for end-stage heart failure*. *New England Journal of Medicine*, 2001. **345**(20): p. 1435-1443.
34. Kirklin, J.K., Naftel, D.C., Pagani, F.D., Kormos, R.L., Stevenson, L.W., Blume, E.D., Myers, S.L., Miller, M.A., Baldwin, J.T., and Young, J.B., *Seventh INTERMACS annual report: 15,000 patients and counting*. *Journal of Heart Lung Transplant*, 2015. **34**(12): p. 1495-504.
35. Helms, C. and Kim-Shapiro, D.B., *Hemoglobin-mediated nitric oxide signaling*. *Free Radical Biology Medicine*, 2013. **61**: p. 464-72.
36. Paul, R., Apel, J., Klaus, S., Schügner, F., Schwindke, P., and Reul, H., *Shear stress related blood damage in laminar couette flow*. *Artificial Organs*, 2003. **27**(6): p. 517-529.
37. Baskurt, O.K. and Meiselman, H.J., *Red blood cell mechanical stability test*. *Clinical Hemorheology and Microcirculation*, 2013. **55**(1): p. 55-62.

38. Crow, S., John, R., Boyle, A., Shumway, S., Liao, K., Colvin-Adams, M., Toninato, C., Missov, E., Pritzker, M., Martin, C., Garry, D., Thomas, W., and Joyce, L., *Gastrointestinal bleeding rates in recipients of nonpulsatile and pulsatile left ventricular assist devices*. *Journal of Thoracic Cardiovascular Surgery*, 2009. **137**(1): p. 208-15.
39. Baskurt, O.K., Uyuklu, M., and Meiselman, H.J., *Protection of erythrocytes from sub-hemolytic mechanical damage by nitric oxide mediated inhibition of potassium leakage*. *Biorheology*, 2004. **41**(2): p. 79-89.
40. Kameneva, M.V. and Antaki, J.F., *Mechanical trauma to blood*. Biomedical and Health Research-Commission of the European Communities then IOS Press, 2007. **69**: p. 206.
41. Lee, S.S., Ahn, K.H., Lee, S.J., Sun, K., Goedhart, P.T., and Hardeman, M.R., *Shear induced damage of red blood cells monitored by the decrease of their deformability*. *Korea-Australia Rheology Journal*, 2004. **16**(3): p. 141-146.
42. Simmonds, M.J., Atac, N., Baskurt, O.K., Meiselman, H.J., and Yalcin, O., *Erythrocyte deformability responses to intermittent and continuous subhemolytic shear stress*. *Biorheology*, 2014. **51**(2-3): p. 171-85.
43. Baskurt, O.K. and Meiselman, H.J., *Red blood cell mechanical stability test*. *Clinical Hemorheology and Microcirculation*, 2013. **55**(1): p. 55-62.
44. Sandza Jr, J., Clark, R., Weldon, C., and Sutera, S., *Subhemolytic trauma of erythrocytes: recognition and sequestration by the spleen as a function of shear*. *ASAIO Journal*, 1974. **20**(1): p. 457-462.
45. Shimono, T., Makinouchi, K., Yada, I., and Nose, Y., *New method of evaluating sublethal damage to erythrocytes by blood pumps*. *Artificial Organs*, 1996. **20**(5): p. 568-571.
46. Hasler, C.R., Owen, G.R., Brunner, W., and Reinhart, W.H., *Echinocytosis induced by haemodialysis*. *Nephrology Dialysis Transplantation*, 1998. **13**(12): p. 3132-7.

47. Papp, J., Toth, A., Sandor, B., Kiss, R., Rabai, M., Kenyeres, P., Juricskay, I., Kesmarky, G., Szabados, S., and Toth, K., *The influence of on-pump and off-pump coronary artery bypass grafting on hemorheological parameters*. *Clinical Hemorheology and Microcirculation*, 2011. **49**(1-4): p. 331-46.
48. Dittrich, S., Priesemann, M., Fischer, T., Boettcher, W., Muller, C., Dahnert, I., Ewert, P., Alexi-Meskishvili, V., Hetzer, R., and Lange, P.E., *Hemorheology and renal function during cardiopulmonary bypass in infants*. *Cardiology in the Young*, 2001. **11**(5): p. 491-7.
49. Polaschegg, H.D. *Red blood cell damage from extracorporeal circulation in hemodialysis*. in *Seminars in dialysis*. 2009. Wiley Online Library.
50. McNamee, A.P., Tansley, G.D., Sabapathy, S., and Simmonds, M.J., *Biphasic impairment of erythrocyte deformability in response to repeated, short duration exposures of supraphysiological, subhaemolytic shear stress*. *Biorheology*, 2016. **53**(3-4): p. 137-149.
51. Simmonds, M.J. and Meiselman, H.J., *Prediction of the level and duration of shear stress exposure that induces subhemolytic damage to erythrocytes*. *Biorheology*, 2017.
52. Watanabe, N., Sakota, D., Ohuchi, K., and Takatani, S., *Deformability of red blood cells and its relation to blood trauma in rotary blood pumps*. *Artificial Organs*, 2007. **31**(5): p. 352-358.
53. Manno, S., Takakuwa, Y., and Mohandas, N., *Identification of a functional role for lipid asymmetry in biological membranes: Phosphatidylserine-skeletal protein interactions modulate membrane stability*. *Proceedings of the National Academy of Sciences*, 2002. **99**(4): p. 1943-1948.
54. Dao, K., O'Rear, E., Johnson, A., and Peitersen, S., *Sensitivity of the erythrocyte membrane bilayer to subhemolytic mechanical trauma as detected by fluorescence anisotropy*. *Biorheology*, 1993. **31**(1): p. 69-76.

55. Grisendi, G., Finetti, E., Manganaro, D., Cordova, N., Montagnani, G., Spano, C., Prapa, M., Guarneri, V., Otsuru, S., and Horwitz, E.M., *Detection of microparticles from human red blood cells by multiparametric flow cytometry*. *Blood Transfusion*, 2015. **13**(2): p. 274-80.
56. Kriebardis, A.G., Antonelou, M.H., Georgatzakou, H.T., Tzounakas, V.L., Stamoulis, K.E., and Papassideri, I.S., *Microparticles variability in fresh frozen plasma: preparation protocol and storage time effects*. *Blood Transfusion*, 2016. **14**(3): p. 228.
57. Sakota, D., Sakamoto, R., Sobajima, H., Yokoyama, N., Waguri, S., Ohuchi, K., and Takatani, S., *Mechanical Damage of Red Blood Cells by Rotary Blood Pumps: Selective Destruction of Aged Red Blood Cells and Subhemolytic Trauma*. *Artificial Organs*, 2008. **32**(10): p. 785-791.
58. Lang, E. and Lang, F., *Triggers, inhibitors, mechanisms, and significance of eryptosis: the suicidal erythrocyte death*. *BioMed Research International*, 2015. **2015**.
59. Sutura, S.P. and Mehrjardi, M.H., *Deformation and fragmentation of human red blood cells in turbulent shear flow*. *Biophysical Journal*, 1975. **15**(1): p. 1-10.
60. Han, C.D., *Slit rheometry, in Rheological Measurement*. 1993, Springer. p. 25-48.
61. White, F., *Flow between long concentric cylinders*. *Fluid mechanics*, McGraw-Hill,, 1999: p. 261-263.
62. Simmonds, M.J. and Meiselman, H.J., *Prediction of the level and duration of shear stress exposure that induces subhemolytic damage to erythrocytes*. *Biorheology*, 2016. **53**(5-6): p. 237-249.
63. Kuck, L., Grau, M., and Simmonds, M.J., *Recovery time course of erythrocyte deformability following exposure to shear is dependent upon conditioning shear stress*. *Biorheology*, 2018(Preprint): p. 1-12.

64. McNamee, A.P., Richardson, K., Horobin, J., Kuck, L., and Simmonds, M.J., *Susceptibility of density-fractionated erythrocytes to subhaemolytic mechanical shear stress*. *The International Journal of Artificial Organs*, 2019. **42**(3): p. 151-157.
65. Rabai, M., Detterich, J.A., Wenby, R.B., Hernandez, T.M., Toth, K., Meiselman, H.J., and Wood, J.C., *Deformability analysis of sickle blood using ektacytometry*. *Biorheology*, 2014. **51**(2-3): p. 159-170.
66. Bull, B., Feo, C., and Bessis, M., *Behavior of elliptocytes under shear stress in the rheoscope and ektacytometer*. *Cytometry: The Journal of the International Society for Analytical Cytology*, 1983. **3**(4): p. 300-304.
67. Paulitschke, M. and Nash, G., *Micropipette methods for analysing blood cell rheology and their application to clinical research*. *Clinical Hemorheology and Microcirculation*, 1993. **13**(4): p. 407-434.
68. Engström, K.G. and Meiselman, H.J., *Fabrication of glass micropipettes: A semi-automatic approach for trimming the pipette tip*. *Biorheology*, 1992. **29**(5-6): p. 499-506.
69. Baskurt, O.K. and Meiselman, H.J., *RBC aggregation: more important than RBC adhesion to endothelial cells as a determinant of in vivo blood flow in health and disease*. *Microcirculation*, 2008. **15**(7): p. 585-590.
70. Baskurt, O.K. and Meiselman, H.J., *Erythrocyte aggregation: basic aspects and clinical importance*. *Clinical Hemorheology and Microcirculation*, 2013. **53**(1-2): p. 23-37.
71. Cokelet, G.R. and Goldsmith, H.L., *Decreased hydrodynamic resistance in the two-phase flow of blood through small vertical tubes at low flow rates*. *Circulation Research*, 1991. **68**(1): p. 1-17.
72. Nash, G.B., Watts, T., Thornton, C., and Barigou, M., *Red cell aggregation as a factor influencing margination and adhesion of leukocytes and platelets*. *Clinical Hemorheology and Microcirculation*, 2008. **39**(1-4): p. 303-310.

73. Baskurt, O.K., *In vivo correlates of altered blood rheology*. *Biorheology*, 2008. **45**(6): p. 629-638.
74. Baskurt, O.K., Yalcin, O., Ozdem, S., Armstrong, J.K., and Meiselman, H.J., *Modulation of endothelial nitric oxide synthase expression by red blood cell aggregation*. *American Journal of Physiology-Heart and Circulatory Physiology*, 2004. **286**(1): p. H222-H229.
75. McNamee, A.P., Horobin, J.T., Tansley, G.D., and Simmonds, M.J., *Oxidative Stress Increases Erythrocyte Sensitivity to Shear-Mediated Damage*. *Artificial Organs*, 2017.
76. Horobin, J.T., Sabapathy, S., and Simmonds, M.J., *Repetitive Supra-Physiological Shear Stress Impairs Red Blood Cell Deformability and Induces Hemolysis*. *Artificial Organs*, 2017.
77. Kormos, R.L., Borovetz, H.S., Griffith, B.P., Hung, T.C., Olsen, D.B., Pennington, D.G., Roohk, V., Atsumi, K.M., Kolff, W.J., and Joist, J.H., *Rheologic Abnormalities in Patients with the Jarvik-7 Total Artificial Heart*. *ASAIO Journal*, 1987. **33**(3): p. 413-417.
78. Kameneva, M.V., Marad, P.F., Brugger, J.M., Repko, B.M., Wang, J.H., Moran, J., and Borovetz, H.S., *In vitro evaluation of hemolysis and sublethal blood trauma in a novel subcutaneous vascular access system for hemodialysis*. *ASAIO journal*, 2002. **48**(1): p. 34-38.
79. Koppensteiner, R., Derfler, K., and Ehringer, H., *Blood rheology after renal transplantation*. *Nephron*, 1996. **74**(2): p. 328-332.
80. Kameneva, M.V., Antaki, J.F., Butler, K.C., Watach, M.J., Kormos, R.L., Griffith, B.P., and Borovetz, H.S., *A Sheep Model for the Study of Hemorheology With Assisted Circulation: Effect of an Axial Flow Blood Pump*. *ASAIO journal*, 1994. **40**(4): p. 959-963.
81. Ding, J., Chen, Z., Niu, S., Zhang, J., Mondal, N.K., Griffith, B.P., and Wu, Z.J., *Quantification of Shear-Induced Platelet Activation: High Shear Stresses for Short Exposure Time*. *Artificial Organs*, 2015. **39**(7): p. 576-583.
82. Selgrade, B.P. and Truskey, G.A., *Computational Fluid Dynamics Analysis to Determine Shear Stresses and Rates in a Centrifugal Left Ventricular Assist Device*. *Artificial Organs*, 2012. **36**(4): p. E89-E96.

83. Başkurt, O., Bor-Küçükataay, M., Yalçın, Ö., Meiselman, H., and Armstrong, J., *Standard aggregating media to test the "aggregability" of rat red blood cells*. *Clinical Hemorheology and Microcirculation*, 2000. **22**(2): p. 161-166.
84. McNamee, A.P., Sabapathy, S., Singh, I., Horobin, J., Guerrero, J., and Simmonds, M.J., *Acute Free-Iron Exposure Does Not Explain the Impaired Haemorheology Associated with Haemochromatosis*. *PLoS One*, 2016. **11**(1): p. e0146448.
85. Dodge, J.T., Mitchell, C., and Hanahan, D.J., *The preparation and chemical characteristics of hemoglobin-free ghosts of human erythrocytes*. *Archives of Biochemistry and Biophysics*, 1963. **100**(1): p. 119-130.
86. Spyridaki, M.-H.E. and Siskos, P.A., *An improved spectrophotometric method for the determination of free, bound and total N-acetylneuraminic acid in biological fluids*. *Analytica Chimica Acta*, 1996. **327**(3): p. 277-285.
87. Borst, O., Abed, M., Alesutan, I., Towhid, S.T., Qadri, S.M., Föller, M., Gawaz, M., and Lang, F., *Dynamic adhesion of eryptotic erythrocytes to endothelial cells via CXCL16/SR-PSOX*. *American Journal of Physiology-Cell Physiology*, 2012. **302**(4): p. C644-C651.
88. Johnson, P.C., *Red cell separation in the mesenteric capillary network*. *American Journal of Physiology-Legacy Content*, 1971. **221**(1): p. 99-104.
89. Mchedlishvili, G., Varazashvili, M., and Gobejishvili, L., *Local RBC aggregation disturbing blood fluidity and causing stasis in microvessels*. *Clinical Hemorheology and Microcirculation*, 2002. **26**(2): p. 99-106.
90. Mehdi, M.M., Singh, P., and Rizvi, S.I., *Erythrocyte sialic acid content during aging in humans: correlation with markers of oxidative stress*. *Disease Markers*, 2012. **32**(3): p. 179-186.
91. Hadengue, A.L., Del-Pino, M., Simon, A., and Levenson, J., *Erythrocyte disaggregation shear stress, sialic acid, and cell aging in humans*. *Hypertension*, 1998. **32**(2): p. 324-330.

92. de Oliveira, S. and Saldanha, C., *An overview about erythrocyte membrane*. *Clinical Hemorheology and Microcirculation*, 2010. **44**(1): p. 63-74.
93. Aoki, T., *A Comprehensive Review of Our Current Understanding of Red Blood Cell (RBC) Glycoproteins*. *Membranes*, 2017. **7**(4): p. 56.
94. Kameneva, M.V., Antaki, J.F., Yeleswarapu, K.K., Watach, M.J., Griffith, B.P., and Borovetz, H.S., *Plasma protective effect on red blood cells exposed to mechanical stress*. *ASAIO Journal*, 1997. **43**(5): p. M571-5.
95. Chien, S., *Red cell deformability and its relevance to blood flow*. *Annual Review of Physiology*, 1987. **49**(1): p. 177-192.
96. Schmid-Schönbein, H. and Wells, R., *Fluid drop-like transition of erythrocytes under shear*. *Science*, 1969. **165**(3890): p. 288-291.
97. Fischer, T.M., Stohr-Lissen, M., and Schmid-Schonbein, H., *The red cell as a fluid droplet: tank tread-like motion of the human erythrocyte membrane in shear flow*. *Science*, 1978. **202**(4370): p. 894-896.
98. Fischer, T.M., *On the energy dissipation in a tank-treading human red blood cell*. *Biophysical Journal*, 1980. **32**(2): p. 863-868.
99. Fischer, T.M., *Tank-tread frequency of the red cell membrane: dependence on the viscosity of the suspending medium*. *Biophysical Journal*, 2007. **93**(7): p. 2553-2561.
100. Goldsmith, H., Marlow, J., and MacIntosh, F.C., *Flow behaviour of erythrocytes-i. Rotation and deformation in dilute suspensions*. *Proceedings of the Royal Society of London. Series B. Biological Sciences*, 1972. **182**(1068): p. 351-384.
101. Fedosov, D.A., Caswell, B., and Karniadakis, G.E., *A multiscale red blood cell model with accurate mechanics, rheology, and dynamics*. *Biophysical Journal*, 2010. **98**(10): p. 2215-25.

102. Horobin, J.T., Sabapathy, S., and Simmonds, M.J., *Repetitive Supra-Physiological Shear Stress Impairs Red Blood Cell Deformability and Induces Hemolysis*. *Artificial Organs*, 2017. **41**(11): p. 1017-1025.
103. McNamee, A.P., Tansley, G.D., and Simmonds, M.J., *Sublethal mechanical trauma alters the electrochemical properties and increases aggregation of erythrocytes*. *Microvascular Research*, 2018. **120**: p. 1-7.
104. Yao, W., Wen, Z., Yan, Z., Sun, D., Ka, W., Xie, L., and Chien, S., *Low viscosity Ektacytometry and its validation tested by flow chamber*. *Journal of Biomechanics*, 2001. **34**(11): p. 1501-1509.
105. Parrow, N.L., Violet, P.-C., Tu, H., Nichols, J., Pittman, C.A., Fitzhugh, C., Fleming, R.E., Mohandas, N., Tisdale, J.F., and Levine, M., *Measuring Deformability and Red Cell Heterogeneity in Blood by Ektacytometry*. *JoVE (Journal of Visualized Experiments)*, 2018(131): p. e56910.
106. Mihailescu, M. and Costescu, J., *Diffraction pattern study for cell type identification*. *Optics Express*, 2012. **20**(2): p. 1465-1474.
107. Nemeth, N., Kiss, F., and Miszti-Blasius, K., *Interpretation of osmotic gradient ektacytometry (osmoscan) data: a comparative study for methodological standards*. *Scandinavian Journal of Clinical and Laboratory Investigation*, 2015. **75**(3): p. 213-222.
108. Bayer, R., Caglayan, S., and Guenther, B. *Discrimination between orientation and elongation of RBC in laminar flow by means of laser diffraction*. in *Biochemical Diagnostic Instrumentation*. 1994. International Society for Optics and Photonics.
109. Olia, S.E., Maul, T.M., Antaki, J.F., and Kameneva, M.V., *Mechanical blood trauma in assisted circulation: sublethal RBC damage preceding hemolysis*. *The International Journal of Artificial Organs*, 2016. **39**(4): p. 150-159.
110. Lipowsky, H.H., Cram, L., Justice, W., and Eppihimer, M., *Effect of erythrocyte deformability on in vivo red cell transit time and hematocrit and their correlation with in vitro filterability*. *Microvascular Research*, 1993. **46**(1): p. 43-64.

111. Driessen, G., Fischer, T., Haest, C., Inhoffen, W., and Schmid-Schönbein, H., *Flow behaviour of rigid red blood cells in the microcirculation*. International Journal of Microcirculation, Clinical and Experimental, 1984. **3**(2): p. 197-210.
112. Baskurt, O.K., Hardeman, M.R., Uyuklu, M., Ulker, P., Cengiz, M., Nemeth, N., Shin, S., Alexy, T., and Meiselman, H.J., *Parameterization of red blood cell elongation index–shear stress curves obtained by ektacytometry*. Scandinavian Journal of Clinical and Laboratory Investigation, 2009. **69**(7): p. 777-788.
113. Sutera, S.P., *Flow-induced trauma to blood cells*. Circulation Research, 1977. **41**(1): p. 2-8.
114. Wen, Z., Gao, T., Yan, Z., Song, L., Dou, H., Sun, D., Lü, Z., Shi, Y., and Xiao, H., *Biophysical meanings of orientation and deformation of RBCs in shear flow field of low viscosity with new Ektacytometry*. Science in China Series C: Life Sciences, 1998. **41**(2): p. 195-202.
115. Artmann, G.M., Sung, K., Horn, T., Whittemore, D., Norwich, G., and Chien, S., *Micropipette aspiration of human erythrocytes induces echinocytes via membrane phospholipid translocation*. Biophysical Journal, 1997. **72**(3): p. 1434-1441.
116. Nemeth, N., Deak, A., Szentkereszty, Z., and Peto, K., *Effects and influencing factors on hemorheological variables taken into consideration in surgical pathophysiology research*. Clinical Hemorheology and Microcirculation, 2018. **69**(1-2): p. 133-140.
117. Reinhart, W.H. and Chien, S., *Roles of cell geometry and cellular viscosity in red cell passage through narrow pores*. American Journal of Physiology-Cell Physiology, 1985. **248**(5): p. C473-C479.
118. Kamyabi, N., Khan, Z.S., and Vanapalli, S.A., *Flow-induced transport of tumor cells in a microfluidic capillary network: role of friction and repeated deformation*. Cellular and Molecular Bioengineering, 2017. **10**(6): p. 563-576.

119. Driessen, G., Haest, C., Heidtmann, H., Kamp, D., and Schmid-Schönbein, H., *Effect of reduced red cell "deformability" on flow velocity in capillaries of rat mesentery*. Pflügers Archiv, 1980. **388**(1): p. 75-78.
120. Driessen, G., Scheidt-Bleichert, H., Sobota, A., Inhoffen, W., Heidtmann, H., Haest, C., Kamp, D., and Schmid-Schönbein, H., *Capillary resistance to flow of hardened (diamide treated) red blood cells (RBC)*. Pflügers Archiv, 1982. **392**(3): p. 261-267.
121. Wakeman, L., Munro, R., Russell, C., Benton, A., Hartnell, S., and Al-Ismail, S., *New Reference Ranges in Haematology for Healthy Adults Using the Modern Sysmex XE-2100 Automated Analyser*. Blood, 2005. **106**(11): p. 3740-3740.
122. Nash, G.B. and Meiselman, H.J., *Red cell and ghost viscoelasticity. Effects of hemoglobin concentration and in vivo aging*. Biophysical Journal, 1983. **43**(1): p. 63-73.
123. Cahalan, S.M., Lukacs, V., Ranade, S.S., Chien, S., Bandell, M., and Patapoutian, A., *Piezo1 links mechanical forces to red blood cell volume*. Elife, 2015. **4**: p. e07370.
124. Manno, S., Takakuwa, Y., and Mohandas, N., *Identification of a functional role for lipid asymmetry in biological membranes: Phosphatidylserine-skeletal protein interactions modulate membrane stability*. Proceedings of the National Academy of Sciences, 2002. **99**(4): p. 1943-8.
125. Mizuno, T., Tsukiya, T., Taenaka, Y., Tatsumi, E., Nishinaka, T., Ohnishi, H., Oshikawa, M., Sato, K., Shioya, K., Takewa, Y., and Takano, H., *Ultrastructural alterations in red blood cell membranes exposed to shear stress*. ASAIO Journal, 2002. **48**(6): p. 668-70.
126. Dao, K., O'Rear, E., Johnson, A., and Peitersen, S., *Sensitivity of the erythrocyte membrane bilayer to subhemolytic mechanical trauma as detected by fluorescence anisotropy*. Biorheology, 1994. **31**(1): p. 69-76.
127. Nash, G.B. and Meiselman, H.J., *Alteration of red cell membrane viscoelasticity by heat treatment: effect on cell deformability and suspension viscosity*. Biorheology, 1985. **22**(1): p. 73-84.

128. Watanabe, N., Sakota, D., Ohuchi, K., and Takatani, S., *Deformability of red blood cells and its relation to blood trauma in rotary blood pumps*. *Artificial Organs*, 2007. **31**(5): p. 352-8.
129. Johnson, C.P., Tang, H.-Y., Carag, C., Speicher, D.W., and Discher, D.E., *Forced unfolding of proteins within cells*. *Science*, 2007. **317**(5838): p. 663-666.
130. Khan, Z.S., Kamyabi, N., Hussain, F., and Vanapalli, S.A., *Passage times and friction due to flow of confined cancer cells, drops, and deformable particles in a microfluidic channel*. *Convergent Science Physical Oncology*, 2017. **3**(2): p. 024001.
131. Allen, C.á. and Bayraktutan, U., *Oxidative stress and its role in the pathogenesis of ischaemic stroke*. *International Journal of Stroke*, 2009. **4**(6): p. 461-470.
132. Hebbel, R.P., Leung, A., and Mohandas, N., *Oxidation-induced changes in microrheologic properties of the red blood cell membrane*. *Blood*, 1990. **76**(5): p. 1015-1020.
133. Baskurt, O.K. and Yavuzer, S., *Some hematological effects of oxidants*. *Advances in Environmental Science and Technology New York*, 1994. **28**: p. 405-405.
134. West, I.C., *Radicals and oxidative stress in diabetes*. *Diabetic Medicine*, 2000. **17**(3): p. 171-180.
135. Loughrey, C., Young, I., Lightbody, J., McMaster, D., McNamee, P., and Trimble, E., *Oxidative stress in haemodialysis*. *Qjm*, 1994. **87**(11): p. 679-683.
136. Cristol, J., Bosc, J., Badiou, S., Leblanc, M., Lorrho, R., Descomps, B., and Canaud, B., *Erythropoietin and oxidative stress in haemodialysis: beneficial effects of vitamin E supplementation*. *Nephrology Dialysis Transplantation*, 1997. **12**(11): p. 2312-2317.
137. Simmonds, M.J., Meiselman, H.J., Marshall-Gradisnik, S.M., Pyne, M., Kakanis, M., Keane, J., Brenu, E., Christy, R., and Baskurt, O.K., *Assessment of oxidant susceptibility of red blood cells in various species based on cell deformability*. *Biorheology*, 2011. **48**(5): p. 293-304.

138. Heitzer, T., Schlinzig, T., Krohn, K., Meinertz, T., and Münzel, T., *Endothelial dysfunction, oxidative stress, and risk of cardiovascular events in patients with coronary artery disease*. *Circulation*, 2001. **104**(22): p. 2673-2678.
139. Maritim, A., Sanders, a., and Watkins, r.J., *Diabetes, oxidative stress, and antioxidants: a review*. *Journal of Biochemical and Molecular Toxicology*, 2003. **17**(1): p. 24-38.
140. Snyder, L., Fortier, N., Trainor, J., Jacobs, J., Leb, L., Lubin, B., Chiu, D., Shohet, S., and Mohandas, N., *Effect of hydrogen peroxide exposure on normal human erythrocyte deformability, morphology, surface characteristics, and spectrin-hemoglobin cross-linking*. *Journal of Clinical Investigation*, 1985. **76**(5): p. 1971.
141. Paci, R. and Davies, K., *Protein degradation as an index of oxidative stress*. *Methods in Enzymology*, 1990. **186**: p. 485-502.
142. Kojda, G. and Harrison, D., *Interactions between NO and reactive oxygen species: pathophysiological importance in atherosclerosis, hypertension, diabetes and heart failure*. *Cardiovascular research*, 1999. **43**(3): p. 652-671.
143. Lai, C.Q., Shen, J.C.W., Cheng, W.C.W., and Yap, C.H., *A near-superhydrophobic surface reduces hemolysis of blood flow in tubes*. *RSC Advances*, 2016. **6**(67): p. 62451-62459.
144. Baskurt, O.K., Temiz, A., and Meiselman, H.J., *Effect of Superoxide Anions on Red Blood Cell Rheologic Properties*. *Free Radical Biology and Medicine*, 1998. **24**(1): p. 102-110.
145. Bessis, M., Mohandas, N., and Feo, C., *Automated ektacytometry: a new method of measuring red cell deformability and red cell indices*. *Blood Cells*, 1979. **6**(3): p. 315-327.
146. Baskurt, O.K. and Meiselman, H.J., *Data reduction methods for ektacytometry in clinical hemorheology*. *Clinical Hemorheology and Microcirculation*, 2013. **54**(1): p. 99-107.
147. Snyder, L.M., Fortier, N.L., Trainor, J., Jacobs, J., Leb, L., Lubin, B., Chiu, D., Shohet, S., and Mohandas, N., *Effect of hydrogen peroxide exposure on normal human erythrocyte deformability, morphology, surface characteristics, and spectrin-hemoglobin cross-linking*. *Journal of Clinical Investigation*, 1985. **76**(5): p. 1971-1977.

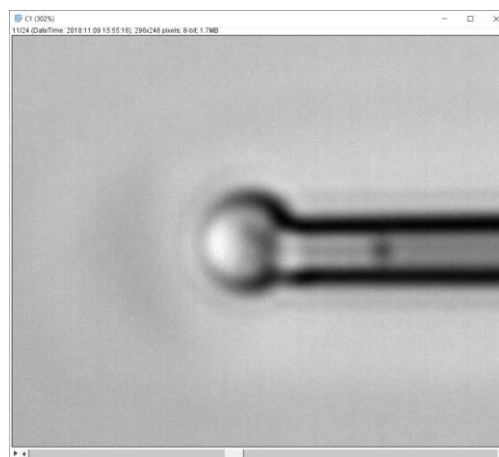
148. Baskurt, O.K. and Meiselman, H.J., *Blood rheology and hemodynamics*. Seminars in Thrombosis and Hemostasis, 2003. **29**(5): p. 435-50.
149. Shinar, E., Rachmilewitz, E.A., and Lux, S.E., *Differing erythrocyte membrane skeletal protein defects in alpha and beta thalassemia*. Journal of Clinical Investigation, 1989. **83**(2): p. 404-10.
150. Sinha, A., Chu, T.T.T., Dao, M., and Chandramohanadas, R., *Single-cell evaluation of red blood cell bio-mechanical and nano-structural alterations upon chemically induced oxidative stress*. Scientific Reports, 2015. **5**: p. 9768.
151. Meram, E., Yilmaz, B.D., Bas, C., Atac, N., Yalcin, O., Meiselman, H.J., and Baskurt, O.K., *Shear stress-induced improvement of red blood cell deformability*. Biorheology, 2013. **50**(3): p. 165-176.
152. Zakkar, M., Guida, G., Suleiman, M., and Angelini, G.D., *Cardiopulmonary bypass and oxidative stress*. Oxidative Medicine and Cellular Longevity, 2015. **2015**.
153. Qiang, Y., Liu, J., Dao, M., Suresh, S., and Du, E., *Mechanical fatigue of human red blood cells*. Proceedings of the National Academy of Sciences, 2019. **116**(40): p. 19828-19834.
154. Horobin, J.T., Sabapathy, S., and Simmonds, M.J., *Red blood cell tolerance to shear stress above and below the subhemolytic threshold*. Biomechanics and Modeling in Mechanobiology, 2019: p. 1-10.

Appendix: automated micropipette image analysis software

The following appendix describes the image analysis software created in ImageJ (National Institutes of Health, Bethesda, USA) for the purpose of automated analysis of RBC micropipette aspiration. Prior to executing the image analysis routine, each micropipette aspiration micrograph image must be captured at 5 Pa intervals, stored in single directory, and the image must be unsharpened with a slight blur.

1. Open the micropipette aspiration image sequence as a stack from a file directory, convert each frame to an 8-bit image, and generate dimensional map for pixel-micron conversion.

```
1 //open images and create stack
2 run("Image Sequence...", "open=C:/Users/asus/Desktop/C1/Image_1460.tif convert sort");
3 //make sure 8bit
4 run("8-bit")
5
6 //get image details
7 ImageNumber = getTitle();
8 Stack.getDimensions(width, height, channels, slices, frames)
```

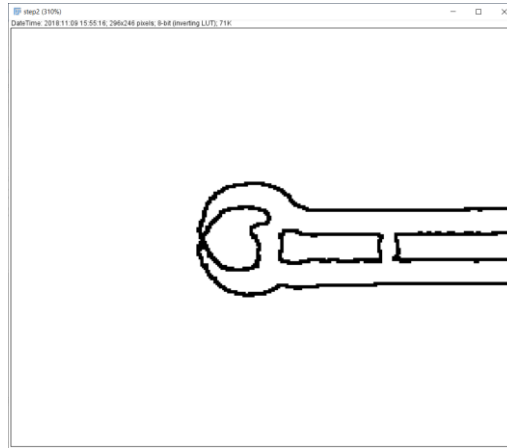


2. Perform initial processing on each frame in the stack to filter, binarise, and detect edges.

```

10 //process pipette image
11 run("Subtract Background...", "rolling=10 light stack");
12 setThreshold(0, 244);
13 setOption("BlackBackground", false);
14 run("Convert to Mask", "method=Default background=Light");
15 run("Despeckle", "slice");
16 run("Remove Outliers...", "radius=5 threshold=50 which=Dark stack");
17 run("Find Edges", "stack");

```



3. Define a data table within ImageJ.

```

19 //create table
20 Table.create(ImageNumber);
21 Table.set("Pipette diameter (micron)",0,0);
22 Table.set("Pressure (Pa)",0,0);
23 Table.set("Cell tongue length (micron)",0,0);

```

4. Ensure that each frame will be processed with the analysis code.

```

25 //run macro on all slices
26 for (i=1;i<frames+1;i++){
27   Stack.setFrame(i);
28   for (j=1;j<slices+1;j++){
29     Stack.setSlice(j);

```

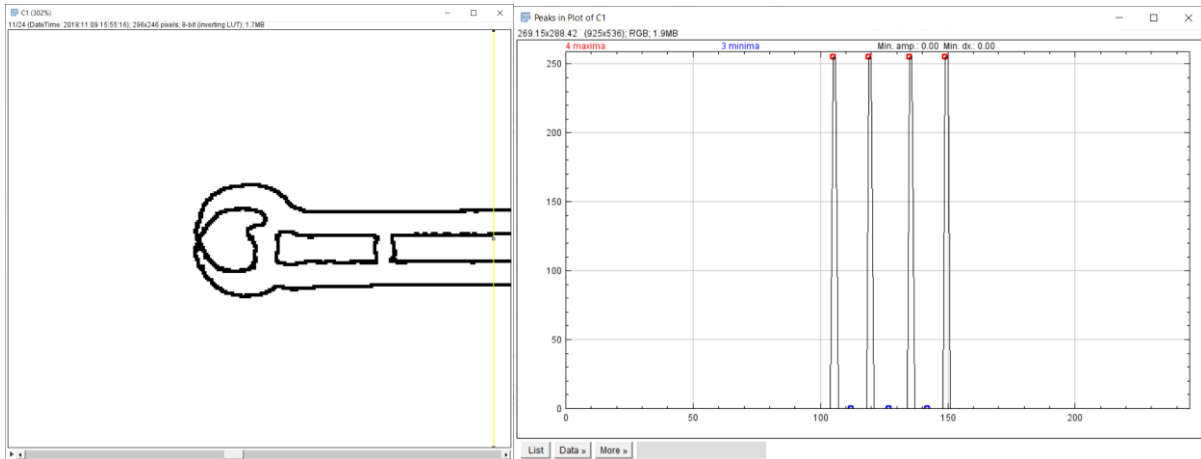
5. Create a vertical line that will intersect with the glass capillary walls that is also independent of the region of interest and cell tongue.

6. Plot the grey value intensity of the vertical line, identifying the maximum amplitudes and intersection with the black lines. Use the innermost black lines as the inner walls of the micropipette, and define these variables for further use.

```

31 //vertical line 1 - get y1 coordinates of top and bottom inner pipette
32 makeLine(width-10,0,width-10,height,1);
33 run("Plot Profile");
34 run("Find Peaks", "min._peak_amplitude=0 min._peak_distance=0 min._value=[] max._value=[] exclude");
35 Plot.showValues();
36 x1 = (getResult("X1", 1));
37 x2 = (getResult("X1", 2));
38 close("Results");
39 close ("Plot*");
40 close ("Peaks*");

```

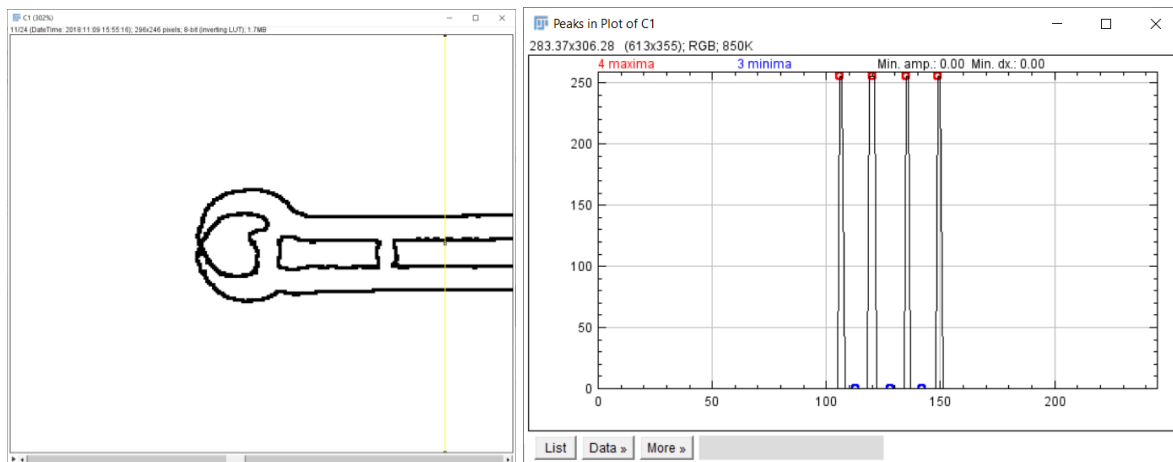


- Repeat Step 5 and Step 6 for another vertical line with a different x location to determine an addition set of (x, y) coordinates of the micropipette inner walls. Define these variables for further use. Using the defined coordinates of the inner walls of the micropipette, the micropipette can be traced to identify the angle and diameter of the pipette tip.

```

42 //vertical line 2 - get y2 coordinates of top and bottom inner pipette
43 makeLine(width-40,0,width-40,height,1);
44 run("Plot Profile");
45 run("Find Peaks", "min._peak_amplitude=0 min._peak_distance=0 min._value=[] max._value=[] exclude");
46 Plot.showValues();
47 x3 = (getResult("X1", 1));
48 x4 = (getResult("X1", 2));
49 close("Results");
50 close ("Plot*");
51 close ("Peaks*");

```



8. Determine the micropipette inner diameter and input the value into the table generated in Step 3.

```

53 //find pipette diameter
54 d=((x1-x2)+(x3-x4))/2*0.10833;
55 Table.set("Pipette diameter (micron)",j,d);

```

9. Plot a straight line at the axial portion of the micropipette using the midpoint determined between previously defined (x, y) coordinates of the micropipette walls.

```

57 //create line at pipette radius
58 makeLine(0, ((x1+x2)/2), width, ((x1+x2)/2));

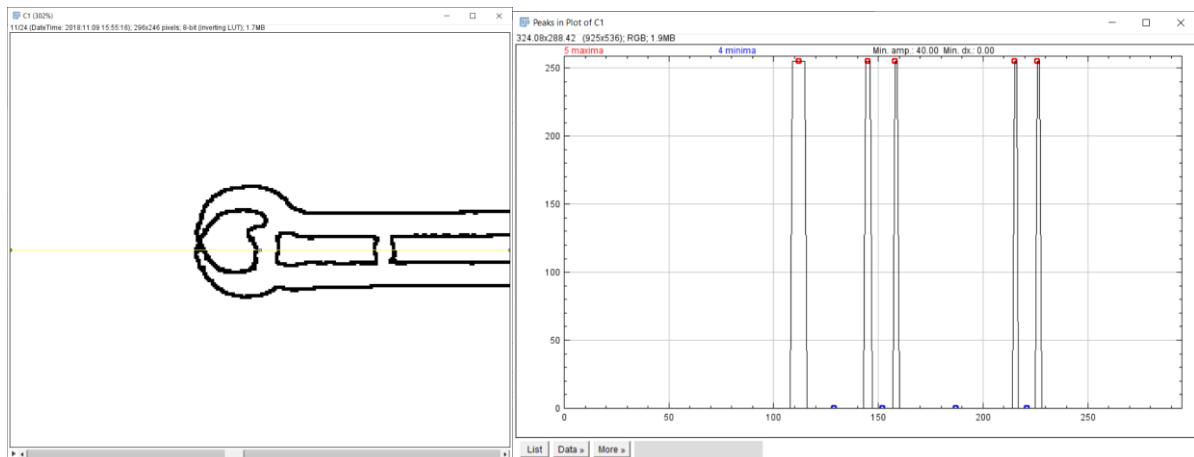
```

10. Plot the gray value intensity and identify maxima representing the pipette tip and the aspirated portion of the RBC tongue.

```

60 //measure tongue length
61 run("Plot Profile");
62 run("Find Peaks", "min._peak_amplitude=40 min._peak_distance=0 min._value=[] max._value=[] exclude");
63 Plot.showValues();
64 //identify tongue
65 x5 = (getResult("X1", 0)+getResult("X1", 1))/2;
66 //identify pipette tip
67 x6 = getResult("X1", 2);
68 //calculate tongue length
69 x7 = x5-x6;
70 close("Results");
71 close ("Plot*");
72 close ("Peaks*");

```



11. Calculate the distances between various maxima and input the values into the data table generated in Step 3 for each frame (at a known pressure).

```

74 //print results to table
75     Table.set("Pipette diameter (micron)",j,d);
76     Table.set("Pressure (Pa)",j,j*5);
77     Table.set("Cell tongue length (micron)",j,x7*0.10833);
78     Table.update;
79     }
80 }
81
82 //Table.save(filePath)

```

Pipette diameter (micron)	Pressure (Pa)	Cell tongue length (micron)
1.679	15	3.358
1.679	20	4.117
1.625	25	4.767
1.679	30	5.417
1.625	35	5.958
1.679	40	6.175
1.679	45	6.500
1.679	50	6.662
1.679	55	6.771
1.625	60	7.096
1.679	65	7.366
1.625	70	7.475
1.625	75	7.583
1.679	80	7.746
1.625	85	7.908
1.679	90	8.125
1.679	95	8.125
1.625	100	8.233
1.625	105	8.341
1.625	110	8.450

12. Save and export the results.

List of abbreviations and symbols

Symbols

g	acceleration due to gravity
L_p	aspirated portion of the cell
a	cross-sectional area
f	Darcy-Weisbach friction factor
ρ	density
D	diameter
ε	dielectric constant of the buffer
Δ	differential/change
γ^{thr}	disaggregation shear rate threshold
η	dynamic viscosity
E	electric field strength
u	electrophoretic mobility
Le	entrance development length for laminar flow
v	fluid velocity
h_f	friction head loss
I.D.	inner diameter
v_r	instantaneous flow velocity

L	length
\times	mathematical operator for multiplication
v_{\max}	maximal flow velocity
N	number of revolutions per minute
p	p-value test statistic
π	pi
\pm	plus-minus
R	radius
r_b	radius of bob
r_c	radius of cup
r_p	radius of the micropipette
Re	Reynolds number
μ	shear elastic modulus
$\dot{\gamma}$	shear rate
τ	shear stress
Q	volumetric flow rate
V	volume
τ_0	wall shear stress
ζ	zeta potential

Units of measurement

pH	acidity; $-\log[\text{H}^+]$
cm	centimetre
d	day(s)
°	degree(s)
$\text{kg}\cdot\text{m}^3$	density; kilogram per cubic metre
fL	femtolitre
F	force
$\text{g}\cdot\text{L}^{-1}$	gram per litre
g	gravitational constant
$\text{L}\cdot\text{L}^{-1}$	haematocrit; litre per litre
Hz	hertz
h	hour(s)
I	Impulse
kDa	kilodaltons
kg	kilogram
kPa	kilopascal
L	litre(s)
μL	microlitre

μm	micrometre
$\mu\text{m}\cdot\text{s}^{-1}$	micrometre per second
m	metre
M	molarity
μM	micromolar
$\text{mg}\cdot\text{dL}^{-1}$	milligram per decilitre
$\text{mg}\cdot\text{mL}^{-1}$	milligram per millilitre
mL	millilitre
$\text{mL}\cdot\text{min}^{-1}$	millilitre per minute
$\text{mL}\cdot\text{s}^{-1}$	millilitre per second
mm	millimetre
mmHg	millimetre of mercury
$\text{mOsmol}\cdot\text{kg}^{-1}$	milliosmole per kilogram; osmolality
mV	millivolts
mW	milliwatts
min	minute(s)
N	newton
Nm	nanometre
$\text{N}\cdot\text{s}\cdot\text{m}^{-2}$	newton-second per square metre

Pa	pascal
%	percentage
pg	picogram
pN	piconewton
$\text{pN}\cdot\mu\text{m}^{-1}$	piconewton per micrometre
$\text{rev}\cdot\text{min}^{-1}$	revolutions per minute
n	sample size
s	second(s)
s^{-1}	shear rate; inverse seconds
$^{\circ}\text{C}$	temperature; degrees Celsius
t	time
$\text{mPa}\cdot\text{s}$	viscosity; millipascal-second
w/v	weight per volume
yr	year(s)

Variables and abbreviated terms

a.u.	arbitrary units
ATP	adenosine triphosphate
B3	band 3 protein
BSA	bovine serum albumin
CFD	computational fluid dynamics
C.I.	confidence interval
Con	control
DX70	dextran, 70 kDa
EI	elongation index
EPM	electrophoretic mobility
EDTA	ethylenediaminetetraacetic acid
G	gauge
GHO	ghost cells
Hb	haemoglobin
HT	heat treatment
I.D.	inner diameter
RBC-NOS	intracellular red blood cell nitric oxide synthase
EI _{max}	maximal elongation index

MCH	mean corpuscular haemoglobin
MCHC	mean corpuscular haemoglobin concentration
MCV	mean corpuscular volume
MCS	mechanical circulatory support
ND	neutral density
NO	nitric oxide
NOS	nitric oxide synthase
AI ₁₂₀	parameterised red blood cell aggregation over 120-s
PMS	phenazine methylsulfate
PBS	phosphate-buffered saline
PLA	plasma
PVP	Polyvinylpyrrolidinone
RBC	red blood cell
M ₀	red blood cell aggregation at stasis in plasma or dextran
M ₁	red blood cell aggregation at 3 s ⁻¹ in plasma or dextran
RCC	red cell concentrates
SA	sialic acid
SEM	standard error of the mean
SS	shear stress

SS_{half} or $SS_{1/2}$	shear stress required for half-maximal elongation index
$T_{1/2}$	time required for half-maximal aggregation
UV	ultraviolet
VAD	ventricular assist device